

# STRATEGIES FOR RADAR-COMMUNICATION SPECTRUM SHARING

---

A Dissertation  
Submitted to  
the Temple University Graduate Board

---

In Partial Fulfillment  
of the Requirements for the Degree  
DOCTOR OF PHILOSOPHY

---

by  
Ammar Ahmed  
Diploma Date May 2021

Examining Committee Members:

Dr. Yimin D. Zhang, Advisory Chair, Department of Electrical and Computer Engineering

Dr. Dennis Silage, Department of Electrical and Computer Engineering

Dr. Joseph Picone, Department of Electrical and Computer Engineering

Dr. Yu Wang, External Member, Department of Computer and Information Sciences

©  
Copyright  
2021

by

Ammar Ahmed  
All Rights Reserved

## ABSTRACT

Spectrum sharing has become increasingly important since the past decade due to the ongoing congestion of spectral resources. Higher data rates in wireless communications require expansion of existing frequency allocations. Significant research efforts have been made in the direction of cognitive radio to effectively manage the existing frequency usage. Recently, coexistence of multiple platforms within the same frequency bands is considered effective to mitigate spectral congestion. This requires both systems to work collaboratively to mitigate their mutual interference. This challenging problem can be significantly simplified if both systems are controlled by the same entity. Joint radar-communication (JRC) system is such an example where radar and communication system objectives are achieved by the same physical platform.

In this dissertation, we consider three different types of JRC systems. These JRC systems respectively exploit a single transmit antenna, an antenna array for beamforming, and a distributed JRC network, and develop novel signal processing techniques to optimize the performance of these systems. Special attention is given to the resource optimization objectives and numerous resource allocation schemes are developed and investigated.

First, we consider a single transmit antenna-based JRC system which exploits dual-purpose transmit orthogonal frequency division multiplexing (OFDM) waveforms to perform radar and communication objectives simultaneously. We optimize the power allocation of the OFDM subcarriers based on the frequency-sensitive target response and communication channel characteristics. For this purpose, we employ mutual information as the optimization metric. In the simulation examples considered for this system, we observed that the JRC system enjoys approximately 20% improvement in the performance of communication subsystem with a mere 5% reduction in radar subsystem performance.

Second, we propose a quadratic amplitude modulation (QAM) based sidelobe modulation scheme for beamforming-based JRC systems which enhances the communication data rate by enabling a novel multiple access strategy. The main principle of this proposed strategy lies in enabling the beamformer to transmit signals with distinct amplitudes and phases in different directions. We also investigate optimal power allocation for such a spectrum sharing approach by employing a spatial power control-based beamforming approach. Furthermore, the robustness of these beamforming-based JRC systems is improved using chance constrained programming. In this context, we observe that the chance constrained optimization can be relaxed to form a deterministic and convex problem by employing the statistical profile of the communication channels. When dealing with JRC systems that are equipped with more antennas than the number of radio frequency chains, we perform the resource optimization in terms of minimized power usage and optimal selection of antennas resulting in an efficient utilization of hardware up-conversion chains. In the simulation examples considered for these schemes, we observe that, even with a reduction of nearly 30% of the transmit antennas, the beamforming-based JRC system is able to perform the required radar and communication tasks without any disadvantage.

Our last contribution is on a distributed JRC system, which is the first effort in this research direction, enabling spectrum sharing for networked radar systems co-existing with the communication systems. We devise a power allocation strategy for such a system by employing convex optimization techniques. In this strategy, the target localization error and the Shannon capacity are respectively considered as the optimization criteria for radar and communication systems. For the simulation example considered in this case, we observe that the proposed resource allocation strategy achieves a communication performance that was approximately 5 times greater than that achieved by the radar-only counterpart. Moreover, the target localization performance achieved by the JRC system using the proposed approach was approximately 4 times better than the performance achieved by the communication-only approach.

To my loved ones.

## ACKNOWLEDGMENTS

This dissertation could not be completed without the help and support of many people. Primarily, I would like to express my deep gratitude to my advisor, Dr. Yimin D. Zhang, for his guidance and support during my years at Temple University. His passion, diligence, and conscientious work ethics towards research and life have motivated me to grow both professionally and as an individual. I am grateful to him for playing a pivotal role and constantly teaching me the art and science of research par excellence. It is truly an honor to be his Ph.D. student. I am also thankful to Dr. Braham Himed from Air Force Research Laboratory for his continuous mentorship and support. Sincere thanks are extended to the members of my dissertation advisory committee members, Dr. Dennis Silage and Dr. Joseph Picone, who contributed their time, knowledge, and mentorship. I am also thankful to Dr. Yu Wang for his valuable time, expertise, and for agreeing to serve as the external examiner. Moreover, the experience gained as a teaching assistant for the courses offered by Dr. Dennis Silage and Dr. Fauzia Ahmad truly boosted my confidence.

The coursework taught at Temple University played a critical role in shaping the direction of my research. In this context, I would like to thank Dr. Dennis Silage, Dr. Joseph Picone, Dr. Yimin D. Zhang, and Dr. Frank Ferrese for their wonderful courses in signal processing, communications, information theory, and optimization strategies. I would also like to thank Temple University College of Engineering and Air Force Research Laboratory for providing the financial support throughout my research. I would also like to express my gratitude to the current and past members of the Advanced Signal Processing Laboratory for their great ideas during our group discussions. I have also greatly benefited from the technical discussions in the graduate seminar with internal and external experts.

Finally, I thank my parents and family for their patience and unconditional love. Without their trust, love and many sacrifices, I would not have been what I am today.

## TABLE OF CONTENTS

	Page
ABSTRACT . . . . .	iii
ACKNOWLEDGMENTS . . . . .	vi
LIST OF ABBREVIATIONS . . . . .	xi
LIST OF TABLES . . . . .	xii
LIST OF FIGURES . . . . .	xiii
 CHAPTER	
1 INTRODUCTION . . . . .	1
1.1 Overview . . . . .	1
1.2 Notations . . . . .	4
1.3 Single Transmit Antenna-based JRC System . . . . .	4
1.3.1 Signal Model . . . . .	5
1.3.2 Radar Subsystem . . . . .	6
1.3.3 Communication Subsystem . . . . .	7
1.4 Beamforming-based JRC System . . . . .	7
1.4.1 Signal Model . . . . .	8
1.4.2 Beamforming Weight Vector Design . . . . .	9
1.4.3 ASK-based Schemes . . . . .	9
1.4.4 PSK-based Schemes . . . . .	11
1.5 Research Contributions . . . . .	12
1.5.1 Subcarrier Allocation and Power Optimization for Single Transmit Antenna-based JRC Systems . . . . .	12
1.5.2 Throughput Enhancement for Beamforming-based JRC Systems . . . . .	13
1.5.3 Chance Constrained Beamforming-based JRC Systems . . . . .	13

	Page	
1.5.4	Power Allocation for Beamforming-based JRC Systems	13
1.5.5	Sensor Selection for Beamforming-based JRC Systems	14
1.5.6	Distributed JRC Systems . . . . .	14
1.6	Publications . . . . .	15
2	SINGLE TRANSMIT ANTENNA-BASED JRC SYSTEMS . . . . .	20
2.1	Signal Model . . . . .	21
2.2	Optimization Criteria . . . . .	24
2.2.1	Radar subsystem . . . . .	24
2.2.2	Communication Subsystem . . . . .	24
2.3	Optimal Power Distribution and Subcarrier Allocation . . .	25
2.3.1	Radar-Centric Design . . . . .	25
2.3.2	Cooperative Design . . . . .	27
2.4	Numerical Results . . . . .	28
2.5	Remarks . . . . .	31
3	THROUGHPUT ENHANCEMENT OF BEAMFORMING BASED JRC SYSTEMS . . . . .	32
3.1	Proposed QAM Based Sidelobe Modulation . . . . .	33
3.1.1	Signaling Strategy . . . . .	33
3.1.2	Information Decoding at Communication Receivers .	39
3.1.3	Sum Data Rate Analysis . . . . .	41
3.2	Simulation Results . . . . .	43
3.2.1	Beampattern Synthesis and Data Rate Analysis for Equal Number of Sidelobe Levels and Phase Constellations	43
3.2.2	Bit Error Rate Analysis for Same Overall Throughput	47
3.3	Remarks . . . . .	50
4	CHANCE CONSTRAINED BEAMFORMING FOR JRC SYSTEMS . .	51
4.1	Joint Radar-Communication System . . . . .	51
4.1.1	Beamformer Design . . . . .	52
4.1.2	Signaling Strategy . . . . .	53
4.2	Chance Constrained Beamforming Design for JRC System .	54

	Page
4.2.1	54
4.2.2	56
4.3	58
4.4	60
5	61
5.1	63
5.1.1	63
5.1.2	66
5.1.3	67
5.2	67
5.3	71
6	72
6.1	74
6.2	76
6.2.1	78
6.2.2	82
6.3	84
6.4	86
6.4.1	86
6.4.2	87
6.4.3	91
6.4.4	94
6.4.5	97
6.4.6	98
6.5	99
7	100

	Page
7.1 System Model . . . . .	100
7.1.1 Radar Subsystem . . . . .	100
7.1.2 Communication Subsystem . . . . .	102
7.2 Optimal Power Allocation for Distributed JRC MIMO System	103
7.2.1 Radar-Only Operation . . . . .	103
7.2.2 Communication-Only Operation . . . . .	104
7.2.3 Joint Radar-Communication System . . . . .	105
7.3 Information Embedding . . . . .	106
7.4 Simulation Results . . . . .	107
7.5 Remarks . . . . .	110
8 FUTURE DIRECTIONS . . . . .	111
REFERENCES CITED . . . . .	113
APPENDICES . . . . .	125
A RADAR TERMINOLOGY . . . . .	125
B SOFTWARE IMPLEMENTATION . . . . .	130

**LIST OF ABBREVIATIONS**

<b>Abbreviation</b>	<b>Explanation</b>
AM	Amplitude Modulation
ASK	Amplitude Shift Keying
BER	Bit Error Rate
CRB	Cramer-Rao Bound
CDF	Cumulative Distribution Function
CU	Communication Unit
DOFs	Degrees-of-Freedom
JRC	Joint Radar-Communications
MI	Mutual Information
MILP	Mixed-Integer Linear Program
MIMO	Multiple-Input Multiple-Output
OFDM	Orthogonal Frequency Division Multiplexing
OFDMA	Orthogonal Frequency Division Multiple Access
PDF	Probability Density Function
PSK	Phase Shift Keying
QAM	Quadrature Amplitude Modulation
QPSK	Quadrature Amplitude Shift Keying
RCS	Radar Cross-section
SNR	Signal-to-Noise Ratio
ULA	Uniform Linear Array

## LIST OF TABLES

Table	Page
2.1 Achieved mutual information for the single antenna-based JRC system	31
3.1 Comparison of beamforming-based JRC systems . . . . .	42
6.1 Transmit antenna selection for individual beamformers . . . . .	81
6.2 Transmit antenna selection for grouped beamformers by employing group sparsity . . . . .	84
7.1 Power allocation example for distributed JRC system . . . . .	109

## LIST OF FIGURES

Figure	Page
1.1 Illustration of three different types of radar-communication spectrum sharing systems: (a) passive radar, (b) coexistence, (c) JRC system. . . . .	2
1.2 Illustration of three different types of JRC systems: (a) single transmit antenna-based JRC, (b) transmit array-based JRC, (c) distributed JRC.	3
1.3 Illustrative example of shared sub-carrier allocation for JRC system [54].	5
1.4 Illustrative example of exclusive sub-carrier allocation for JRC system [51]. . . . .	6
2.1 JRC system consisting of a dual-purpose transmitter performing radar and communication tasks simultaneously. . . . .	21
2.2 Subcarrier allocation and power distribution strategy for a JRC system. Two communication users are shown in the example. . . . .	22
2.3 Channel conditions for radar and communications. . . . .	29
2.4 Power allocation and subcarrier distribution for radar-centric design. .	29
2.5 Power allocation and subcarrier distribution for cooperative design ( $\gamma_{\text{flex}} = 0.95$ ). . . . .	30
3.1 Transmit array-based JRC system. . . . .	35
3.2 The proposed JRC strategy using QAM-based sidelobe modulation. . .	36
3.3 The proposed QAM-based JRC approach using QAM-based sidelobe modulation . . . . .	37
3.4 Focused beampattern synthesis for the existing and the proposed JRC approaches . . . . .	44
3.5 Focused beampattern synthesis for the existing and the proposed JRC approaches . . . . .	46
3.6 Comparative analysis of the communication throughput of the existing and the proposed JRC approaches . . . . .	47
3.7 Comparative analysis of the bit error rate achieved by the existing and the proposed JRC approaches . . . . .	49
4.1 Beamforming patterns for different desired probabilities $\eta$ ( $M = 25, \theta_{\text{rad}} = 0^\circ, \theta_1 = 20^\circ, \theta_2 = 40^\circ, \Delta_u = 0.1, \alpha_{\text{rad}} = 0.1, \sigma_u = 1$ ). . . . .	58

Figure	Page
4.2 Beamforming patterns for different channel scale parameters $\sigma_u$ ( $M = 25, \theta_{\text{rad}} = 0^\circ, \theta_1 = 20^\circ, \theta_2 = 40^\circ, \Delta_u = 0.1, \alpha_{\text{rad}} = 0.1, \eta = 0.9$ ) . . . . .	60
5.1 The proposed JRC strategy. . . . .	64
5.2 Example beampatterns using the proposed approach (ULA with $M = 20, U = 2$ at $40^\circ$ and $50^\circ$ ). . . . .	68
5.3 Range estimation and symbol error rate performance for the proposed technique. . . . .	70
6.1 Basic principle of the joint radar-communication system. . . . .	74
6.2 The proposed antenna selection strategy for joint radar-communication system. . . . .	77
6.3 Focused beampatterns synthesis using the optimal antenna selection strategy in Algorithm I ( $M = 40, \Theta_{\text{rad}} = 0^\circ, \Theta_{\text{trans}} = [-6^\circ 0^\circ] \cup (0^\circ 6^\circ], \Theta_{\text{sl}} = [-90^\circ - 6^\circ] \cup (6^\circ 90^\circ], G_{\text{rad}} = 1, \gamma_{\text{tol}} = 10^{-3}, \varepsilon_{\text{sl}} = 0.1$ (20 dB below $G_{\text{rad}}$ ): (a) Transmit power distribution pattern, (b) Total number of selected antennas with respect to the number of iterations, (c) Spatial antenna selection profile for each iteration. . . . .	88
6.4 Flat-top beampattern synthesis using the antenna selection strategy in Algorithm I ( $M = 40, \Theta_{\text{rad}} = [-7^\circ 7^\circ], \Theta_{\text{trans}} = [-17^\circ - 7^\circ] \cup (7^\circ 17^\circ], \Theta_{\text{sl}} = [-90^\circ - 17^\circ] \cup (17^\circ 90^\circ], G_{\text{rad}} = 1, \gamma_{\text{tol}} = 10^{-3}, \varepsilon_{\text{sl}} = 0.1$ (20 dB below $G_{\text{rad}}$ ): (a) Transmit power distribution pattern, (b) Total number of selected antennas with respect to the number of iterations, (c) Spatial antenna selection profile with increasing number of iterations . . . . .	89
6.5 Focused beampattern synthesis using the antenna selection strategy in Algorithm I for different communication objectives ( $M = 40, \Theta_{\text{rad}} = 0^\circ, \Theta_{\text{trans}} = [-6^\circ 0^\circ] \cup (0^\circ 6^\circ], \Theta_{\text{sl}} = [-90^\circ - 6^\circ] \cup (6^\circ 90^\circ], G_{\text{rad}} = 1, \gamma_{\text{tol}} = 10^{-3}, \varepsilon_{\text{sl}} = 0.1$ (20 dB below $G_{\text{rad}}$ ) : (a) Transmit power distribution pattern, (b) Final antenna selection profile for each beampattern, (c) Overall antenna selection profile containing the antennas selected at least once by any of the beamforming weight vectors. . . . .	90
6.6 Flat-top beampattern synthesis using the antenna selection strategy in Algorithm I for different communication objectives ( $M = 40, \Theta_{\text{rad}} = [-7^\circ 7^\circ], \Theta_{\text{trans}} = [-17^\circ - 7^\circ] \cup (7^\circ 17^\circ], \Theta_{\text{sl}} = [-90^\circ - 17^\circ] \cup (17^\circ 90^\circ], G_{\text{rad}} = 1, \gamma_{\text{tol}} = 10^{-3}, \varepsilon_{\text{sl}} = 0.1$ (20 dB below $G_{\text{rad}}$ ): (a) Transmit power distribution pattern, (b) Final antenna selection profile for each beampattern, (c) Overall antenna selection profile containing the antennas selected at least once by any of the beamforming weight vectors. . . . .	92

Figure	Page
6.7 Focused beampattern synthesis by employing the group-sparsity for antenna selection Algorithm II ( $M = 40, \Theta_{\text{rad}} = 0^\circ, \Theta_{\text{trans}} = [-6^\circ 0^\circ] \cup (0^\circ 6^\circ], \Theta_{\text{sl}} = [-90^\circ - 6^\circ] \cup (6^\circ 90^\circ], G_{\text{rad}} = 1, \gamma_{\text{tol}} = 10^{-3}, \varepsilon_{\text{sl}} = 0.1$ (20 dB below $G_{\text{rad}}$ ): (a) Transmit power distribution pattern, (b) Number of selected antennas with increasing number of iterations, (c) Spatial antenna selection profile for the first 5 iterations. . . . .	93
6.8 Flat-top beampattern synthesis by employing the group-sparsity based antenna selection Algorithm II ( $M = 40, \Theta_{\text{rad}} = [-7^\circ 7^\circ], \Theta_{\text{trans}} = [-17^\circ - 7^\circ] \cup (7^\circ 17^\circ], \Theta_{\text{sl}} = [-90^\circ - 17^\circ] \cup (17^\circ 90^\circ], G_{\text{rad}} = 1, \gamma_{\text{tol}} = 10^{-3}, \varepsilon_{\text{sl}} = 0.1$ (20 dB below $G_{\text{rad}}$ ): (a) Transmit power distribution pattern, (b) Number of selected antennas with increasing number of iterations, (c) Spatial antenna selection profile for the first 5 iterations. . . . .	95
6.9 Flat-top beampattern synthesis by employing the group-sparsity based antenna selection Algorithm II using QAM-based sidelobe modulation ( $M = 40, \Theta_{\text{rad}} = [-7^\circ 7^\circ], \Theta_{\text{trans}} = [-17^\circ - 7^\circ] \cup (7^\circ 17^\circ], \Theta_{\text{sl}} = [-90^\circ - 17^\circ] \cup (17^\circ 90^\circ], G_{\text{rad}} = 1, \gamma_{\text{tol}} = 10^{-3}, \varepsilon_{\text{sl}} = 0.1$ (20 dB below $G_{\text{rad}}$ ): (a) Transmit power distribution pattern for the first four beampatterns, (b) Number of selected antennas with increasing number of iterations, (c) Spatial antenna selection profile for the first 5 iterations. . . . .	96
6.10 Computation time required to compute the beamforming weight vectors using the proposed approaches. . . . .	97
6.11 Relative frequency of antenna utilization for randomly generated simulation events. . . . .	98
7.1 Distributed JRC MIMO system. . . . .	101
7.2 Simulation layout for distributed JRC MIMO system. . . . .	108

# CHAPTER 1

## INTRODUCTION

### 1.1 Overview

Spectrum sharing has recently gained a significant research attention due to the ongoing congestion of wireless spectrum caused by the broadband wireless communications and ever-increasing deployment of new applications that consume the same spectral resources [1–6]. Modern wireless communication systems require immense expansion of existing spectral allocations in order to achieve high data rates to ensure the success of future generations of wireless systems. Moreover, new technical advancements and emerging applications which bring various advantages to the end users require new allocations of frequency resources [7]. In this context, great efforts have been invested in the field of cognitive radios to improve the spectral efficiency so as to effectively manage the usage of electromagnetic spectrum [8]. Recently, coexistence of multiple platforms within the same frequency bands has been found effective to mitigate the spectral congestion by simultaneously sharing the same spectral resources for multiple applications.

Although different terminologies have been employed in the literature for a variety of concurrent radar and communication operations within same spectral bands, we broadly classify these systems into three different types. The first type of such systems employs a passive radar that exploits the waveforms transmitted by a communication system for radar operation. Although the passive radar does not have a control on the transmitted waveform due to the non-cooperative illuminating sources, it enjoys the inherent secrecy attributed to the receive-only nature of the radar and the multi-static observations from rich sources of opportunity [9–11]. The second type of spectrum sharing system employs coexisting radar and communication operations where both radar and communication subsystems cooperate with each other





The objective of resource allocation for such a system is to optimize the transmit energy of the dual-purpose waveform based on the propagation channels of both radar and CUs [51, 54]. The second type of JRC system employs a transmit antenna array that directs a high-energy beam towards the surveillance region of the radar, whereas the CUs are assumed to be located in the sidelobe region [26, 29, 46]. Such system are more flexible than the single transmitter based systems as they are capable to transmit different signals in different directions due to their spatial multiplexing capabilities. The third type of JRC system consists of a distributed JRC network [52, 55] which enjoys spatial diversity for radar and communications. The information transmission can be done by waveform diversity and receiver beamforming in such systems.

## 1.2 Notations

Lower-case and upper-case bold characters are used to respectively denote vectors and matrices.  $(\cdot)^T$ ,  $(\cdot)^*$ , and  $(\cdot)^H$  respectively represent the transpose, conjugate, and the Hermitian transpose operators. Moreover,  $|\cdot|$ ,  $|\cdot|_0$ ,  $|\cdot|_1$ , and  $|\cdot|_2$  denote the absolute value,  $\ell_0$ -,  $\ell_1$ - and  $\ell_2$ -norms, respectively. The notation  $\mathbf{1}_{L \times 1}$  represents the  $L$ -length column vector of all ones, whereas  $\mathbf{I}_L$ ,  $\mathbf{0}_L$ , and  $\mathbf{1}_L$  respectively represent the identity matrix, matrix of all zeros, and matrix of all ones, each having a dimension of  $L \times L$ .  $\text{diag}(\mathbf{x})$  denotes a diagonal matrix whose diagonal elements are contained by the vector  $\mathbf{x}$ , whereas  $\det(\cdot)$  shows the determinant of a matrix. Furthermore,  $\text{tr}(\cdot)$  denotes the matrix trace, and  $\mathbb{E}[\cdot]$  represents the expectation operator. The notation  $\odot$  shows the Hadamard product,  $*$  is the convolution operator, and  $j = \sqrt{-1}$  represents the imaginary number. Finally,  $\mathbf{h}(x)$  denotes the differential entropy of the random variable  $x$ ,  $\mathbf{I}(x; y)$  denotes the mutual information (MI) between random variables  $x$  and  $y$ , whereas  $\log(\cdot)$  denotes base-2 logarithm.

## 1.3 Single Transmit Antenna-based JRC System

In such a system, a single dual-purpose transmit antenna is responsible to transmit OFDM waveforms that are shared for both radar and communication purpose. A

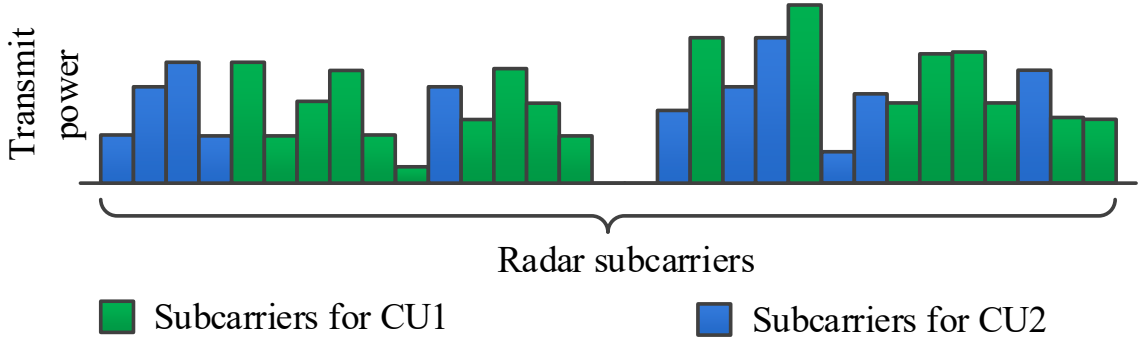


Figure 1.3. Illustrative example of shared sub-carrier allocation for JRC system [54].

single radar target and two CUs are considered in the vicinity of the JRC system. Both communication channel gains and radar target responses are assumed to vary with frequency. Depending on the desired mode of operation, the OFDM subcarriers can either be shared between radar and communications [54] (as in Fig. 1.3) or radar and communications can use their separate subcarriers [51] (as in Fig. 1.4).

### 1.3.1 Signal Model

Let the transmit dual-purpose waveform consist of an  $L$ -symbol OFDM signal  $\mathbf{x}$  such that  $K \leq L$  subcarriers are exploited. The transmit waveform is represented as:

$$\mathbf{x} = \mathbf{F}_{\text{IDFT}}\mathbf{s}, \quad (1.1)$$

where  $\mathbf{F}_{\text{IDFT}}$  is the  $L \times K$  inverse discrete Fourier transform (IDFT) matrix whose columns correspond to unit power OFDM subcarriers of unique frequencies, and  $\mathbf{s} = [s_1, \dots, s_K]^T$  is a  $K \times 1$  vector whose elements correspond to the amplitudes and phases of the respective OFDM waveforms. Each subcarrier can use a digital modulation scheme for information transfer such as quadratic phase shift keying (QPSK). The information is carried in the phase of each subcarrier, such that the phase of  $s_k$  represents the desired phase for the  $k$ th subcarrier.

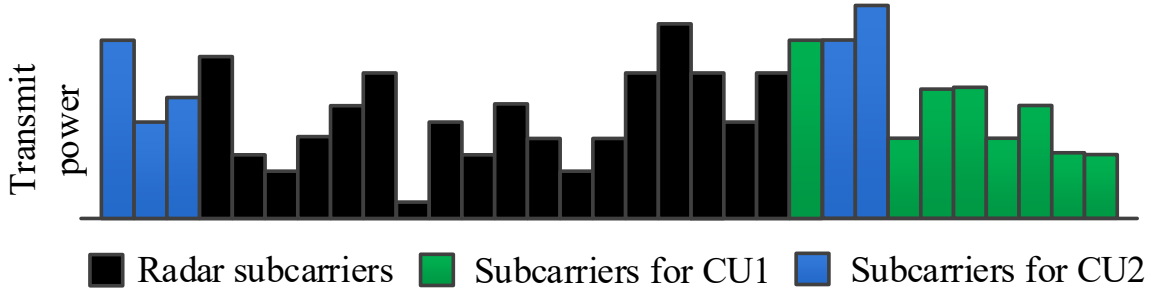


Figure 1.4. Illustrative example of exclusive sub-carrier allocation for JRC system [51].

### 1.3.2 Radar Subsystem

The transmitted OFDM signal is reflected by the target having a frequency-sensitive response and reaches the radar receiver. Denote  $h_k$  as the radar channel coefficients, including the radar cross-section (RCS) and the path loss, corresponding to the  $K$  subcarriers. The target response to all the  $K$  subcarriers can be expressed in vectorized form as  $\mathbf{h} = [h_1, \dots, h_K]^T$ . The corresponding radar channel impulse response is given by  $\tilde{\mathbf{h}} = \mathbf{F}_{\text{IDFT}}\mathbf{h}$ . Therefore, the target-reflected signal received at the radar can be represented as follows:

$$\tilde{\mathbf{y}}_{\text{rad}} = \tilde{\mathbf{h}} * \mathbf{x} + \tilde{\mathbf{n}}, \quad (1.2)$$

where  $\tilde{\mathbf{n}}$  is the zero-mean complex additive white Gaussian noise vector. All  $K$  subcarriers of the received signal can be recovered by discrete Fourier transform (DFT) of Equation (1.2). The received radar signal takes the following form [54, 56]:

$$\mathbf{y}_{\text{rad}} = \mathbf{H}\mathbf{s} + \mathbf{n}, \quad (1.3)$$

where  $\mathbf{H} = \text{diag}(\mathbf{h})$ , and  $\mathbf{n} \sim \mathcal{CN}(\mathbf{0}_K, \mathbf{\Sigma}_n)$  is the  $K \times 1$  vector containing the DFT of  $\tilde{\mathbf{n}}$  where  $\mathbf{\Sigma}_n = \text{diag}\{\sigma_{n,1}^2, \dots, \sigma_{n,K}^2\}$  and  $\sigma_{n,k}^2$  is the noise power of the  $k$ th subcarrier.

### 1.3.3 Communication Subsystem

Similar to Equation (1.3) for the radar subsystem, the OFDM signal reaching the  $u$ th CU is expressed as:

$$\mathbf{y}_{\text{com},u} = \mathbf{G}_u \mathbf{s} + \mathbf{m}_u, \quad u = 1, \dots, U, \quad (1.4)$$

where  $\mathbf{G}_u = \text{diag}(\mathbf{g}_u)$  with  $\mathbf{g}_u = [g_{u,1}, \dots, g_{u,K}]^T$  denoting the channel coefficients of the  $K$  subcarriers associated with the  $u$ th CU. In addition, the noise term  $\mathbf{m}_u \sim \mathcal{CN}(\mathbf{0}_K, \Sigma_{\mathbf{m}_u})$  is independent of  $\mathbf{G}_u$  where  $\Sigma_{\mathbf{m}_u} = \text{diag}\{\sigma_{\mathbf{m}_u,1}^2, \dots, \sigma_{\mathbf{m}_u,K}^2\}$ .

In Chapter 2, we will further discuss these systems in detail.

## 1.4 Beamforming-based JRC System

In beamforming-based JRC systems, a sensor array is exploited to steer radar and communication signals in different directions. The waveforms for both radar and communication operations are transmitted from the same physical antenna array. In this case, communication is considered to be the secondary objective of the JRC system and is enabled by embedding information in the radar waveforms such that the primary radar operation is not compromised.

Fig. 1.2(b) shows the basic principle of beamforming-based JRC system. The notable techniques in this research direction include the sidelobe control methods based on amplitude modulation (AM) [27], multi-waveform amplitude shift keying (ASK) [28–30], and phase shift keying (PSK) [31–33]. The sidelobe AM method [27] exploits multiple beamforming weight vectors corresponding to different sidelobe levels at the CUs located in the sidelobe region of radar. Each sidelobe level is mapped to a unique communication symbol. In the multi-waveform ASK-based method [28], multiple orthogonal radar waveforms are employed such that each waveform is transmitted by one of the two beamformers implementing two different sidelobe levels. The CU decodes the transmitted information by matched filtering the received waveform and extracting the sidelobe level information.

Although the aforementioned ASK-based method exploits waveform diversity, only two sidelobe levels are utilized. The method in [30] increases the effective signal-to-noise ratio (SNR) at the CUs by using only one beamforming weight vector corresponding to the maximum allowable sidelobe level. Unfortunately, all the ASK-based methods discussed above can only broadcast the same communication information to all the CUs.

In PSK-based JRC methods [31–33], information embedding is achieved by a dictionary of beamforming weight vectors having the same beampattern but different phase response towards the CUs. The CUs detect the corresponding phase symbols embedded in the received radar waveforms to determine the transmitted information either by coherent demodulation or with the help of a reference radar waveform transmitted through a reference beamforming weight vector. However, the PSK-based method cannot exploit the flexibility of having different sidelobe levels.

#### 1.4.1 Signal Model

Consider a JRC system equipped with an  $M$ -element transmit antenna array of an arbitrary configuration. Let  $P$  denote the total power transmitted by the antenna array during each radar pulse, and  $\{\psi_1(t), \psi_2(t), \dots, \psi_{\hat{K}}(t)\}$  be the  $\hat{K}$  possible radar waveforms orthogonal to each other such that:

$$\frac{1}{T} \int_0^T \psi_{k_1}(t) \psi_{k_2}(t) dt = \delta(k_1 - k_2), \quad k_1, k_2 = 1, \dots, \hat{K}, \quad (1.5)$$

where  $t$  is the fast time,  $T$  is the time duration of each radar pulse,  $k_1$  and  $k_2$  are positive integers, and  $\delta(\cdot)$  is the Kronecker delta function.

The objective of existing sidelobe control-based JRC schemes is to send information symbols to the CUs located in the sidelobe region without introducing perturbation to the primary radar operation [26–35]. This implies that the average transmit power of the radar waveform must not vary during each transmitted pulse. In order to realize this objective, ASK-based schemes exploit different beamforming vectors to transmit different sidelobe levels in the directions of CUs while keeping the radar's main beam at a constant amplitude. On the other hand, PSK-based schemes rely on

the transmission of different phases towards the CUs during each radar pulse such that the amplitude levels towards the CUs and the radar's main beam are not perturbed.

### 1.4.2 Beamforming Weight Vector Design

The following optimization can be used to synthesize the beamforming weight vectors for JRC schemes [26, 29–33]:

$$\begin{aligned} & \min_{\mathbf{u}_n} \max_{\theta_r} |e^{j\varphi(\theta_r)} - \mathbf{u}_n^H \mathbf{a}(\theta_r)|, \quad \theta_r \in \Theta_{\text{rad}}, \\ & \text{subject to } |\mathbf{u}_n^H \mathbf{a}(\theta_{\text{sl}})| \leq \varepsilon_{\text{sl}}, \quad \theta_{\text{sl}} \in \bar{\Theta}, \\ & \mathbf{u}_n^H \mathbf{a}(\theta_u) = \Delta_n, \quad 1 \leq n \leq N, 1 \leq u \leq U. \end{aligned} \tag{1.6}$$

Here,  $\Theta_{\text{rad}}$  is the set of angles at which the radar main beam (main lobe) operates,  $\bar{\Theta}$  is the complement set of  $\Theta_{\text{rad}}$  representing the sidelobe region,  $\mathbf{a}(\theta)$  is the response vector of the transmitting antenna array at the angle  $\theta$ ,  $\varphi(\theta)$  is the phase profile of user's choice,  $\mathbf{u}_n$  is the desired beamforming vector which achieves the sidelobe level  $\Delta_n$  at all the CUs located at angles  $\theta_u \in \bar{\Theta}$ ,  $U$  is the total number of CUs located in the sidelobe region,  $\varepsilon_{\text{sl}}$  is the allowable sidelobe level of the radar,  $N$  denotes the total number of allowable sidelobe levels.

In the following, we summarize the sidelobe control-based JRC schemes [26–35].

### 1.4.3 ASK-based Schemes

The information embedding in the radar waveform by exploiting ASK-based techniques [26–30] can be realized by projecting varying sidelobe levels towards the directions of CUs located in the sidelobe region of the radar. These sidelobe levels change from one pulse to other but remain constant during the course of each radar pulse. We can generate  $N$  beamforming weight vectors by using the optimization in Eq. (1.6) such that each vector results in a unique sidelobe level  $\Delta_n$  in the directions of CUs. If one radar waveform is exploited, the signal transmitted from the JRC

platform during one radar pulse using one of the  $N$  available beampatterns can be expressed as follows [26, 27]:

$$\mathbf{s}(t, \tau) = \sqrt{P} \sum_{n=1}^N b_n(\tau) \mathbf{u}_n^* \psi_k(t), \quad (1.7)$$

where  $\tau$  is the slow time (i.e., pulse index)<sup>1</sup>,  $\psi_k(t)$  is the arbitrary waveform selected from  $\hat{K}$  possible radar waveforms,  $b_n(\tau)$  is the binary selection coefficient such that  $\sum_{n=1}^N b_n(\tau) = 1$  for each radar pulse,  $P$  is the transmit power of the radar.

Multiple orthogonal radar waveforms can be exploited to improve the detection performance of radar and increase the information rate of communication [26, 28–30]. In [28, 29],  $K(\leq \hat{K})$  orthogonal radar waveforms are utilized and the transmitted signal vector for this scheme is given as:

$$\mathbf{s}(t, \tau) = \sqrt{\frac{P}{K}} \sum_{k=1}^K (b_k(\tau) \mathbf{u}_{\text{low}}^* + (1 - b_k(\tau)) \mathbf{u}_{\text{high}}^*) \psi_k(t), \quad (1.8)$$

where only two beamforming weight vectors  $\mathbf{u}_{\text{low}}$  and  $\mathbf{u}_{\text{high}}$  are exploited which, respectively, result in the sidelobe levels of  $\Delta_{\text{low}}$  and  $\Delta_{\text{high}}$  ( $\Delta_{\text{low}} < \Delta_{\text{high}}$ ) at all the CUs. The value of each coefficient  $b_k(\tau)$  is either 0 or 1 during each radar pulse. These coefficients select the desired beamforming weight vector for each of the  $K$  transmitted waveforms, thereby carrying one bit of information for each of these waveforms. During each radar pulse, a radar waveform is transmitted with an amplitude of either  $\Delta_{\text{low}} \sqrt{P/K}$  or  $\Delta_{\text{high}} \sqrt{P/K}$  towards each CU for the detection of embedded information. This means that the same communication symbols are broadcast to all the receivers. Obviously, it is not possible to transmit different information streams to different CUs located at different directions.

Another ASK-based JRC technique employs only one beamforming weight vector, which corresponds to the highest allowable sidelobe level at all the CUs resulting in highest possible SNR for the CUs. During each radar pulse,  $\hat{K} - 1$  bits are transmitted such that the coefficients corresponding to  $K(\leq \hat{K} - 1)$  bits are equal to 1 and the

<sup>1</sup>See Section A of Appendix A for detail.

remaining  $\hat{K} - K - 1$  bits are equal to 0. This is achieved by transmitting  $\hat{K}$  distinct orthogonal waveforms. The transmitted signal is given as [30]:

$$\mathbf{s}(t, \tau) = \sqrt{\frac{P}{K}} \sum_{k=1}^{\hat{K}-1} b_k(\tau) \mathbf{u}_{\text{high}}^* \psi_k(t) + \sqrt{P} \prod_{k=1}^{\hat{K}-1} (1 - b_k(\tau)) \mathbf{u}_{\text{high}}^* \psi_{\hat{K}}(t). \quad (1.9)$$

Each coefficient  $b_k(\tau)$  for  $1 \leq k \leq \hat{K} - 1$  is either 0 or 1 such that only  $K$  coefficients are equal to 1 and the rest of them are equal to 0. The second term in the above equation expresses the case when all zeros are transmitted (i.e., all coefficients  $b_k(\tau)$  for  $1 \leq k \leq \hat{K} - 1$  are equal to 0) using the reference orthogonal waveform  $\psi_{\hat{K}}(t)$ . In this scheme same information is broadcast to all the CUs because the transmission is formulated to achieve same sidelobe level at each CU.

#### 1.4.4 PSK-based Schemes

The fundamental principle underlying PSK-based JRC is to embed communication information by controlling the phase of the signals transmitted towards the CUs while keeping the amplitude levels constant in the direction of communication [26, 31–33]. This is achieved by exploiting the radiation pattern invariance property of uniform linear arrays (ULAs) which states that, for each of the possible transmit radiation patterns, there exists a set of beamforming weight vectors  $\mathbf{U} = [\mathbf{u}_1, \mathbf{u}_2, \dots, \mathbf{u}_{2^{M-1}}]$  such that each column of  $\mathbf{U}$  provides exactly the same radiation pattern but exhibits different phase profile. The complete set  $\mathbf{U}$  can be determined if any of the beamforming vectors presented in  $\mathbf{U}$  is known [57]. The transmitted signal for PSK-based JRC can be expressed as [26, 31, 32]:

$$\mathbf{s}(t, \tau) = \sqrt{\frac{P}{K}} \sum_{k=1}^K \mathbf{U}^* \mathbf{b}_k(\tau) \psi_k(t), \quad K \leq \hat{K}, \quad (1.10)$$

where  $\mathbf{b}_k(\tau)$  is a binary vector of size  $(2^{M-1} \times 1)$  such that all of its elements are zero except one element which is equal to 1. The vector  $\mathbf{b}_k(\tau)$  is responsible to select the desired beamforming vector  $\mathbf{u}_k$  from  $\mathbf{U}$ . Here,  $\mathbf{u}_1$  is calculated by solving the optimization problem in Eq. (1.6) and rest of the beamforming vectors in  $\mathbf{U}$  are calculated using the method developed in [57]. If coherent communication is

considered, each radar pulse consists of  $K$  orthogonal waveforms transmitted towards CUs with the embedded phase information given as:

$$\phi_k = \angle \{ \mathbf{u}_k^H \mathbf{a}(\theta_u) \}, \quad 1 \leq k \leq K, \quad (1.11)$$

where  $\angle\{\cdot\}$  denotes the angle of a complex number. For non-coherent communications, we select  $\psi_1(t)$  as the reference waveform transmitted using the reference beamforming weight vector  $\mathbf{u}_1$  by setting  $\mathbf{b}_1(\tau) = [1, \mathbf{0}_{2^{M-1}-1}]^T$ , where  $(\cdot)^T$  is the transpose operator, and  $\mathbf{0}_{2^{M-1}-1}$  is a row vector of all zeros having the length of  $2^{M-1} - 1$ . In this case, each radar pulse projects the set of  $(K - 1)$  phase rotations towards the CUs. The phase  $\phi_k$  corresponding to the  $k$ -th waveform can be calculated as:

$$\phi_k = \angle \left\{ \frac{\mathbf{u}_k^H \mathbf{a}(\theta_u)}{\mathbf{u}_1^H \mathbf{a}(\theta_u)} \right\}, \quad 2 \leq k \leq K. \quad (1.12)$$

## 1.5 Research Contributions

We primarily focus on spectrum sharing strategies based on JRC transmission, i.e. considering the waveform transmission systems which satisfy the objectives of both radar and communication subsystems simultaneously. Important contributions of our proposed research directions as follows:

### 1.5.1 Subcarrier Allocation and Power Optimization for Single Transmit Antenna-based JRC Systems

We propose a novel JRC system which exploits multiple subcarriers for performing radar and communication operations simultaneously. A dual-purpose transmit antenna is exploited to optimize the transmit power of different subcarriers to fulfill the radar objectives. These subcarriers used by the radar are also allocated to different CUs to achieve the communications objectives. We aim to optimize the JRC system based on the mutual information between the frequency-dependent target response and the received waveform. The communication performance is optimized by

allocating the radar subcarriers to different CUs by using MI maximization as the criterion. The work in this direction is reported in Chapter 2.

### **1.5.2 Throughput Enhancement for Beamforming-based JRC Systems**

We propose a novel JRC strategy to embed QAM-based communication information in the radar waveforms by exploiting sidelobe control and waveform diversity. The proposed information embedding technique can support multiple CUs located in the sidelobe region of the radar. In addition to the information broadcasting, the developed approach enables multi-user access by allowing simultaneous transmission of distinct information streams to the CUs located in different directions. We show that the proposed technique ensures a significant data rate enhancement compared to the existing techniques. Moreover, the developed JRC strategy generalizes the mathematical framework of the existing sidelobe control-based information embedding techniques. This research work is extensively discussed in Chapter 3.

### **1.5.3 Chance Constrained Beamforming-based JRC Systems**

We present an intelligent sensor array-based JRC system which exploits chance constrained programming to develop a robust beamforming design. Probabilistic chance constraints are introduced for the communication operation where the communication objectives are achieved with a desired success rate in the presence of communication channel uncertainties. The chance constraint optimization is then relaxed to form a deterministic and convex problem by employing the statistical profile of the communication channels. This research work is discussed in Chapter 4.

### **1.5.4 Power Allocation for Beamforming-based JRC Systems**

We propose a novel JRC strategy by exploiting directional power control and waveform diversity. The proposed technique ensures the highest possible magnitude of the radar main beam, resulting in an improved SNR ratio for the radar operation. This

maximization objective is achieved while considering the pre-allocated or adjustable transmit energy requirement for radar and communication operations. The secondary communication objective enabling multi-user access is realized by transmitting distinct amplitude levels and phases towards different communication receivers located in the sidelobe region of the radar. As an example, power allocation for different subcarriers projected towards the radar main beam and the communication receivers is discussed by considering the frequency response of target returns. This research work is presented in Chapter 5.

### 1.5.5 Sensor Selection for Beamforming-based JRC Systems

In a system with more sensors than the number of radio frequency chains, optimal sensor selection is anticipated as an attractive means to achieve superior performance with a low hardware cost because of the ever-decreasing cost of the sensor deployment compared to the radio frequency chains and processors. We address optimal sensor selection for adaptive beamforming-based JRC systems by exploiting a constrained re-weighted  $\ell_1$  norm minimization. Such minimization was originally proposed for sparsity-based regression problems. It is observed that the re-weighted  $\ell_1$  minimization approaches to  $\ell_0$  norm minimization by solving an iterative convex problem. This research work is included in Chapter 5.

### 1.5.6 Distributed JRC Systems

A distributed JRC system consists of widely separated transmitters and receivers that perform the tasks of both radar and communication subsystems. We present a novel distributed JRC MIMO system capable of simultaneously performing radar and communication tasks. The radar objective is to achieve the desired target localization performance whereas the communication objective is to optimize the overall data rate. The distributed JRC MIMO system performs both objectives by optimizing the power allocation of the different transmitters in the JRC system. A dictionary of radar waveforms is used at each transmitter and the communication information

is embedded in the radar waveform by exploiting waveform diversity. The proposed strategy can serve multiple CUs located in the vicinity of the distributed JRC MIMO system. We discuss this research work in Chapter 7.

In the following chapters, we will discuss these research directions in detail. Mathematical analysis and simulation results are provided to illustrate the performance of the proposed techniques.

## 1.6 Publications

During the dissertation research, the author has worked on three projects: (a) spectrum sharing strategies for JRC systems, (b) spatial and temporal spectrum sensing, and (c) target parameter estimation for over-the-horizon radar. Following is the comprehensive set of publications resulting from the Ph.D. research.

### Invention Disclosures

1. **A. Ahmed**, Y. D. Zhang, and B. Himed, “System and method for distributed dual-function radar-communication,” U.S. Non-Provisional Application No. 16/854,251; filed: April 21, 2020.

### Book Chapters

1. **A. Ahmed** and Y. D. Zhang, “Resource allocation for joint radar-communications,” in K. V. Mishra, B. S. M. R. Rao, B. Ottersten, and L. Swindlehurst (eds.), *Signal Processing for Joint Radar Communications*, Wiley, 2021.

### Journal Publications

1. **A. Ahmed** and Y. D. Zhang, “Distributed Joint Radar-Communication System,” under preparation.

2. **A. Ahmed** and Y. D. Zhang “Non-redundant sparse array designs,” submitted to *IEEE Transactions on Signal Processing*.
3. **A. Ahmed**, Y. D. Zhang, and B. Himed, “Target altitude estimation in over-the-horizon radar,” submitted to *Signal Processing*.
4. **A. Ahmed**, Y. D. Zhang, and B. Himed “Joint target and ionosphere parameter estimation in over-the-horizon radar,” submitted to AFRL for public release.
5. **A. Ahmed**, S. Zhang, and Y. D. Zhang, “Antenna selection strategy for transmit beamforming-based joint radar-communication system,” *Digital Signal Processing*, vol. 105, pp. 102768, Oct. 2020.
6. **A. Ahmed**, Y. D. Zhang, and Y. Gu, “Dual-function radar-communications using QAM-based sidelobe modulation,” *Digital Signal Processing*, vol. 82, pp. 166–174, Nov. 2018.

### Conference Publications

1. **A. Ahmed**, Y. D. Zhang, and B. Himed, “Doppler signature analysis of over-the-horizon radar signals with target altitude perturbation,” in Proc. IEEE Radar Conference, Atlanta, GA, May 2021.
2. **A. Ahmed** and Y. D. Zhang, “Radar-based dataset development for human activity recognition,” IEEE Signal Processing in Medicine and Biology Symposium, Philadelphia, PA, Dec. 2020.
3. **A. Ahmed** and Y. D. Zhang, “Non-redundant sparse array with flexible aperture,” Asilomar Conference on Signals, Systems, and Computers, Pacific Grove, CA, Nov. 2020.
4. **A. Ahmed**, Y. D. Zhang, and B. Himed, “Doppler signature separation of mixed O/X-mode over-the-horizon radar signals,” IEEE Radar Conference, Florence, Italy, Sept. 2020.

5. **A. Ahmed**, D. Silage, and Y. D. Zhang, "High-resolution target sensing using multi-frequency sparse array," IEEE Sensor Array and Multichannel Signal Processing Workshop, Hangzhou, China, June 2020.
6. S. Zhang, **A. Ahmed**, Y. D. Zhang, and S. Sun, "DOA estimation exploiting interpolated multi-frequency sparse array," IEEE Sensor Array and Multichannel Signal Processing Workshop, Hangzhou, China, June 2020.
7. **A. Ahmed**, D. Silage, and Y. D. Zhang, "Chance constrained beamforming for joint radar-communication systems," IEEE Sensor Array and Multichannel Signal Processing Workshop, Hangzhou, China, June 2020.
8. **A. Ahmed**, S. Zhang, and Y. D. Zhang, "Optimized sensor selection for joint radar-communication systems," IEEE International Conference on Acoustics, Speech, and Signal Processing, Barcelona, Spain, May 2020.
9. **A. Ahmed**, Y. D. Zhang, and B. Himed, "Doppler signature analysis of mixed O/X-mode signals in over-the-horizon radar," IEEE International Radar Conference, Rockville, MD, April-May 2020.
10. S. Zhang, **A. Ahmed**, and Y. D. Zhang, "Sparsity-based time-frequency analysis for automatic radar waveform recognition," IEEE International Radar Conference, Rockville, MD, April-May 2020.
11. **A. Ahmed**, S. Zhang, V. S. Amin, Y. D. Zhang, "Spectrum sharing strategy for radio frequency-based medical services," IEEE Signal Processing in Medicine and Biology Symposium, Philadelphia, PA, Dec. 2019.
12. **A. Ahmed**, Y. D. Zhang, A. Hassanien, B. Himed, "OFDM-based joint radar-communication system: optimal sub-carrier allocation and power distribution by exploiting mutual information," Asilomar Conference on Signals, Systems, and Computers, Pacific Grove, CA, Nov. 2019.

13. S. Zhang, **A. Ahmed**, Y. D. Zhang, "Robust source localization exploiting collaborative UAV network," Asilomar Conference on Signals, Systems, and Computers, Pacific Grove, CA, Nov. 2019.
14. **A. Ahmed**, S. Zhang, and Y. D. Zhang, "Multi-target motion parameter estimation exploiting collaborative UAV network," IEEE International Conference on Acoustics, Speech, and Signal Processing, Brighton, U.K., May 2019.
15. **A. Ahmed**, Y. D. Zhang, and J-K. Zhang, "Coprime array design with minimum lag redundancy," IEEE International Conference on Acoustics, Speech, and Signal Processing, Brighton, U.K., May 2019.
16. **A. Ahmed**, Y. D. Zhang, and B. Himed, "Distributed dual-function radar-communication MIMO system with optimized resource allocation," IEEE Radar Conference, Boston, MA, April 2019.
17. S. Zhang, **A. Ahmed**, and Y. D. Zhang "Sparsity-based collaborative sensing in a scalable wireless network", SPIE Defense + Commercial Sensing, Baltimore, MD, April 2019.
18. **A. Ahmed**, Y. Gu, D. Silage, and Y. D. Zhang, "Power-efficient multi-user dual-function radar-communications," IEEE International Workshop on Signal Processing Advances in Wireless Communications, Kalamata, Greece, June 2018.
19. **A. Ahmed**, Y. D. Zhang, and B. Himed, "Multi-user dual-function radar-communications exploiting sidelobe control and waveform diversity," IEEE Radar Conference, Oklahoma City, OK, April 2018.
20. **A. Ahmed**, Y. D. Zhang, and B. Himed, "Cumulant-based direction-of-arrival estimation using multiple co-prime frequencies," Asilomar Conference on Signals, Systems, and Computers, Pacific Grove, CA, Oct. 2017.

21. **A. Ahmed**, Y. D. Zhang, and B. Himed, "Effective nested array design for fourth-order cumulant-based DOA estimation," IEEE Radar Conference, Seattle, WA, May 2017. (**best student paper award - 3rd place**)

## CHAPTER 2

### SINGLE TRANSMIT ANTENNA-BASED JRC SYSTEMS

In this chapter, we present a novel joint radar-communication system which exploits OFDM waveforms for performing radar and communication operations simultaneously. A dual-purpose OFDM transmitter is exploited that optimizes the transmit power of different subcarriers to fulfill the radar objectives. These OFDM subcarriers used by the radar are also allocated to different CUs to achieve the communications objectives. All the subcarriers are primarily used by the radar and the secondary communication operation is enabled by embedding the information in OFDM waveforms. We discuss the optimal power distribution for the OFDM subcarriers and their allocation to different communication users based on MI maximization.

MI has been widely used as a performance metric for radar and communication systems [49,58–62]. This is because MI maximization is related to the maximization of the probability of detection in radar systems for a fixed probability of false alarm [58]. From a communications perspective, MI maximization is analogous to maximizing the channel capacity of the communication systems [60]. Since MI maximization is a convex optimization problem by definition, it becomes an attractive measure for JRC system design as compared to other optimization criteria, like probability of detection and Cramer-Rao bound, which generally yield non-convex problems [51].

In this chapter, we exploit the MI between the frequency-dependent target response and the transmit waveform in order to optimize the radar performance. Similarly, communication performance is optimized by allocating the radar subcarriers to different communication users by using MI maximization as the criterion. For the communication system, the problem has been discussed in terms of maximizing the overall MI as well as achieving the worst-case MI for each user. Two optimization

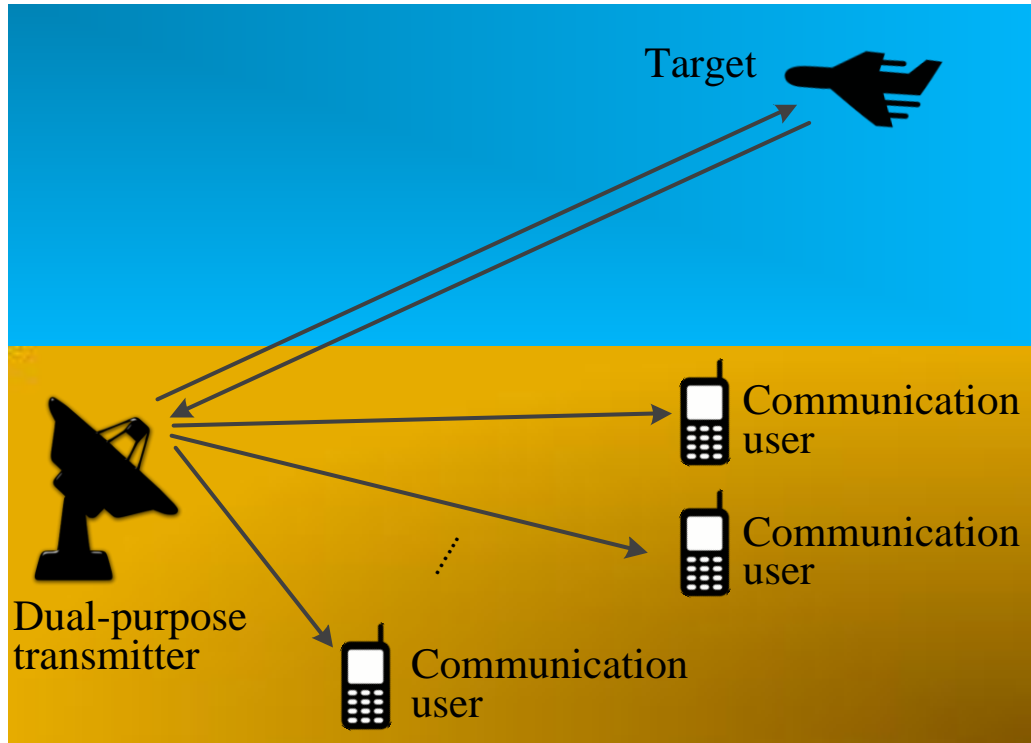


Figure 2.1. JRC system consisting of a dual-purpose transmitter performing radar and communication tasks simultaneously.

strategies are discussed and compared which optimize the two systems respectively using a radar-centric design and a cooperative design.

## 2.1 Signal Model

We consider a JRC system consisting of a single-antenna dual-purpose transmitter responsible for transmitting a dual-purpose radar-communication waveform in the presence of one radar target and  $U$  CUs. The target response and communication channels are assumed to vary with the frequency. The transmitter emits OFDM waveforms such that all the subcarriers are used by the radar, whereas these subcarriers are further allocated to different communication users so as to enable a secondary communication operation. Fig. 2.1 illustrates an example of such system whereas

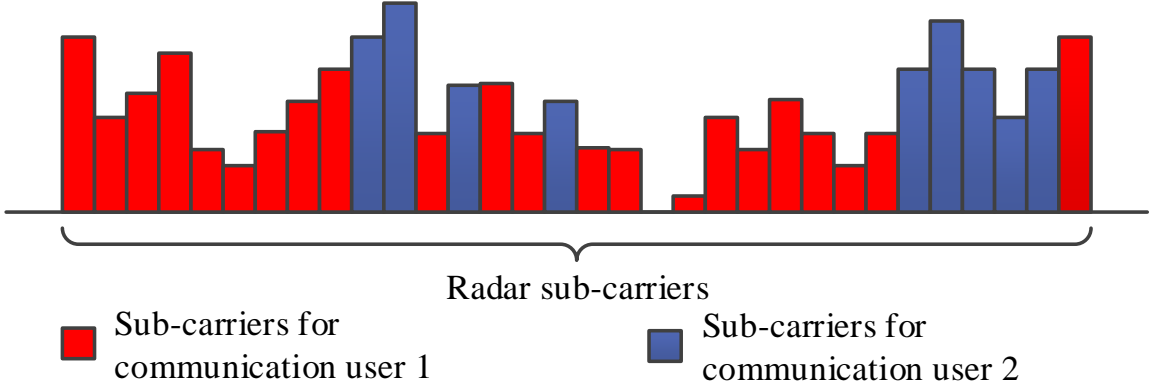


Figure 2.2. Subcarrier allocation and power distribution strategy for a JRC system. Two communication users are shown in the example.

Fig. 2.2 illustrates an example power distribution among the subcarriers and their allocation to the CUs.

The  $L$ -symbol OFDM vector  $\mathbf{x}$  emitted from a dual-purpose transmitter, which consists of  $K$  subcarriers with  $K \leq L$ , can be represented as:

$$\mathbf{x} = \mathbf{F}_{\text{IDFT}}\mathbf{s}, \quad (2.1)$$

where  $\mathbf{F}_{\text{IDFT}}$  is the  $L \times K$  inverse discrete Fourier transform (IDFT) matrix, and each column of  $\mathbf{F}_{\text{IDFT}}$  corresponds to an OFDM subcarrier having a unique subcarrier frequency. Note that the columns of  $\mathbf{F}_{\text{IDFT}}$  are orthonormal, i.e.,  $\mathbf{F}_{\text{IDFT}}^H \mathbf{F}_{\text{IDFT}} = \mathbf{I}_K$ . In addition,  $\mathbf{s} = [s_1, \dots, s_K]^T$  is a  $K \times 1$  vector whose elements correspond to the amplitudes and phases of the respective OFDM waveforms.

We use quadratic phase shift keying (QPSK) in each subcarrier. As such, the phase of  $s_k$  carries the communication information in the  $k$ th subcarrier whereas its magnitude determines the corresponding transmit power  $\xi_k = |s_k|^2$ , which will be optimized later. The total transmit power of the OFDM signal is given as:

$$P_{\text{total}} = \mathbf{x}^H \mathbf{x} = \mathbf{s}^H \mathbf{F}_{\text{IDFT}}^H \mathbf{F}_{\text{IDFT}} \mathbf{s} = \mathbf{s}^H \mathbf{s} = \sum_{k=1}^K \xi_k = \text{tr}\{\mathbf{\Xi}\}, \quad (2.2)$$

where  $\mathbf{\Xi} = \text{diag}\{\boldsymbol{\xi}\}$  is a diagonal matrix with  $\boldsymbol{\xi} = [\xi_1, \dots, \xi_K]^T$ . We denote the maximum possible transmit power for the  $k$ th subcarrier by  $\xi_{k,\text{max}}$  and let  $\boldsymbol{\xi}_{\text{max}} =$

$[\xi_{1,\max}, \dots, \xi_{K,\max}]^T$ , whereas the maximum total transmit power is represented by  $P_{\text{total,max}}$ .

The transmitted OFDM signal is reflected by the target with frequency-dependent characteristics and reaches the radar receiver. Denote  $\mathbf{h} = [h_1, \dots, h_K]^T$  as the radar channel coefficients, including the radar cross-section (RCS), for the  $K$  subcarriers, and let  $\tilde{\mathbf{h}} = \mathbf{F}_{\text{IDFT}}\mathbf{h}$  be the corresponding channel impulse response. Then, the received signal at the radar receiver is expressed as:

$$\tilde{\mathbf{y}}_{\text{rad}} = \tilde{\mathbf{h}} * \mathbf{x} + \tilde{\mathbf{n}}, \quad (2.3)$$

where  $\tilde{\mathbf{n}}$  is the zero-mean complex additive white Gaussian noise vector.

After performing the discrete Fourier transform, the  $K$  subcarriers of the received OFDM signal are recovered as:

$$\mathbf{y}_{\text{rad}} = \mathbf{H}\mathbf{s} + \mathbf{n}, \quad (2.4)$$

where  $\mathbf{H} = \text{diag}(\mathbf{h})$ , and  $\mathbf{n}$  is the Fourier transform of  $\tilde{\mathbf{n}}$  and denotes the zero-mean additive white complex Gaussian noise vector in the  $K$  subcarriers. We assume that the noise components in the  $K$  subcarriers are independent and identically distributed with known covariance matrix  $\mathbf{\Sigma}_{\mathbf{n}} = \text{diag}\{\sigma_{\mathbf{n},1}^2, \dots, \sigma_{\mathbf{n},K}^2\}$ .

Similarly, the OFDM subcarriers reaching the CU  $u$  can be jointly expressed as

$$\mathbf{y}_{\text{com},u} = \mathbf{G}_u\mathbf{s} + \mathbf{m}_u, \quad u = 1, \dots, U, \quad (2.5)$$

where  $\mathbf{G}_u = \text{diag}(\mathbf{g}_u)$  and  $\mathbf{g}_u = [g_{u,1}, \dots, g_{u,K}]^T$  denotes the channel coefficients of the  $K$  subcarriers associated with the  $u$ th CU. In addition,  $\mathbf{m}_u$  is the zero-mean additive white complex Gaussian noise vector with a known covariance matrix  $\mathbf{\Sigma}_{\mathbf{m}_u} = \text{diag}\{\sigma_{\mathbf{m}_u,1}^2, \dots, \sigma_{\mathbf{m}_u,K}^2\}$ . Furthermore, the statistical properties of the radar and communication channels are known to be  $\mathbf{h} \sim \mathcal{CN}(\mathbf{0}_K, \mathbf{\Sigma}_{\mathbf{h}})$  and  $\mathbf{g}_u \sim \mathcal{CN}(\mathbf{0}_K, \mathbf{\Sigma}_{\mathbf{g}_u})$ , where  $\mathbf{\Sigma}_{\mathbf{h}} = \text{diag}\{\sigma_{\mathbf{h},1}^2, \dots, \sigma_{\mathbf{h},K}^2\}$  and  $\mathbf{\Sigma}_{\mathbf{g}_u} = \text{diag}\{\sigma_{\mathbf{g}_u,1}^2, \dots, \sigma_{\mathbf{g}_u,K}^2\}$  are  $K \times K$  diagonal matrices and  $\mathbf{0}_K$  is the  $K \times 1$  vector of all zeros. Moreover, we assume that  $\mathbf{h}$  and  $\mathbf{n}$  as well as  $\mathbf{g}_u$  and  $\mathbf{m}_u$ ,  $u = 1, \dots, U$ , are mutually independent.

## 2.2 Optimization Criteria

In this section, we develop the MI-based optimization criteria respectively for the radar and communication subsystem of the JRC system.

### 2.2.1 Radar subsystem

We consider the MI between the dual-purpose transmit waveform and the frequency-dependent target response  $\mathbf{h}$  as the performance criterion for the radar subsystem which can be stated as [60]:

$$\mathbf{I}(\mathbf{y}_{\text{rad}}; \mathbf{h}|\mathbf{s}) = \mathbf{h}(\mathbf{y}_{\text{rad}}|\mathbf{s}) - \mathbf{h}(\mathbf{y}_{\text{rad}}|\mathbf{h}, \mathbf{s}) = \mathbf{h}(\mathbf{y}_{\text{rad}}|\mathbf{s}) - \mathbf{h}(\mathbf{n}). \quad (2.6)$$

Using Eq. (2.4), we can find the covariance matrix of  $\mathbf{y}_{\text{rad}}$  as [59]:

$$\mathbf{E}[\mathbf{y}_{\text{rad}}\mathbf{y}_{\text{rad}}^{\text{H}}] = \mathbf{E}[\mathbf{H}\mathbf{s}\mathbf{s}^{\text{H}}\mathbf{H}^{\text{H}} + \mathbf{n}\mathbf{n}^{\text{H}}] = \mathbf{\Xi}\mathbf{\Sigma}_{\text{h}} + \mathbf{\Sigma}_{\text{n}}, \quad (2.7)$$

Thus,  $\mathbf{y}_{\text{rad}}|\mathbf{s} \sim \mathcal{CN}(\mathbf{0}, \mathbf{\Xi}\mathbf{\Sigma}_{\text{h}} + \mathbf{\Sigma}_{\text{n}})$ . Eq. (2.6) takes the following form [60]:

$$\begin{aligned} \mathbf{I}(\mathbf{y}_{\text{rad}}; \mathbf{h}|\mathbf{s}) &= \log \left[ (\pi e)^K \det(\mathbf{\Xi}\mathbf{\Sigma}_{\text{h}} + \mathbf{\Sigma}_{\text{n}}) \right] - \log \left[ (\pi e)^K \det(\mathbf{\Sigma}_{\text{n}}) \right] \\ &= \log(\det(\mathbf{\Xi}\mathbf{\Sigma}_{\text{h}} + \mathbf{\Sigma}_{\text{n}})) - \log \det(\mathbf{\Sigma}_{\text{n}}). \end{aligned} \quad (2.8)$$

Since  $\mathbf{\Xi}\mathbf{\Sigma}_{\text{h}}$  is a diagonal matrix, we can express its determinant as the product of its diagonal elements, thus yielding

$$\mathbf{I}(\mathbf{y}_{\text{rad}}; \mathbf{h}|\mathbf{s}) = \log \left( \prod_{k=1}^K \frac{\xi_k \sigma_{\text{h}_k}^2 + \sigma_{\text{n},k}^2}{\sigma_{\text{n},k}^2} \right) = \sum_{k=1}^K \log \left( 1 + \frac{\xi_k \sigma_{\text{h}_k}^2}{\sigma_{\text{n},k}^2} \right). \quad (2.9)$$

### 2.2.2 Communication Subsystem

Now we consider the MI between the CU and the dual-purpose transmit waveform as the performance criteria for the communication subsystem because maximizing the MI is analogous to maximizing the data rate [60]. For the  $u$ th CU, the MI between the transmitted OFDM signal  $\mathbf{s}$  and the communication channel  $\mathbf{g}_u$  can be written as [60]:

$$\mathbf{I}(\mathbf{y}_{\text{com},u}; \mathbf{g}_u|\mathbf{s}) = h(\mathbf{y}_{\text{com},u}|\mathbf{s}) - h(\mathbf{y}_{\text{com},u}|\mathbf{g}_u, \mathbf{s}) = h(\mathbf{y}_{\text{com},u}|\mathbf{s}) - h(\mathbf{m}_u). \quad (2.10)$$

Because  $\mathbf{y}_{\text{com},u}|\mathbf{s} \sim \mathcal{CN}(\mathbf{0}_K, \mathbf{\Xi}\mathbf{\Sigma}_{\mathbf{g}_u} + \mathbf{\Sigma}_{\mathbf{m}_u})$ , we can re-write Eq. (2.10) as [60]:

$$\mathbf{I}(\mathbf{y}_{\text{com},u}; \mathbf{g}_u|\mathbf{s}) = \log(\det(\mathbf{\Xi}\mathbf{\Sigma}_{\mathbf{g}_u} + \mathbf{\Sigma}_{\mathbf{m}_u})) - \log(\det(\mathbf{\Sigma}_{\mathbf{m}_u})). \quad (2.11)$$

Since  $\mathbf{P}\mathbf{\Sigma}_{\mathbf{g}_u}$  is diagonal, Eq. (2.11) takes the following form:

$$\mathbf{I}(\mathbf{y}_{\text{com},u}; \mathbf{g}_u|\mathbf{s}) = \log\left[\prod_{k=1}^K \frac{\xi_k^H \sigma_{\mathbf{g}_{u,k}}^2 + \sigma_{\mathbf{m}_{u,k}}^2}{\sigma_{\mathbf{m}_{u,k}}^2}\right] = \sum_{k=1}^K \log\left(1 + \frac{\xi_k \sigma_{\mathbf{g}_{u,k}}^2}{\sigma_{\mathbf{m}_{u,k}}^2}\right). \quad (2.12)$$

## 2.3 Optimal Power Distribution and Subcarrier Allocation

In this section, we determine the optimal power for each subcarrier and its allocation among the CUs for the optimal JRC operation. The radar subcarriers are optimally allocated to the communication users to achieve the desired data rate such that an individual subcarrier serves only one CU. This enables interference-free multiple access by transmitting distinct data streams to different CUs over their dedicated subcarriers. In the following, we discuss two optimization strategies for subcarrier allocation and power distribution.

### 2.3.1 Radar-Centric Design

For this scenario, the optimization objective aims at maximizing the MI for radar as in Eq. (2.9). This design gives supreme precedence to radar objectives and the resulting subcarrier power distribution of the dual-purpose OFDM transmitter provides maximum MI for the radar operation. However, it does not guarantee that the communication objectives are satisfied. The transmitted waveform can still be used by the CUs in the vicinity of the dual-purpose transmitter. The OFDM subcarriers, whose individual powers for the optimal radar operation have already been determined, are allocated to different communication users.

## Power distribution

Note that the MI in Eq. (2.9) is a concave function of  $\boldsymbol{\xi}$  and the resulting convex optimization takes the following form:

$$\begin{aligned} \min_{\boldsymbol{\xi}} \quad & - \sum_{k=1}^K \log \left( 1 + \frac{\xi_k \sigma_{h_k}^2}{\sigma_{n,k}^2} \right) \\ \text{s.t.} \quad & \mathbf{1}_K^T \boldsymbol{\xi} \leq P_{\text{total,max}}, \\ & \mathbf{0}_K \leq \boldsymbol{\xi} \leq \boldsymbol{\xi}_{\text{max}}, \end{aligned} \tag{2.13}$$

The constraints emphasize the fact that the power of all OFDM subcarriers is bounded by the total available power while the power of each subcarrier is bounded by the maximum possible individual power.

## Subcarrier allocation

In the following, we formulate a mixed-integer linear program (MILP) which designates the OFDM subcarriers to the individual CUs such that the communication MI is maximized. In order to ensure interference-free multiple access, each subcarrier is dedicated to a single CU. Note that the power of each subcarrier is already determined in (2.13) and the following optimization only allocates the subcarriers to the CUs. Two different optimization criteria are considered.

The first criterion maximizes the sum communication MI, expressed as:

$$\begin{aligned} \min_{\mathbf{w}_k} \quad & - \sum_{u=1}^U \sum_{k=1}^K w_{u,k} \log \left( 1 + \frac{\xi_k \sigma_{g_{u,k}}^2}{\sigma_{m_{u,k}}^2} \right) \\ \text{s.t.} \quad & \mathbf{1}_K^T \mathbf{w}_k = 1, \quad w_{u,k} \in \{0, 1\}, \quad \forall u, \forall k, \end{aligned} \tag{2.14}$$

where  $w_{u,k}$  is a binary selection variable, and  $\mathbf{w}_k = [w_{1,k}, \dots, w_{R,k}]^T$ . If  $w_{u,k} = 1$ , it means that the  $k$ th subcarrier is assigned to the  $u$ th CU. Note that, in the underlying scenario, it is possible that some communication users, which have poor channel conditions, are ignored.

To avoid this issue, the second optimization criterion maximizes the worst-case communication capacity to ensure that each communication user is served with a

fair data rate, irrespective of their channel conditions. This is important for the communication users who cannot tolerate being ignored in case they have bad channel conditions. We address this worst-case optimization problem by exploiting the following min-max MILP:

$$\begin{aligned} \min_{\mathbf{w}_k} \max_r & - \sum_{k=1}^K w_{u,k} \log \left( 1 + \frac{\xi_k \sigma_{g_{u,k}}^2}{\sigma_{m_{u,k}}^2} \right) \\ \text{s.t.} & \mathbf{1}^T \mathbf{w}_k = 1, \quad w_{u,k} \in \{0, 1\}, \quad \forall u, \forall k, \end{aligned} \quad (2.15)$$

which can be equivalently written as:

$$\begin{aligned} \min_{\mathbf{w}_k} & \gamma_{\min} \\ \text{s.t.} & - \sum_{k=1}^K w_{u,k} \log \left( 1 + \frac{\xi_k \sigma_{g_{u,k}}^2}{\sigma_{m_{u,k}}^2} \right) \leq \gamma_{\min}, \quad \forall u, \\ & \mathbf{1}_K^T \mathbf{w}_k = 1, \quad w_{u,k} \in \{0, 1\}, \quad \forall u, \forall k. \end{aligned} \quad (2.16)$$

Note that the power  $\xi_k$  for each subcarrier in the optimization (2.15) and (2.16) was obtained from (2.13). Although the optimization in (2.15) and (2.16) ensures the worst-case MI for the communication users, we should be careful that, if some communication users have an extremely low SNR, a worst-case optimization might drain significant power in the poor communication channels, rendering the overall communication performance to be very low.

### 2.3.2 Cooperative Design

Unlike the radar-centric design where the power of each subcarrier solely depends on the radar objectives, a cooperative design enables cooperation from the radar. In this case, radar shows some flexibility on the maximum possible MI it can achieve.

#### Power distribution

First, the optimization (2.13) is exploited to determine the maximum MI  $\alpha_{\text{opt}}$  the radar can achieve. The radar then decides its flexibility parameter  $\gamma_{\text{flex}}$  whose value varies between 0 and 1, where a higher  $\gamma_{\text{flex}}$  favors the radar objectives. In this way,

the radar function allows the dual-purpose transmitter to vary the power allocation such that the radar MI does not fall below  $\gamma_{\text{flex}}\alpha_{\text{opt}}$ .

The initial values of the subcarrier allocation coefficients  $w_{u,k}$  can be either randomly chosen, or optimized by (2.14) or (2.16). The following optimization then achieves the acceptable radar objective while maximizing the overall communication MI:

$$\begin{aligned}
\min_{\boldsymbol{\xi}} \quad & - \sum_{u=1}^U \sum_{k=1}^K w_{u,k} \log \left( 1 + \frac{\xi_k \sigma_{g_{u,k}}^2}{\sigma_{m_{u,k}}^2} \right) \\
\text{s.t.} \quad & - \sum_{k=1}^K \log \left( 1 + \frac{\xi_k \sigma_{h_k}^2}{\sigma_{n,k}^2} \right) \leq -\gamma_{\text{flex}}\alpha_{\text{opt}}, \\
& \mathbf{1}_K^T \boldsymbol{\xi} \leq P_{\text{total,max}}, \\
& \mathbf{0}_K \leq \boldsymbol{\xi} \leq \boldsymbol{\xi}_{\text{max}}.
\end{aligned} \tag{2.17}$$

### Subcarrier allocation

The optimal value of  $\xi_k$  obtained from (2.17) is fed back to (2.14) or (2.16), depending upon which type of communication optimization criterion is required. The optimization for power distribution (2.17) and that for subcarrier allocation (2.14) or (2.16) are repeated iteratively until there is no significant change in the achieved subcarrier allocation and power distribution. All these optimizations are solvable using popular MILP solvers like Gurobi [63] and Mosek [64].

## 2.4 Numerical Results

Consider a JRC transmitter exploiting 32 subcarriers such that there is one radar target and two CUs. The normalized target channel gains and the normalized communication channel gains, respectively expressed as  $\sigma_{h_k}/\sigma_{n_k}$  and  $\sigma_{g_{u,k}}/\sigma_{m_{u,k}}$  are illustrated in Fig. 2.3. The maximum possible subcarrier power and the total maximum power are normalized to 10 units and 100 units, respectively. We use the Gurobi solver [63] to solve for all the optimizations and the achieved MI for each case is listed in Table I.

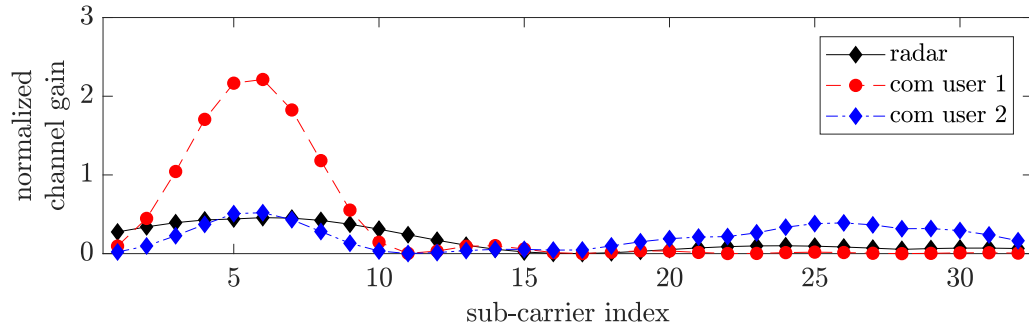
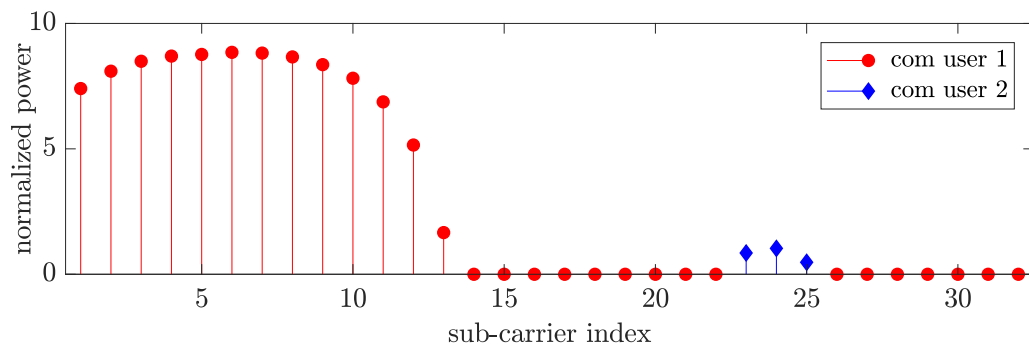
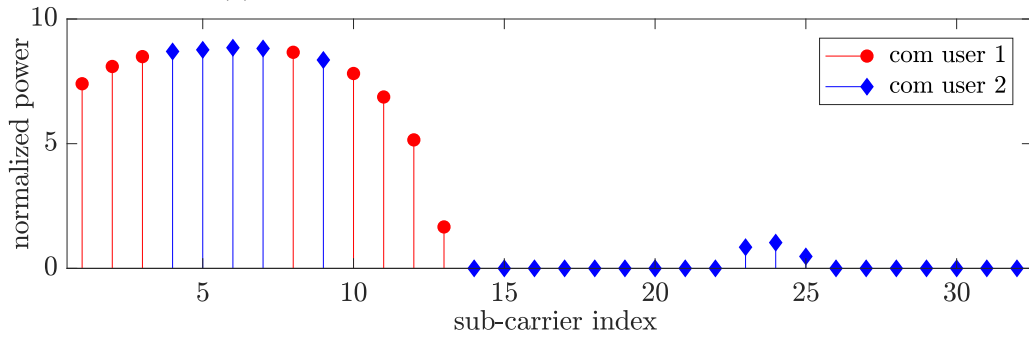


Figure 2.3. Channel conditions for radar and communications.



(a) Maximum communication capacity optimization



(b) Worst-case communication capacity optimization

Figure 2.4. Power allocation and subcarrier distribution for radar-centric design.

First, we discuss the radar-centric design. Fig. 2.4(a) shows the power allocation for different subcarriers using the radar-centric design (2.13) that maximizes the MI for radar. It can be observed that most of the power is allocated to the subcarriers

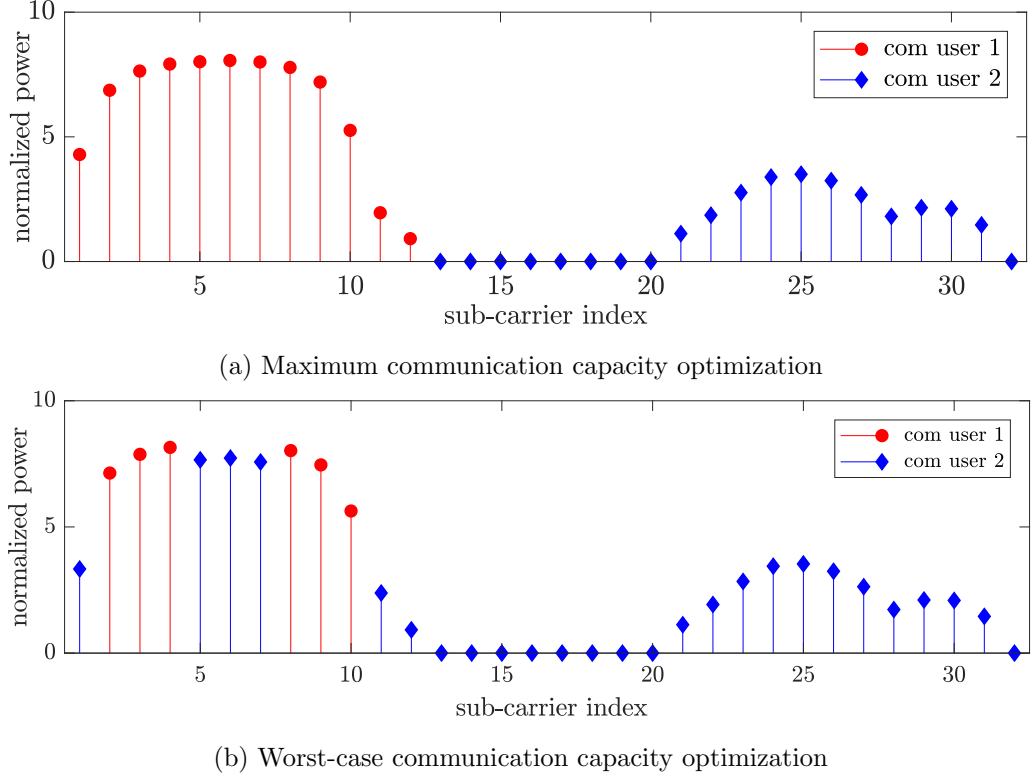


Figure 2.5. Power allocation and subcarrier distribution for cooperative design ( $\gamma_{\text{flex}} = 0.95$ ).

which have a high target RCS. The subcarriers in the red and blue colors depict the OFDM subcarriers respectively allocated to CUs 1 and 2 by maximizing the overall communication MI as in (2.14). It is observed that, although the overall communication MI is maximized, CU 2 is allocated only three low-power subcarriers to enable its communication operation. Fig. 2.4(b) depicts the optimized results using the worst-case optimization (2.16). We can see in Table I that more power is now allocated to the 2nd CU as it has poorer channel conditions than the 1st CU in radar-favored subcarriers. However, in Fig. 2.4(b), the overall communication MI is lower than that in Fig. 2.4(a) as we can observe in Table I.

Next, we discuss the cooperative radar-communication design. For this purpose, the radar's objective is to achieve 95% of the maximum possible MI. Fig. 2.5(a) shows the power allocation and subcarrier distribution for the case of maximum communi-

Table 2.1.  
Achieved mutual information for the single antenna-based JRC system

	Radar-Centric Design		Cooperative Design ( $\gamma_{\text{flex}} = 0.95$ )	
	Maximum	Worst-case	Maximum	Worst-case
	Comm. MI	Comm. MI	Comm. MI	Comm. MI
$I(\mathbf{y}_{\text{rad}}; \mathbf{h} \mathbf{s})$	11.85	11.85	11.26	11.26
$I(\mathbf{y}_{\text{com},1}; \mathbf{g}_1 \mathbf{s})$	15.29	5.66	14.23	7.89
$I(\mathbf{y}_{\text{com},2}; \mathbf{g}_2 \mathbf{s})$	0.48	5.67	4.30	7.71

ation MI. We note in Table 2.1 that, although the radar MI is reduced, the overall communication MI is improved. Similarly, Fig. 2.5(b) illustrates the worst-case optimization which maximizes the worst-case communication MI for both CUs at the expense of reduced overall communication MI.

## 2.5 Remarks

In this chapter, we present a novel JRC system which exploits OFDM waveforms for performing radar and communication operations simultaneously. A dual-purpose OFDM transmitter is exploited which optimizes the transmit power of different subcarriers to fulfill the radar objectives. The same OFDM subcarriers are allocated to different CUs to enable the communication objectives. The MI between frequency-sensitive radar and communication channels is used as the optimization objective for optimizing the system's performance. We discussed the problem for radar-centric and cooperative designs. Moreover, communication performance was discussed in terms of maximum overall mutual information as well as the worst-case communication mutual information. Simulation results show the comparison of the proposed strategies.

## CHAPTER 3

### THROUGHPUT ENHANCEMENT OF BEAMFORMING BASED JRC SYSTEMS

In this chapter, we focus on the communication data rate enhancement of existing beamforming based JRC systems. We propose a novel QAM-based JRC strategy which exploits sidelobe control and waveform diversity, simultaneously, to transmit communication information. The proposed approach enables multi-user access such that we can send distinct QAM based communication streams in different directions while utilizing the same hardware resources as employed by the existing ASK and PSK based techniques. In this context, the proposed technique can provide a higher throughput compared to the conventional approaches, where multiplexing of communication information will be required to transmit different information to different receivers.

It is important to note that the author has developed an ASK-based method [38] which enables multiple access contrary to the aforementioned ASK-based methods. This objective is achieved by simultaneously transmitting different sidelobe levels towards the communication receivers located in different directions. However, we omit the detail of that method because the following strategy discussed in this chapter is a generalized form and [38] can be considered a special case of this strategy.

In contrast to the prior multi-user ASK-based scheme proposed by the author [38] which employs varying sidelobe levels at different communication receivers, the proposed strategy exploits varying sidelobe levels as well as phases of transmitted waveforms to further enhance the data rate. The data rate achieved by the proposed QAM-based scheme is the sum of the data rate separately offered by the amplitude and phase variations. Note that, unlike the existing PSK-based schemes [31–33], which work only for ULAs to utilize the radiation pattern invariance property [57],

the proposed approach also works for arbitrary arrays. Moreover, the proposed technique serves as the generalized mathematical model for the existing sidelobe ASK-based JRC schemes. Simulation results demonstrate the effectiveness of the proposed strategy.

The proposed QAM based sidelobe modulation scheme is different from the existing schemes in the following way:

- The proposed approach enables multi-user access. Different CUs can be served with distinct communication streams, simultaneously. This is contrary to the existing JRC schemes which transmit the same communication information to all the users.
- The proposed approach embeds the communication information as a QAM symbol containing the amplitude as well as the phase part. Existing schemes either use ASK or PSK based schemes which result in the reduced data rate for the same symbol space.

### 3.1 Proposed QAM Based Sidelobe Modulation

#### 3.1.1 Signaling Strategy

We have observed that the existing ASK-based JRC approaches [26, 27, 29] can only broadcast the same information to all the communication receivers by controlling the sidelobe levels during each radar pulse. Since the sidelobe levels towards all the communication directions are same, it is impossible to enable multi-user access, i.e., transmission of different information to the receivers located in different directions is not feasible. On the other hand, the PSK-based JRC strategy can be enabled to transmit distinct communication streams to different users ; however, the use of radiation pattern invariance property [57] is restricted to ULAs only. Moreover, PSK-based schemes cannot exploit the diversity achieved by the ASK principle, restricting the amount of data which can be transmitted. Nevertheless, it is possible to increase the maximum possible data rate by varying sidelobe levels for different

communication receivers and exploiting an efficient PSK-based JRC strategy. However, inability of ASK-based schemes to transmit different communication streams in different directions makes the problem much more cumbersome.

In the proposed approach, a JRC system consisting of an arbitrary linear transmit antenna array can serve different communication receivers located in the sidelobe region with different communication information by exploiting QAM-based communication, i.e., utilizing both amplitude and phase information simultaneously. The proposed JRC system is powered with two degrees-of-freedom (DOFs):

1. The information embedding exploits different amplitude levels to feed distinct communication streams to multiple CUs located in different directions. Such distinct information transmission is made possible by exploiting different sidelobe levels in different directions simultaneously during each radar pulse. These sidelobe levels are kept constant during each radar pulse which constitutes the symbol period.
2. The JRC system can transmit the symbols with different phase differences in different directions, thus providing an extra DOFs in addition to the provision of multiple-level sidelobes.

The proposed scheme is analogous to QAM-based communication system as it exploits amplitude as well as phase shift keying to enable the information embedding using multiple radar waveforms. Moreover, we will show that the proposed scheme serves as the generalized mathematical formulation of the existing JRC techniques [26,29]. Fig. 3.1 show the transmit array-based JRC system transmitting high energy towards the surveillance region, whereas the CUs are located within the sidelobe region. Fig. 3.2 illustrates the basic principle of the proposed QAM-based sidelobe communication approach.

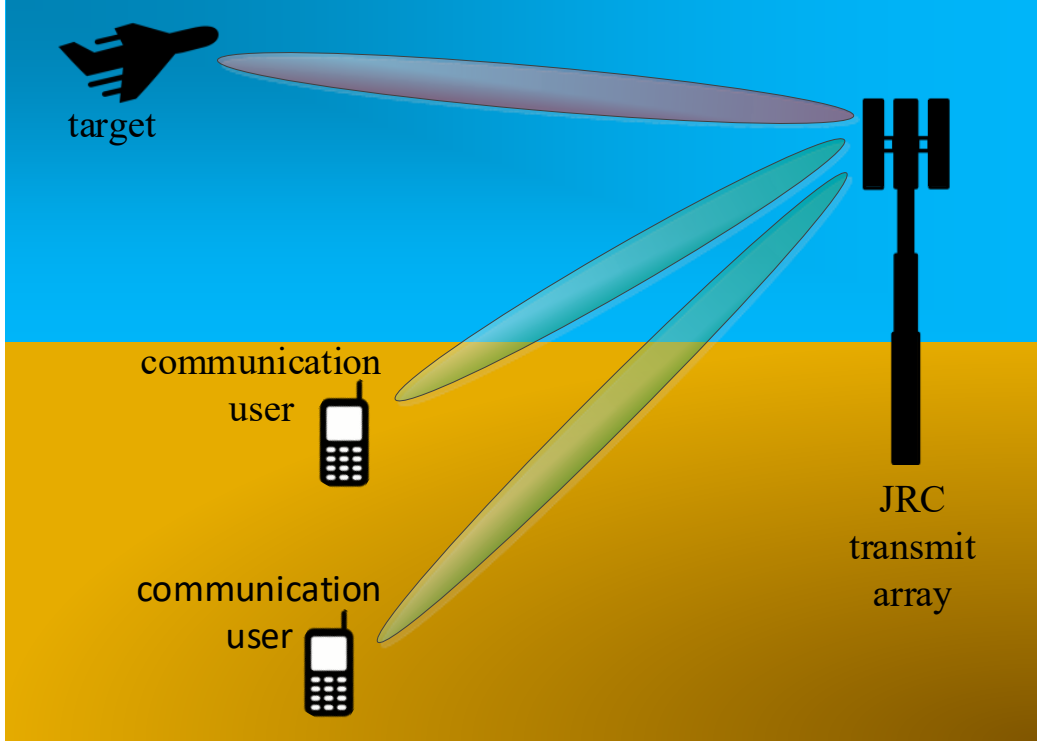


Figure 3.1. Transmit array-based JRC system.

The beamforming weight vectors for the proposed QAM-based communication scheme can be extracted by solving the following optimization:

$$\begin{aligned}
 & \min_{\mathbf{u}_n} \max_{\theta_r} |e^{j\varphi(\theta_r)} - \mathbf{u}_n^H \mathbf{a}(\theta_r)|, \quad \theta_r \in \Theta_{\text{rad}}, \\
 & \text{subject to } |\mathbf{u}_n^H \mathbf{a}(\theta_p)| \leq \varepsilon_{\text{sl}}, \quad \theta_p \in \Theta_{\text{sl}}, \\
 & \mathbf{u}_n^H \mathbf{a}(\theta_u) = \Delta_n(\theta_u) e^{j\phi_n(\theta_u)}, \quad 1 \leq u \leq U, 1 \leq n \leq N.
 \end{aligned} \tag{3.1}$$

Here,  $\mathbf{u}_n$  is the  $n$ -th beamforming weight vector resulting in sidelobe level  $\Delta_n(\theta_u)$  and phase  $e^{j\phi_n(\theta_u)}$  towards the  $u$ -th communication receiver located at  $\theta_u$ . Note that the sidelobe level  $\Delta_n(\cdot)$  and the projected phase  $e^{j\phi_n(\theta_u)}$  are functions of angle  $\theta_u$  of the communication receivers. Each sidelobe level term  $\Delta_n(\theta_u)$  can take any of the  $L$  allowable sidelobe levels and each phase term  $e^{j\phi_n(\theta_u)}$  can take any of the  $Q$  allowable phases. The beamforming weight vector  $\mathbf{u}_n$  in Eq. (3.1) is constructed using  $U$  communication constraints, each corresponding to the desired sidelobe level and

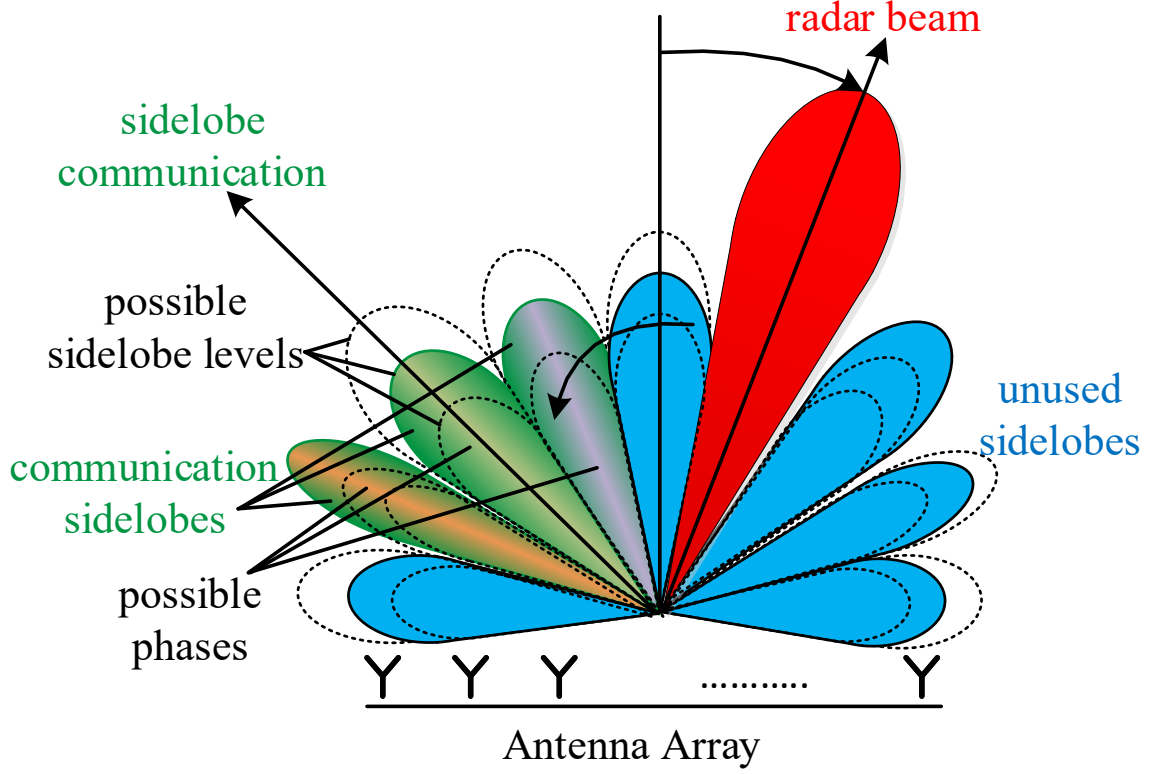


Figure 3.2. The proposed JRC strategy using QAM-based sidelobe modulation.

phase towards the communication receiver located at different angles  $\theta_u$  ( $1 \leq u \leq U$ ). Here,  $\varepsilon$  is the maximum allowable sidelobe level.

The possibility of having  $L$  unique sidelobe levels and  $Q$  unique phases results in  $LQ$  unique combinations for the term  $\Delta_n(\theta_u) e^{j\phi_n(\theta_u)}$  towards  $\theta_u$ . However, each of the  $U$  communication constraints selects only one distinct value of  $\Delta_n(\theta_u) e^{j\phi_n(\theta_u)}$  out of the  $LQ$  possible values for evaluating the beamforming weight vectors. Note that the values of  $\Delta_n(\theta_u) e^{j\phi_n(\theta_u)}$  can be different in different directions  $\theta_u$ , thereby enabling multi-user access, i.e., ensuring independent communication streams towards different directions. Since there are  $LQ$  possible values of  $\Delta_n(\theta_u) e^{j\phi_n(\theta_u)}$  at each communication receiver, there will be a total of  $(LQ)^U$  possible communication constraints for the  $U$  users. A beamforming weight vector  $\mathbf{u}_n$  is designed by selecting  $U$  constraints out of the total  $(LQ)^U$  constraints. Therefore, we can generate  $N = (LQ)^U$  unique

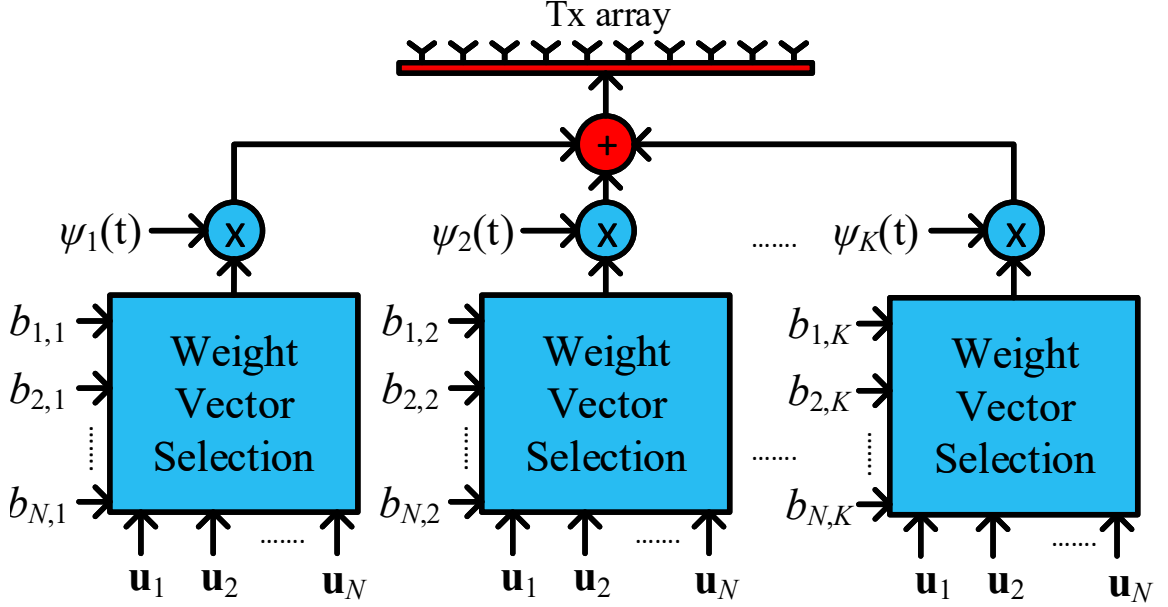


Figure 3.3. The proposed QAM-based JRC approach using QAM-based sidelobe modulation (coefficients  $b_{n,k}$  are the function of  $\tau$ ).

beamforming weight vectors using Eq. (3.1) such that each beamforming weight vector projects a unique set of  $U$  QAM symbols towards the communication directions. The desired beamforming weight vector corresponding to the required amplitude levels and phases towards communication directions can be selected from the set of  $(LQ)^U$  beamforming weight vectors for information transmission.

For the proposed approach, it is possible to transmit radar waveforms with the same (broadcast case) or different (multi-user access case) information by respectively choosing the same or different sidelobe levels and phases at all the communication receivers simultaneously. The signal transmitted from the JRC antenna array is expressed as:

$$\mathbf{s}(t, \tau) = \sqrt{\frac{P}{K}} \sum_{k=1}^K \mathbf{U}^* \mathbf{b}_k(\tau) \psi_k(t), \quad (3.2)$$

where  $\mathbf{U} = [\mathbf{u}_1, \mathbf{u}_2, \dots, \mathbf{u}_N]$  is an  $M \times N$  matrix which serves as the dictionary of  $N$  beamforming weight vectors optimized using Eq. (3.1), and  $\mathbf{b}_k(\tau) = [b_{1,k}(\tau), b_{2,k}(\tau), \dots, b_{N,k}(\tau)]^T$  is an  $N \times 1$  binary selection vector selecting the desired beam-

forming weight vector from the dictionary  $\mathbf{U}$  for each transmitted waveform  $\psi_k(t)$ . Moreover,  $t$  is the fast time and  $\tau$  is the slow time index.<sup>1</sup> All the elements in  $\mathbf{b}_k(\tau)$  are 0 except only one element which is equal to 1. We utilize  $K(\leq \hat{K})$  orthogonal waveforms during each radar pulse and it is possible to use different values of  $K$  for each pulse. Note that the individual sidelobe levels and phases towards each communication receiver obtained by the weight vectors present in  $\mathbf{U}$  are not the same, thus enabling us to transmit distinct QAM-based communication streams towards each communication receiver.

The proposed transmission scheme allows  $L$  unique sidelobe levels and  $Q$  unique phases at each receiver, each transmitted waveform carries  $\log(LQ)$  bits of distinct information for each receiver. The proposed signaling strategy is outlined in Fig. 3.3.

The transmitted signal  $\mathbf{s}(t, \tau)$  can be rewritten in a compact form as:

$$\mathbf{s}(t, \tau) = \sqrt{\frac{P}{K}} \mathbf{U} \mathbf{B}(\tau) \boldsymbol{\psi}(t), \quad (3.3)$$

where

$$\begin{aligned} \mathbf{B}(\tau) &= \left[ \mathbf{b}_1(\tau), \mathbf{b}_2(\tau), \dots, \mathbf{b}_K(\tau) \right], \\ \boldsymbol{\psi}(t) &= \left[ \psi_1(t), \psi_2(t), \dots, \psi_K(t) \right]^T. \end{aligned} \quad (3.4)$$

The radar system transmits waveforms in the form of pulses. For this purpose, we define *coherent communication* as the protocol where the start time of pulses is always known at the communication receivers. On the other hand, communication receivers are blind about the pulse start time in *non-coherent communication*. For both protocols, we assume that all the radar waveforms are known at the communication receivers. Since the start time of the pulses are known for coherent communications, all the orthogonal waveforms can be used to transmit information. On the other hand, a reference waveform (pilot tone) is reserved in non-coherent communication to detect the start time of the pulses. This is achieved by the sliding window matched filtering with the reference waveform.

---

<sup>1</sup>See Section A of Appendix A for detail.

For the case of coherent communications where carrier synchronization is not an issue, the transmitted information in the direction  $\theta_u$  can be expressed as:

$$G_T(\theta_u) = \mathbf{u}_n^H \mathbf{a}(\theta_u) = \Delta_n(\theta_u) e^{j\phi_n(\theta_u)}, \quad 1 \leq n \leq N, \quad (3.5)$$

where  $\Delta_n(\theta_u)$  and  $e^{j\phi_n(\theta_u)}$  vary with respect to  $\theta_u$ .

For the case of non-coherent communications where it is difficult to achieve carrier synchronization, we can exploit a reference waveform  $\psi_1(t)$  along with a reference beamforming vector  $\mathbf{u}_1$  (collectively forming the reference pilot tone). In this way, the transmitted information in the direction  $\theta_u$  can be expressed as:

$$G_T(\theta_u) = \frac{\mathbf{u}_n^H \mathbf{a}(\theta_u)}{\mathbf{u}_1^H \mathbf{a}(\theta_u)}, \quad 2 \leq n \leq N. \quad (3.6)$$

Note in Eqs. (3.5) and (3.6) that  $\mathbf{u}_n$  varies with  $\tau$  depending on the value of  $\mathbf{b}_k(\tau)$  in Eq. (3.2), and  $G_T(\theta_u)$  provides an estimate of the transmitted QAM symbol, where  $|G_T(\theta_u)|$  and  $\angle\{G_T(\theta_u)\}$  respectively represent the amplitude and the phase components of the transmitted QAM symbols in the communication direction  $\theta_u$ .

### 3.1.2 Information Decoding at Communication Receivers

The signal received at the  $u$ -th communication receiver located in the sidelobe region at angle  $\theta_u$  can be described as:

$$x_u(t, \tau) = \alpha_u(\tau) \mathbf{a}^T(\theta_u) \mathbf{s}(t, \tau) + n(t), \quad (3.7)$$

where  $\alpha_u(\tau)$  is the complex-valued channel response which is considered constant during each radar pulse, and  $n(t)$  is the zero-mean complex white Gaussian noise. Matched filtering the received signal  $x_u(t, \tau)$  in (3.7) to each of the  $\hat{K}$  possible waveforms at the  $u$ -th communication receiver yields the following scalar output:

$$\begin{aligned} y_{u,k}(\tau) &= \frac{1}{T} \int_{t=0}^T x_u(t, \tau) \psi_k(t) dt \\ &= \begin{cases} \sqrt{\frac{P}{K}} \alpha_u(\tau) \Delta_n(\theta_u) e^{j\phi_n(\theta_u)} + n_k(\tau), & \text{if } \psi_k(t) \text{ was transmitted,} \\ n_k(\tau), & \text{otherwise.} \end{cases} \end{aligned} \quad (3.8)$$

Here,  $n_k(\tau)$  is the zero-mean complex white Gaussian noise at the output of the matched filter. By analyzing  $y_{u,k}(\tau)$  at the  $u$ -th receiver using all radar waveforms  $\psi_k(t)$ ,  $1 \leq k \leq \hat{K}$ , it is possible to determine the transmitted sidelobe levels  $\Delta_n(\theta_u)$  and phases  $e^{j\phi_n(\theta_u)}$  which decodes the embedded communication information.

For the case of coherent communication, the receiver at  $\theta_u$  determines the transmitted QAM signals during each radar pulse as:

$$G_U(\theta_u) = y_{u,k}(\tau). \quad (3.9)$$

For the case of non-coherent communication,  $y_{r,1}(\tau)$  is considered as the reference, and the receiver determines the transmitted QAM signals during each radar pulse as:

$$G_U(\theta_u) = \frac{y_{u,k}(\tau)}{y_{u,1}(\tau)}. \quad (3.10)$$

In Eqs. (3.9) and (3.10),  $G_U(\theta_u)$  denotes the received QAM communication symbol having magnitude  $|G_U(\theta_u)|$  and phase  $\angle\{G_U(\theta_u)\}$  at the receiver located at angle  $\theta_u$ .

We can observe that the proposed multi-waveform sidelobe QAM-based signaling strategy treats each of the existing JRC techniques discussed in [27, 33, 35, 38] as a special case. Table 3.1 shows the parameters which can be changed in Eq. (3.2) to yield these existing JRC signaling methods. This implies that the proposed signaling scheme represents a generalized mathematical framework of existing JRC schemes.

The following proposition addresses the number of users which can be supported by the proposed JRC technique.

**Proposition 1:** For the JRC system consisting of an  $M$ -element uniform linear array (ULA), the number of maximum possible supportable CUs located in unique directions is  $M - 1$ .

**Proof:** For the case of ULA, we can consider the beamforming weight vector in Eq. (3.1) as a polynomial of degree  $M - 1$  having a maximum of  $M - 1$  unique roots. If all these  $M - 1$  roots correspond to the equality constraints in Eq. (3.1), it may still be possible to solve for other constraints without losing any DOFs in ideal cases. However, some of the DOFs might be utilized to satisfy the inequality constraint

and the minimization function in Eq. (3.1). Thus, the maximum possible number of supported CUs located in distinct directions for ULA is  $M - 1$ .

### 3.1.3 Sum Data Rate Analysis

In this section, we evaluate the sum of the number of bits which can be transmitted during one radar pulse using the proposed QAM-based JRC technique to the sidelobe communication receivers located at distinct angles. We consider  $U$  receivers utilizing  $L(\geq 1)$  sidelobe levels and  $Q(\geq 1)$  phase constellations with  $LQ > 1$  such that  $K \leq \hat{K}$  fixed number of orthogonal waveforms are used during each radar pulse. The following proposition addresses the achievable data rate.

**Proposition 2:** The maximum data rate achieved from the proposed QAM-based JRC strategy is  $UK \log(LQ)$  for coherent communication.

**Proof:** According to Eq. (3.2), for each radar waveform  $\psi_k(t)$ , we can transmit  $L$  possible sidelobe levels and  $Q$  distinct phases to each communication receiver. Thus, each communication receiver deciphers  $\log(LQ)$  bits of distinct information during each radar pulse for each of the  $K$  transmitted radar waveforms. Therefore, the sum data rate for all the  $U$  communication receivers becomes  $UK \log(LQ)$  for the case of coherent communications. Similarly, the sum data rate offered by the proposed strategy for non-coherent communication is  $U(K - 1) \log(LQ)$  if one waveform is used as the reference waveform.

The achievable data rate offered by the proposed QAM-based information embedding strategy is compared with existing JRC methods [26,27,35,38] in Table 3.1. It is evident that the proposed technique outperforms existing approaches in terms of overall throughput or sum data rate because it benefits from multiple sidelobe levels and phase possibilities simultaneously at different communication receivers. Moreover, the ability to transmit different information streams (sidelobe levels and phases) to different users further enhances the maximum achievable data rate.

Table 3.1.  
Comparison of beamforming-based JRC systems

Signaling Strategy	Parameters for Eq. (3.1)–(3.2)	Maximum data rate (bits/pulse)
Sidelobe AM [27]	$K = 1, N = L \geq 2,$ $Q = 1, U = 1.$	$\log L$
Multiwaveform ASK [28, 35]	$N = L = 2, Q = 1,$ fixed $K(\leq \hat{K})$ , varying $U$ , $\mathbf{u}_1 = \mathbf{u}_{\text{low}}, \mathbf{u}_2 = \mathbf{u}_{\text{high}},$ $b_{1,k}(\tau) = 1 - b_{2,k}(\tau)$	$K \log L$
Multi-waveform single-level ASK [30]	$N = L = 1, Q = 1,$ $\mathbf{u}_1 = \mathbf{u}_{\text{high}},$ varying $K$ and $U$ , For all zeros: $K = 1, b_{1,K} = 1$ else: $b_{1,1} = 0, b_{1,k} = 0$ or $1,$ $\sum_{k=2}^{\hat{K}} b_{1,k} = K.$	$K \leq \hat{K}$
Multi-user ASK [38]	varying $N, L, U, K,$ $Q = 1, 1 < K \leq \hat{K}$	$UK \log L$
Multi-waveform coherent PSK [33]	$N = L = 1, \mathbf{u}_1 = \mathbf{u}_{\text{high}},$ fixed $K(\leq \hat{K}),$ varying $U$ and $Q(\geq 2).$	$K \log Q$
Multi-waveform non-coherent PSK [33]	$N = L = 1, \mathbf{u}_1 = \mathbf{u}_{\text{high}},$ fixed $K(2 \leq K \leq \hat{K}),$ varying $U$ and $Q(\geq 2)$	$(K - 1) \log Q$
Coherent Multi-user QAM (proposed) [46]	varying $N, L, U, Q, K$	$UK \log(LQ)$
Non-coherent Multi-user QAM (proposed) [46]	varying $N, L, U, Q, K,$ $1 < K \leq \hat{K}$	$U(K - 1) \log(LQ)$

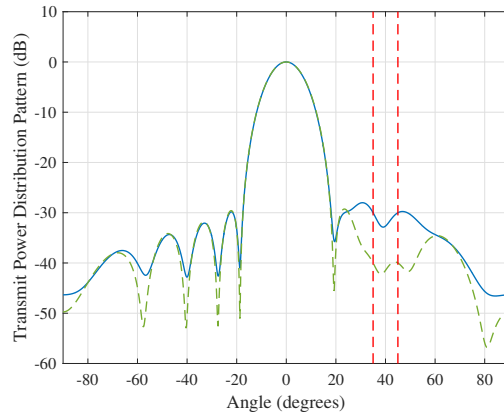
## 3.2 Simulation Results

In this section, we present simulation results to illustrate the performance of the proposed QAM-based JRC strategy. In all simulations, we consider a ULA of 10 transmit antennas to serve two CUs located in the sidelobe region of the radar. We have used CVX toolbox [65–68] with MATLAB to solve all the optimizations. Moreover, the communication system protocol is also modeled in MATLAB.

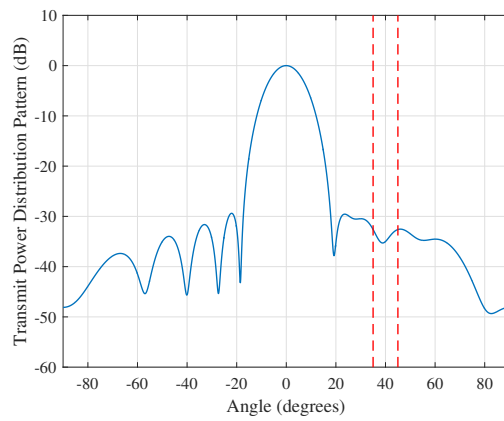
### 3.2.1 Beam pattern Synthesis and Data Rate Analysis for Equal Number of Sidelobe Levels and Phase Constellations

We consider that the JRC system is capable of projecting two sidelobe levels and transmitting the waveforms with two different phases towards the communication receivers located in the sidelobe region at angles  $35^\circ$  and  $45^\circ$ , respectively. For this case, we have  $U = L = Q = 2$ . Here, the primary function of the radar is to project the main beam at  $0^\circ$ . For the communication purpose, ASK- and PSK-based schemes will have the ability to exploit only the magnitude or phase variation, respectively. In contrast, the QAM-based scheme can utilize the variation in both magnitude as well as the phase of the transmitted waveform.

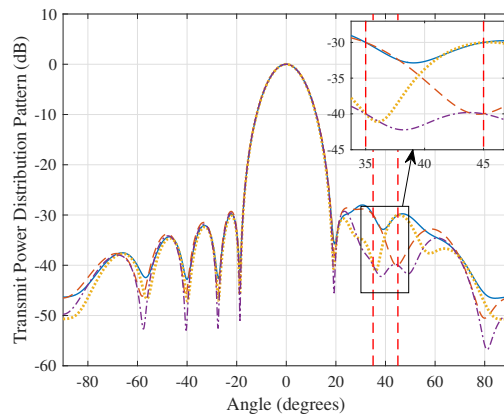
Fig. 3.4(a) shows the transmit power pattern corresponding to two beamforming weight vectors for multi-waveform ASK [29]. These beamforming vectors respectively broadcast the amplitude of either  $-30$  dB or  $-40$  dB in the directions of communication receivers. The sidelobe level at both communication receivers also remains identical for the existing ASK-based schemes [29] during each radar pulse. For PSK-based method [33], two beamforming vectors are generated to have the same magnitude response but different phase response in the directions of communication receivers. Fig. 3.4(b) shows the power pattern of these beamforming weight vectors projecting a sidelobe level of  $-32.61$  dB at both communication receivers. Each of the two beamforming vectors for the PSK-based method broadcast a unique phase towards all the communication receivers during each radar pulse. Just like ASK-based methods, the transmitted information is broadcast to all the CUs.



(a)



(b)

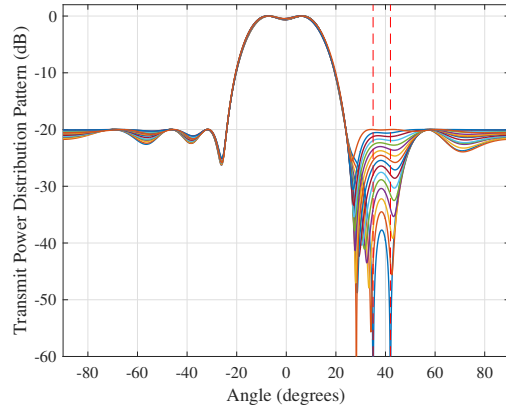


(c)

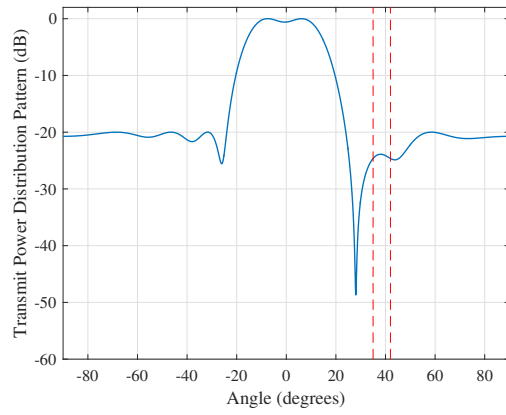
Figure 3.4. Beampatterns for JRC strategies ( $U = 2, Q = 2, L = 2$ ): (a) Multi-waveform ASK-based method [35], (b) Multi-waveform PSK-based method [35], (c) Proposed QAM-based method [46].

Unlike the ASK-based technique, the QAM-based method can assign different sidelobe levels at the two communication receivers. Moreover, in contrast to the existing PSK-based strategy, the proposed QAM-based technique can transmit different phases to different receivers at the same time. Thus, the QAM-based strategy can independently project two different levels of amplitudes as well as phases at the two receivers so as to transmit distinct information to each user. We can generate 16 beamforming weight vectors for  $U = 2, L = 2, Q = 2$  using Eq. (3.1). Fig. 3.4(c) shows the four possible power patterns for the proposed QAM-based scheme generated using Eq. (3.1). Since the number of possible transmitted phases towards each receiver are 2, each beampattern for the QAM-based scheme corresponds to four distinct beamforming weight vectors projecting the same magnitude but different phase responses towards the two communication receivers.

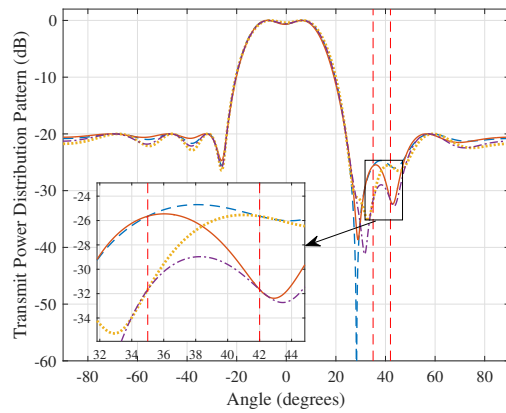
Let us examine the achievable throughput (sum data rate) for this experiment. Note that the average power transmitted to each communication receiver is kept constant for all the three schemes. For a single radar waveform, the ASK-based method exploiting two sidelobe levels will be able to transmit (broadcast)  $\log L = 1$  bit per waveform for each radar pulse. Coherent PSK-based method utilizing two phase options will also be able to broadcast  $\log Q = 1$  bit per radar waveform for each radar pulse. On the other hand, the coherent QAM-based information embedding strategy is able to transmit 2 bits per user resulting in a total throughput of  $U \log(LQ) = 4$  bits transmitted using each radar waveform during each radar pulse. For two waveforms, this data rate for all the coherent schemes will double. The non-coherent schemes will utilize one waveform as the reference and one waveform will be used for communication purpose; therefore, the data rate of coherent scheme will be half compared to the coherent counterpart if two orthogonal waveforms are utilized. Fig. 3.6 shows the maximum throughput with respect to the number of available waveforms for this simulation parameters ( $U = L = Q = 2$ ). The simulation results clearly illustrate the superiority of our proposed technique in terms of sum data rate.



(a)



(b)



(c)

Figure 3.5. Beampatterns for JRC strategies. (a) Multi-waveform ASK-based method [35], (b) Multi-waveform PSK-based method [33], (c) Proposed QAM-based method [46].

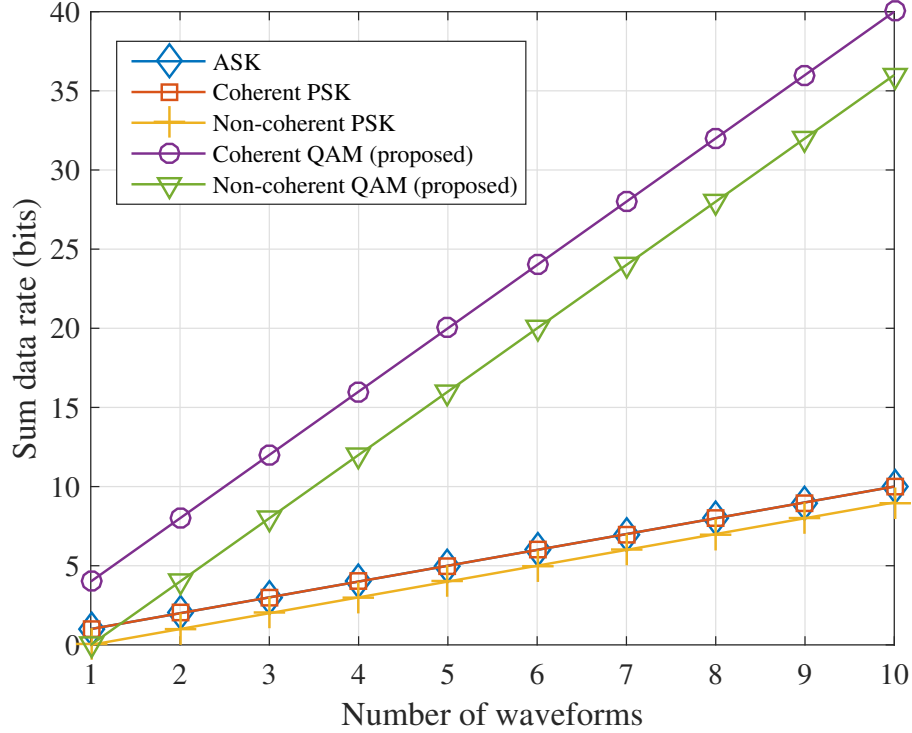


Figure 3.6. The comparison of throughput for the case of  $U = L = Q = 2$  and varying number of available waveforms.

### 3.2.2 Bit Error Rate Analysis for Same Overall Throughput

In the second example, we investigate the possibility of synthesizing beamforming weight vectors for the case of extended radar's main beam and compare the bit error rate (BER) for the JRC strategies by keeping the sum data rate and transmitted power constant.

We consider two CUs ( $U = 2$ ) at  $35^\circ$  and  $42^\circ$  with respect to the JRC transmit antenna array. The desired main lobe region is from  $-10^\circ$  to  $10^\circ$  and two orthogonal waveforms ( $K = 2$ ) are available to the JRC system. The objective is to transmit 4 bits of information to each CU (a total throughput of 8 bits).

For the case of multi-waveform ASK [35], we have to design 16 beamforming weight vectors having sidelobe levels uniformly distributed from 0 to 0.1 towards the intended communication directions ( $L = 16$ ,  $K \log L = 8$  bits throughput). For the PSK-based

technique [33], 16 beamforming vectors having sidelobe level of 0.2347 towards the CUs are synthesized such that the respective phases of these beamforming vectors at the receivers is uniformly distributed from  $0^\circ$  to  $360^\circ$  ( $Q = 16, K \log Q = 8$  bits throughput).

Since there are only two available waveforms, the non-coherent PSK will have 32 beamforming weight vectors to match the data rate because one waveform will be used as a reference to realize non-coherent communications ( $Q = 32, (K - 1) \log Q = 8$ ).

For the case of the proposed coherent QAM-based sidelobe modulation, we have generated 16 beamforming vectors using Eq. (3.1) such that there are a total number of four groups of QAM-based beamforming weight vectors corresponding to the same amplitude response. Each group comprises four beamforming weight vectors corresponding to unique phase combinations at the both communication receivers. We have the ability to transmit waveforms towards the communication receivers with two distinct power levels and four phase possibilities. In a similar manner, the non-coherent QAM-based strategy will result in the generation of 32 beampatterns such that we have the ability to project the radar waveforms at two power levels and four unique phase constellations at each communication receiver.

The beampatterns for the designed beamforming vectors for the case of ASK, PSK and QAM-based information embedding is shown in Fig. 3.5. We observe that the multi-waveform ASK and all the coherent communication based algorithms result in an equal number of beamforming weight vectors. Moreover, non-coherent based JRC techniques also have the same number of beamforming vectors.

Fig. 3.7 compares the BER performance of the proposed technique with existing techniques. For error reduction, all the symbols for the JRC transmission schemes are grey coded before transmission. We observe that the proposed QAM-based method is more capable to resilient to noise compared to existing JRC techniques. This is because the proposed QAM-based method is designed to offer a higher throughput with the same resources and, therefore, results in increased distance between the signals in the symbol space. The QAM symbol space in this simulation contains 8 symbols compared to 16 symbols each for PSK and ASK, respectively. In addition

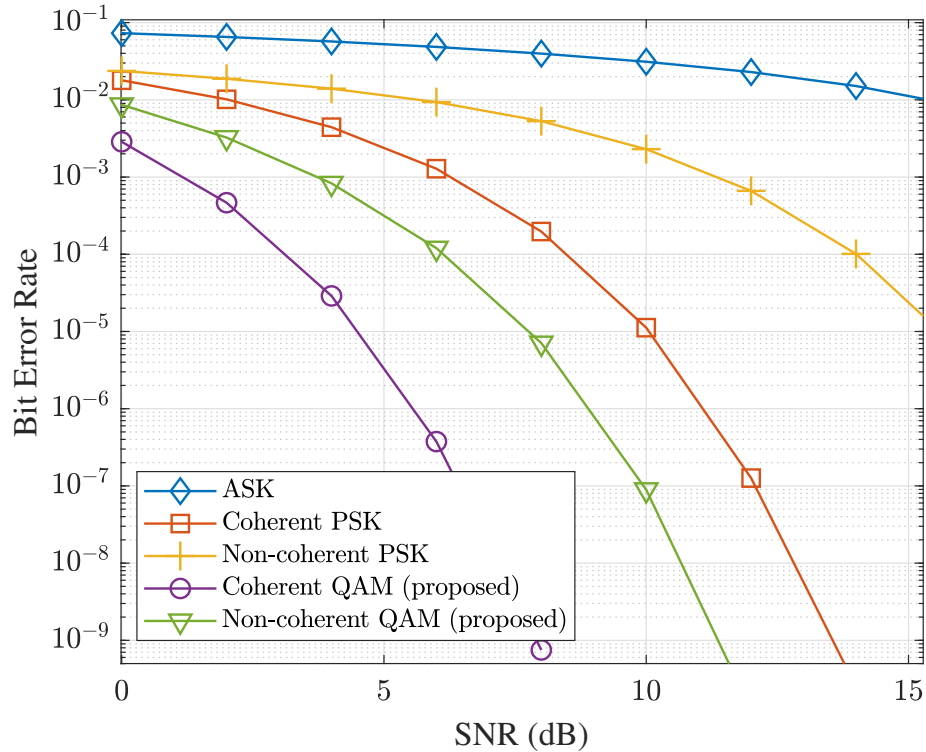


Figure 3.7. Bit error rate analysis for the multi-waveform ASK-based method [29], multi-waveform PSK-based method (coherent and non-coherent case) [33] and the proposed QAM-based method (coherent and non-coherent case).

to this, 8-QAM symbols are distributed as two levels of amplitudes and 4 levels of phases which further increases the effective distance between the transmitted symbol constellations. This increased distance between the symbol constellations along with the flexibility to transmit different symbols to different users results in reduced BER for the proposed QAM-based technique. Moreover, the coherent communication based methods have better performance compared to the non-coherent counterparts because the number of symbols in the symbol space is increased for the latter, resulting in higher error rates. However, the proposed non-coherent QAM-based information embedding strategy still outperforms the existing methods in terms of the BER.

In short, the simulation results illustrate the effectiveness of the proposed QAM-based information embedding in comparison to the existing schemes in terms of BER and the overall throughput of the communication system.

### 3.3 Remarks

A novel multi-waveform QAM-based scheme exploiting sidelobe control and waveform diversity was proposed, which enables the transmission of distinct communication information to the communication receivers located in distinct directions. The information embedding has been discussed for coherent as well as non-coherent communication cases. Compared to the existing ASK and PSK-based signaling strategies, the proposed method achieves higher transmission capacity by simultaneously enabling both amplitude and phase shift keying in the radar sidelobe region. Moreover, the ability to transmit distinct information in different directions enhances the sum data rate by a factor of number of CUs. As such, the proposed signaling strategy also serves as a generalized mathematical framework of existing JRC strategies. Simulation results evidently verify the effectiveness of the proposed scheme.

## CHAPTER 4

### CHANCE CONSTRAINED BEAMFORMING FOR JRC SYSTEMS

We present an intelligent sensor array-based joint radar-communication system which exploits chance constrained programming to develop a robust beamforming design. Probabilistic chance constraints are introduced for the communication operation where the communication objectives are achieved with a desired success rate in the presence of communication channel uncertainties. In the presence of communication channel uncertainties, such an approach will ensure the communication system quality in a probabilistic sense. Our communication objective will be to achieve the desired communication signal power at communication receivers with a specific probability. For this purpose, we assume non-stationary communication channels such that their statistical profile is known to the intelligent sensor array. Using this statistical profile, we then relax the chance constraints to their equivalent convex deterministic counterparts [69]. Simulation results illustrate the performance of the proposed strategy.

#### 4.1 Joint Radar-Communication System

Consider a JRC system equipped with an  $M$ -element linear intelligent sensor array of an arbitrary configuration. There are  $R$  single-antenna communication receivers located in the sidelobe region of the radar. The JRC system employs  $K$  orthogonal waveforms  $\psi_1(t), \psi_2(t), \dots, \psi_K(t)$  such that

$$\frac{1}{T} \int_0^T \psi_{k_1}(t) \psi_{k_2}^*(t - \zeta) dt = \delta(k_1 - k_2) \delta(t - \zeta), \quad (4.1)$$

where  $1 \leq k_1, k_2 \leq K$ ,  $t$  is the fast time,  $T$  is the pulse duration,  $\psi_{k_2}(\zeta)$  is the time delayed version of  $\psi_{k_2}(t)$  delayed by  $\zeta$  ( $< T$ ), and  $\delta(\cdot)$  represents the Kronecker delta function.

Both radar and communication operations are performed by the same transmit array exploiting their respective waveforms  $\psi_{\text{rad}}(t)$  and  $\psi_{\text{com}}(t)$ . The mutual interference between the radar and communication systems is mitigated by employing orthogonal waveforms and spatial filtering. Similar to [47], we assume that  $\psi_{\text{rad}}(t) = \psi_1(t)$  and  $\psi_{\text{com}}(t)$  is selected from the remainder of the  $K - 1$  orthogonal waveforms depending on which information is transmitted.

#### 4.1.1 Beamformer Design

During each radar pulse, the JRC system exploits two beamforming weight vectors  $\mathbf{u}_{\text{rad}}$  and  $\mathbf{u}_{\text{com}}$  which correspond to the waveforms  $\psi_{\text{rad}}(t)$  and  $\psi_{\text{com}}(t)$ , respectively.

Denote  $\mathbf{a}(\theta)$  as the array response vector of the transmit JRC array in the direction  $\theta$ , and  $\theta_{\text{rad}}$  as the direction of the radar main lobe, whereas  $\Theta_{\text{com}}$  is the set containing the directions of all the CUs. Note that all the CUs are located in the sidelobe of the radar, i.e.,  $\Theta_{\text{com}} \subset \Theta_{\text{rad}}^c$ , where  $\Theta_{\text{rad}}^c$  represents the radar sidelobe region which excludes the main lobe and its corresponding transition region.

The beamforming weight vectors  $\mathbf{u}_{\text{rad}}$  and  $\mathbf{u}_{\text{com}}$  can be designed as [69]:

$$\begin{aligned}
 & \min_{\mathbf{u}_{\text{rad}}, \mathbf{u}_{\text{com}}} \quad \mathbf{u}_{\text{rad}}^H \mathbf{u}_{\text{rad}} + \mathbf{u}_{\text{com}}^H \mathbf{u}_{\text{com}} \\
 & \text{subject to} \quad \mathbf{u}_{\text{rad}}^H \mathbf{a}(\theta_{\text{rad}}) = 1, \\
 & \quad \mathbf{u}_{\text{rad}}^H \mathbf{a}(\theta_u) = 0, \quad \theta_u \in \Theta_{\text{com}}, \\
 & \quad \mathbf{u}_{\text{rad}}^H \mathbf{a}(\theta_{\text{rad,sl}}) \leq \alpha_{\text{rad}}, \quad \theta_{\text{rad,sl}} \in \Theta_{\text{rad}}^c, \\
 & \quad \mathbf{u}_{\text{com}}^H \mathbf{a}(\theta_{\text{rad}}) = 0, \\
 & \quad \mathbf{u}_{\text{com}}^H \mathbf{a}(\theta_u) \geq \Delta_u, \quad \theta_u \in \Theta_{\text{com}},
 \end{aligned} \tag{4.2}$$

where  $\alpha_{\text{rad}}$  denotes the worst-case amplitude level of the radar waveform towards all the angles  $\theta_{\text{rad,sl}}$  in the radar sidelobe region  $\Theta_{\text{rad}}^c$  and  $\Delta_u > 0$  is the desired communication amplitude transmitted towards the  $u$ th communication receiver. Due to the power minimization objective of the above optimization, the communication amplitudes will always approach  $\Delta_u$ , i.e.,  $\mathbf{u}_{\text{com}}^H \mathbf{a}(\theta_u) = \Delta_u$  (note that the imaginary part is equal to zero). Since  $\mathbf{u}_{\text{rad}}$  and  $\mathbf{u}_{\text{com}}$  are designed to be orthogonal in the radar

and communications directions, we may choose  $\Delta_u$  to be higher than  $\alpha_{\text{rad}}$  without compromising the radar operation. Note that, as  $\Delta_u$  is real, the imaginary part of  $\mathbf{u}_{\text{com}}^H \mathbf{a}(\theta_u)$  approaches zero.

#### 4.1.2 Signaling Strategy

The JRC system exploits the dictionary of communication waveforms which is assumed to be known at the communication receivers. This dictionary is given by

$$\mathbf{\Psi}(t) = [\psi_2(t), \psi_3(t), \dots, \psi_K(t)]^T. \quad (4.3)$$

The composite signal transmitted from the JRC platform during each radar pulse is represented as [47]:

$$\mathbf{x}(t, \tau) = \mathbf{u}_{\text{rad}}^* \psi_{\text{rad}}(t) + \mathbf{u}_{\text{com}}^* \psi_{\text{com}}(t), \quad (4.4)$$

where  $\tau$  is the slow-time index,  $\psi_{\text{rad}}(t) = \psi_1(t)$ , and  $\psi_{\text{com}}(t)$  is given by

$$\psi_{\text{com}}(t) = \boldsymbol{\beta}^T(\tau) \mathbf{\Psi}(t), \quad (4.5)$$

where  $\boldsymbol{\beta}(\tau)$  is a  $(K - 1) \times 1$  binary selection vector which specifies the desired communication waveform from the dictionary  $\mathbf{\Psi}(t)$  for each slow-time index given that  $\boldsymbol{\beta}^T(\tau) \mathbf{1}_{K-1} = 1, \forall \tau$ .

For the time-invariant communication channels, i.e., the channels do not change with the slow time  $\tau$ , we denote the channel gain between the JRC transmitter and the  $u$ th communication receiver as  $h_u$ . Then, the received signal at the  $u$ th CU takes the following form:

$$s_u(t, \tau) = h_u \mathbf{x}^T(t) \mathbf{a}(\theta_u) + n_u(t) = h_u \tilde{\Delta}_u \psi_{\text{com}}(t) + n_u(t), \quad (4.6)$$

where  $\tilde{\Delta}_u \geq \Delta_u$  and  $n_u(t)$  is the additive complex white Gaussian noise

The communication information is extracted at the communication receivers by estimating the modulated waveform transmitted by the JRC transmit array during

each radar pulse. This is performed by matched filtering of the received signal in Eq. (4.6) with all the communication waveforms as:

$$\begin{aligned} r_u(\tau) &= \frac{1}{T} \int_{t=0}^T s(t, \tau) \psi_k(t) dt \\ &= \begin{cases} h_u \tilde{\Delta}_u + \tilde{n}_u(\tau), & \text{if } \psi_k(t) \text{ was transmitted,} \\ \tilde{n}_u(\tau), & \text{otherwise,} \end{cases} \end{aligned} \quad (4.7)$$

where  $r_u(\tau)$  is the output of the matched filter during the slow-time index  $\tau$  and  $\tilde{n}_u(\tau)$  is the corresponding noise output at the  $u$ th communication receiver.

## 4.2 Chance Constrained Beamforming Design for JRC System

In this section, we present chance constrained beamforming for the JRC system under Rayleigh fading communication channels. Our objective is to optimize the communication performance of the system by incorporating robustness in the beamformer design against communication channel uncertainties through the exploitation of chance constraints. The resulting nonlinear optimization is further relaxed into a convex form by employing the information of probability density function (PDF) of the channel conditions.

### 4.2.1 Incorporating Robustness through Chance Constraint

We assume that the magnitude of the communication channel gain for different radar pulses follows the Rayleigh distribution, i.e. the communication channels vary with the slow time  $\tau$ , such that  $|h_u(\tau)| = \bar{h}_u \tilde{h}_u, \forall \tau$ , where  $\bar{h}_u$  is a constant accounting for the propagation loss and  $\tilde{h}_u \sim \mathcal{R}(\sigma_u)$  with  $\mathcal{R}(\sigma_u)$  denoting Rayleigh distribution with scale parameter (mode) of  $\sigma_u$ . Such a model is relevant as long as the large-scale channel parameters remain constant. Note that  $|h_u(\tau)|$  will follow  $\mathcal{R}(\bar{h}_u \sigma_u)$ .

At the  $u$ th communication receiver, the required minimum signal amplitude is  $\bar{\Delta}_u = \bar{h}_u \Delta_u$ . This amplitude requirement is satisfied by (4.2) for non-fading channels. For fading channels, however, the communication channel gain  $|h_u(\tau)|$  is a stochastic process, and the worse-case value of the received signal amplitude at the  $u$ th

communication receiver,  $\Delta_u |h_u(\tau)| = \bar{\Delta}_u |h_u(\tau)| / \bar{h}_u$ , varies over time. Therefore, the desired communication objective is ensured only if  $|h_u(\tau)| / \bar{h}_u = \tilde{h}_u \geq 1$  holds. As  $|h_u(\tau)| \sim \mathcal{R}(\bar{h}_u \sigma_u)$ , the achieved signal amplitude at the  $u$ th communication receiver can fall below the desired amplitude with a probability  $P(|h_u(\tau)| < \bar{h}_u) = P(\tilde{h}_u < 1)$ .

This illustrates the suboptimal performance exhibited by the optimization (4.2) and emphasizes a need for robust design which incorporates these channel uncertainties.

In order to maintain the communication signal level to be higher than the desired amplitude with a required probability, we employ chance constrained optimization as follows [69]:

$$\begin{aligned}
& \min_{\mathbf{u}_{\text{rad}}, \mathbf{u}_{\text{com}}} && \mathbf{u}_{\text{rad}}^H \mathbf{u}_{\text{rad}} + \mathbf{u}_{\text{com}}^H \mathbf{u}_{\text{com}}, \\
& \text{subject to} && \mathbf{u}_{\text{rad}}^H \mathbf{a}(\theta_{\text{rad}}) = 1, \\
& && \mathbf{u}_{\text{rad}}^H \mathbf{a}(\theta_u) = 0, && \theta_u \in \Theta_{\text{com}}, \\
& && \mathbf{u}_{\text{rad}}^H \mathbf{a}(\theta_{\text{rad,sl}}) \leq \alpha_{\text{rad}}, && \theta_{\text{rad,sl}} \in \Theta_{\text{rad}}^c, \\
& && \mathbf{u}_{\text{com}}^H \mathbf{a}(\theta_{\text{rad}}) = 0, \\
& && P\left(\mathbf{u}_{\text{com}}^H \mathbf{a}(\theta_u) \tilde{h}_u \geq \Delta_u\right) \geq \eta, \quad \theta_u \in \Theta_{\text{com}},
\end{aligned} \tag{4.8}$$

where  $\eta$  is the desired probability ensuring the quality of service such that the constraint  $\mathbf{u}_{\text{com}}^H \mathbf{a}(\theta_u) \tilde{h}_u \geq \Delta_u$  should be true. Since  $\mathbf{u}_{\text{com}}^H \mathbf{a}(\theta_u)$  has a zero imaginary part,  $\mathbf{u}_{\text{com}}^H \mathbf{a}(\theta_u) \tilde{h}_u$  always represents the real transformation of the Rayleigh random variable  $\tilde{h}_u$ .

The optimization problem (4.8) ensures that we achieve the received communication signal level higher than the desired amplitude with a probability  $\eta$ . Such strategy is practical as it will subsequently result in a controlled BER for the communication system by ensuring the desired signal power at the communication receivers.

Note that, if we directly modify the optimization problem (4.2) by replacing the last constraint by  $\mathbf{u}_{\text{com}}^H \mathbf{a}(\theta_u) \geq \Delta_u / \tilde{h}_u$ , such strategy will try to ensure the desired signal level of  $\bar{\Delta}_u$  even if the communication channel undergoes deep fading, resulting in significant power loss. In contrary, the proposed strategy (4.8) ameliorates this requirement by ensuring the communication performance for the  $\eta \times 100\%$  of the

communication interval. This implies that the chance constraints will not be satisfied for  $(1 - \eta) \times 100\%$  of the slow time indexes in the worst channel conditions (left tail of Rayleigh distribution where channel gain is significantly low), thus impeding unnecessary power loss. Practically, the small probability of unsatisfactory signal amplitude is compensated by channel coding to render the desirable BER performance [70].

#### 4.2.2 Convex Relaxation

The chance constraint-based optimization in (4.8) is difficult to solve due to its nonlinearity and the dynamic behavior of the communication channel gain. In the following, we relax this chance constraint into a deterministic constraint by employing the statistical information of the communication channel gain. For this purpose, it is assumed that the PDFs of the communication channels are either known or can be obtained for the chance constraint problem under consideration.

**Theorem 1:** Denote  $\Phi(c) = 1 - e^{-c^2/2}$  as the cumulative distribution function (CDF) of  $c \sim \mathcal{R}(1)$ , and  $\Phi^{-1}(\eta) = [-2\ln(1 - \eta)]^{0.5}$  as the inverse function of  $\Phi(c)$ , where  $\eta$  is the probability. Then, for a Rayleigh random variable  $a \sim \mathcal{R}(\sigma_a)$ , the chance constraint  $\text{P}\{ya \geq b\} \geq \eta$  is equivalent to  $y\sigma_a\Phi^{-1}(1 - \eta) \geq b$  where  $y$  and  $b$  are positive constants.

**Proof:** Let  $\Phi_a(a)$  denote the CDF of  $a$ . We can write

$$\text{P}\{ya \geq b\} = \text{P}\{a \geq b/y\} = 1 - \Phi_a(b/y). \quad (4.9)$$

Because  $a$  follows the distribution  $\mathcal{R}(\sigma_a)$ , its CDF is given by  $\Phi_a(a) = 1 - e^{-a^2/(2\sigma_a^2)}$ . The corresponding inverse function of  $\Phi_a(a)$  takes the form  $\Phi_a^{-1}(\eta) = \sigma_a\Phi^{-1}(\eta)$ .

The chance constraint under consideration subsequently takes the following forms:

$$\begin{aligned}
& \text{P}\{ya \geq b\} \geq \eta \\
\implies & 1 - \Phi_a(b/y) \geq \eta \\
\implies & y\Phi_a^{-1}(1 - \eta) \geq b \\
\implies & y\sigma_a\Phi^{-1}(1 - \eta) \geq b.
\end{aligned}$$

Note that  $\Phi^{-1}(1 - \eta)$  is always positive because the desired probability always follows  $0 \leq \eta \leq 1$  for  $0 \leq c \leq \infty$ . Moreover,  $\sigma_a\Phi^{-1}(1 - \eta)$  is a constant which makes the above constraint deterministic and linear.  $\square$

In the above theorem, we see that the chance constraint can be relaxed into a deterministic constraint using the PDF for the JRC case under consideration. Using this theorem, we replace the chance constraint in (4.8) by the deterministic convex (linear) constraint which results in the following convex optimization formulation [69]:

$$\begin{aligned}
& \min_{\mathbf{u}_{\text{rad}}, \mathbf{u}_{\text{com}}} && \mathbf{u}_{\text{rad}}^{\text{H}} \mathbf{u}_{\text{rad}} + \mathbf{u}_{\text{com}}^{\text{H}} \mathbf{u}_{\text{com}}, \\
& \text{subject to} && \mathbf{u}_{\text{rad}}^{\text{H}} \mathbf{a}(\theta_{\text{rad}}) = 1, \\
& && \mathbf{u}_{\text{rad}}^{\text{H}} \mathbf{a}(\theta_u) = 0, \\
& && \mathbf{u}_{\text{rad}}^{\text{H}} \mathbf{a}(\theta_{\text{rad,sl}}) \leq \alpha_{\text{rad}}, \\
& && \mathbf{u}_{\text{com}}^{\text{H}} \mathbf{a}(\theta_{\text{rad}}) = 0, \\
& && \mathbf{u}_{\text{com}}^{\text{H}} \mathbf{a}(\theta_u) \sigma_u \Phi^{-1}(1 - \eta) \geq \Delta_u.
\end{aligned} \tag{4.10}$$

In practice, we are usually interested in  $\eta \geq 0.9$  for efficient communication. Several different values of  $\eta$  are considered in the simulation evaluations.

It is interesting to observe that for  $\sigma_u = 1$ , if  $\eta = 0.6065$ ,  $\Phi^{-1}(1 - \eta) = 1$  and the optimization (4.10) becomes exactly the same as optimization (4.2). This implies that the solution to the optimization (4.2) ensures the efficient communication only for 60.65% of the communication time.

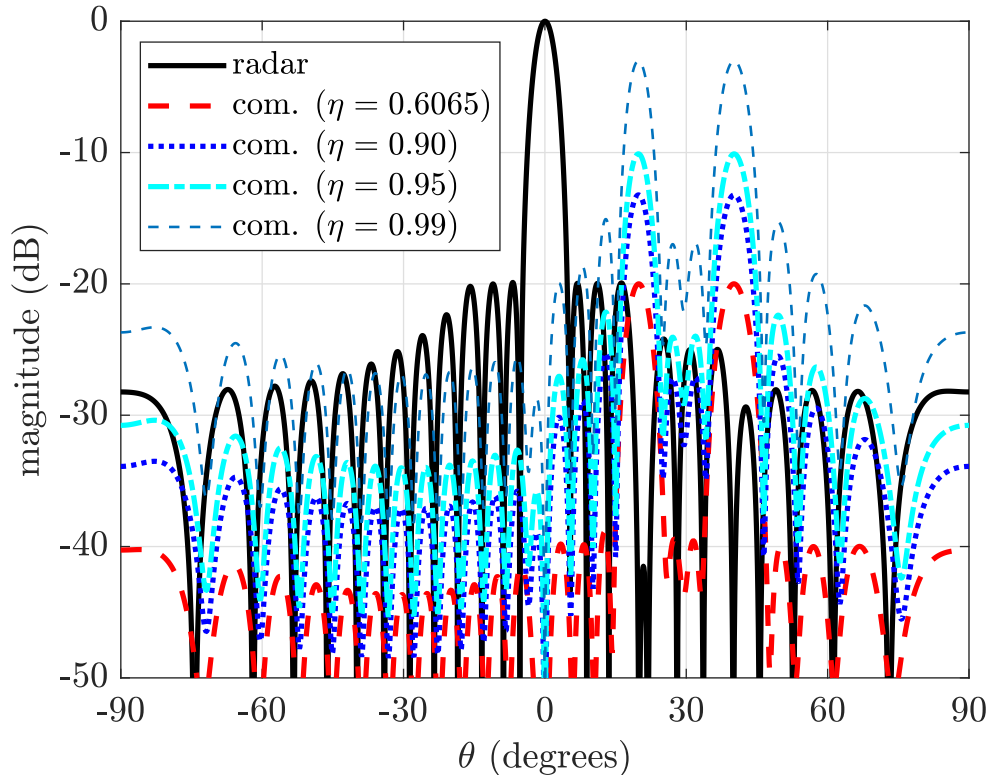


Figure 4.1. Beamforming patterns for different desired probabilities  $\eta$  ( $M = 25, \theta_{\text{rad}} = 0^\circ, \theta_1 = 20^\circ, \theta_2 = 40^\circ, \Delta_u = 0.1, \alpha_{\text{rad}} = 0.1, \sigma_u = 1$ ).

### 4.3 Simulation Results

In this section, we present simulation results illustrating the performance of the JRC system exploiting the proposed chance constrained optimization. In all simulation examples, the transmit JRC system is equipped with a 25-element uniform linear array and the interelement spacing is half a wavelength. The radar main beam is directed towards  $\theta_{\text{rad}} = 0^\circ$ , whereas two CUs are located at  $\theta_1 = 20^\circ$  and  $\theta_2 = 40^\circ$ , respectively. The desired amplitude of the communication signal towards both CUs is assumed to be  $\Delta_u = 0.1$ . The maximum allowable sidelobe level for radar waveform is  $\alpha_{\text{rad}} = 0.1$ . We use the SDPT3 solver [71, 72] with the CVX [65, 66] toolbox for solving the optimization problems.

In the first simulation, we assume  $\sigma_u = 1$  for all the communication channels. The communication beampatterns have been plotted for the cases of  $\eta = 0.6065, 0.9, 0.99$  and  $0.999$ . Fig. 4.1 illustrates the beampatterns extracted for the radar and communication signals by employing the optimization (4.10). Note that the radar beampattern is the same for all cases and its amplitude is below the desired sidelobe levels in its sidelobe regions. Because the radar and communication waveforms are orthogonal to each other, their mutual interference between the radar and communication directions is small, i.e., the radar beampattern has nulls towards the communication directions, and vice versa.

Now we consider the impact of the different values of probability  $\eta$  to the amplitudes of communication beamformers in the directions of communication receivers. It is observed that, in order to achieve the communication objective with a higher probability, higher communication power is transmitted in the direction of CUs. The results shown for  $\eta = 0.6065$  render the results of optimization problem (4.2). In this case, the power utilization is low, and the communication objective is achieved only for 60.65% of the slow time indexes, corresponding to worse communication performance among the results being compared here.

In the second simulation, we fix the probability  $\eta$  to be 0.9. The scale parameter of Rayleigh distribution  $\sigma_u$  for underlying communication channels varies in this simulation for different beamforming weight vectors. However, both CUs experience the same channel conditions. It is observed again in Fig. 4.2 that radar and communication beampatterns minimize their mutual interference. Moreover, as the scale parameter of communication channels increases, less communication power is required to ensure the success probability of  $\eta = 0.9$  for the communication objectives. This is because an increase in the scale parameter for Rayleigh distribution results in an increase in the mean of the distribution which corresponds to higher channel gains.

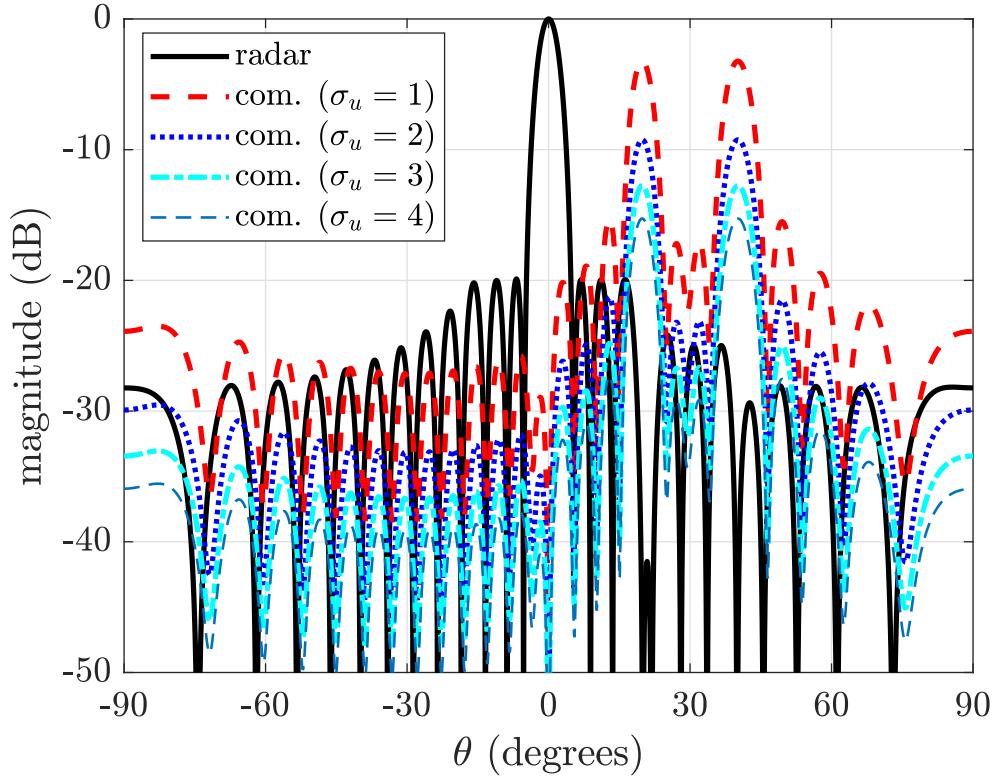


Figure 4.2. Beamforming patterns for different channel scale parameters  $\sigma_u$  ( $M = 25, \theta_{\text{rad}} = 0^\circ, \theta_1 = 20^\circ, \theta_2 = 40^\circ, \Delta_u = 0.1, \alpha_{\text{rad}} = 0.1, \eta = 0.9$ ).

#### 4.4 Remarks

In this chapter, we present the chance constrained programming-based optimization strategy for JRC system. We introduce probabilistic constraints for the communication operation which optimize the transmit power according to the channel conditions and prevent the drain of communication power in case of momentous deep fades. It is also observed that we need more communication power for the cases where communication channels have lower gain or if a high communication success rate is required. Simulation results illustrate the performance of the proposed strategy.

## CHAPTER 5

### POWER-EFFICIENT MULTI-USER JRC SYSTEMS

In this chapter, we propose a novel JRC strategy to ensure maximum transmit power in the radar main beam while exploiting directional power control and waveform diversity. The primary radar objective is achieved without compromising the communication information transmission to the users located in the sidelobe region of radar. Unlike the conventional JRC schemes which transmit equal power in all the radar waveforms [26, 27, 35, 46], the proposed method is able to control the transmit power for each waveform towards radar and communication directions depending on the target reflections. Optimized power allocation results in the highest SNR at the radar receiver to improve target detection. The proposed approach enables multi-user access by transmitting distinct communication symbols in different directions while exploiting the same hardware resources as used by the existing methods [26, 27, 35, 46]. Therefore, the proposed JRC strategy provides much greater flexibility in system design compared to other existing methods. Simulation results demonstrate the effectiveness of the proposed JRC method.

Consider a JRC system consisting of  $M$  linear transmit array elements arranged in an arbitrary fashion. The primary function of the JRC system is to ensure the unperturbed radar operation while performing a secondary communication activity. The objective of the radar operation is to maintain a desired magnitude of the radar signal towards the radar main lobe. Moreover, the JRC system provides communication information to  $U$  users located in the sidelobe region of the radar in different directions. Denote  $P_{\text{total}}$  as the total power transmitted by the antenna array and  $\psi_1(t), \psi_2(t), \dots, \psi_{\hat{K}}(t)$  as the  $\hat{K}$  mutually orthogonal waveforms which are available

to the JRC system. Here,  $t$  is the fast time and each waveform  $\psi_k(t)$  ( $1 \leq k \leq \hat{K}$ ) is normalized to unit average power such that:

$$\frac{1}{T_p} \int_0^{T_p} \psi_{k_1}(t) \psi_{k_2}(t) dt = \delta(k_1 - k_2), \quad 1 \leq k_1, k_2 \leq \hat{K}, \quad (5.1)$$

where  $T_p$  denotes the radar pulse period. To realize the objectives of the JRC system, different beamforming weight vectors are synthesized to enable multiple information streams at the communication receivers while keeping the radar main beam at a constant amplitude. The following optimization problem is formulated for this purpose [46]:

$$\begin{aligned} & \min_{\mathbf{u}_n} \max_{\theta_i} |G e^{j\varphi(\theta_i)} - \mathbf{u}_n^H \mathbf{a}(\theta_i)|, \quad \theta_i \in \Theta_{\text{rad}}, \\ & \text{subject to } |\mathbf{u}_n^H \mathbf{a}(\theta_p)| \leq \varepsilon, \quad \theta_p \in \Theta_{\text{sll}}, \\ & \mathbf{u}_n^H \mathbf{a}(\theta_u) = \delta_u e^{j\phi(\theta_u)}, \quad \theta_u \in \Theta_{\text{com}}, \end{aligned} \quad (5.2)$$

where  $\Theta_{\text{rad}}$  denotes the directions at which the radar main beam operates,  $\Theta_{\text{com}}$  contains the directions of communication receivers, and  $\Theta_{\text{sll}}$  denotes the complement set of  $\Theta_{\text{rad}} \cup \Theta_{\text{com}}$  representing the remaining sidelobe level. In addition,  $\mathbf{a}(\theta)$  is the array manifold vector of the transmit antenna array at angle  $\theta$ ,  $G$  is the desired magnitude of radar main lobe, and  $\varphi(\theta)$  is the desired phase profile of radar at angle  $\theta$ . Further,  $\mathbf{u}_n$  is the desired beamforming weight vector which achieves the sidelobe level  $\delta_u$  with phase  $\phi(\theta_u)$  at the communication receiver located at an angle  $\theta_u$  ( $1 \leq u \leq U$ ). Each pair of  $\delta_u$  and  $\phi(\theta_u)$  can take any of the  $L$  possible sidelobe levels and  $Q$  allowable phase symbols, respectively. Moreover,  $\mathbf{u}_n$  guarantees a sidelobe level having a maximum value of  $\varepsilon$  in the sidelobe region  $\Theta_{\text{sll}}$ .

The transmitted signal from the JRC system can be expressed as:

$$\mathbf{s}(t, \tau) = \sqrt{\frac{P_{\text{total}}}{K}} \sum_{k=1}^K \mathbf{U} \mathbf{b}_k(\tau) \psi_k(t), \quad (5.3)$$

where  $\tau$  is the slow time, and  $\mathbf{U} = [\mathbf{u}_1^*, \mathbf{u}_2^*, \dots, \mathbf{u}_N^*]$  is an  $M \times N$  dictionary matrix which includes  $N$  beamforming weight vectors optimized using Eq. (5.2) such that each beamforming vector results in a unique set of amplitude levels and phase offsets in the directions of communication receivers while keeping the radar beam at a constant amplitude. In addition,  $\mathbf{b}_k(\tau) = [b_{1,k}(\tau), b_{2,k}(\tau), \dots, b_{N,k}(\tau)]^T$  is an  $N \times 1$  selection

vector which chooses the desired beamforming weight vector  $\mathbf{u}_k$  from the dictionary matrix  $\mathbf{U}$  for each transmitted waveform  $\psi_k(t)$ . All the elements in  $\mathbf{b}_k(\tau)$  are zero except only one element equal to 1. We utilize  $K$  ( $\leq \hat{K}$ ) orthogonal waveforms during a radar pulse and it is possible to use different values of  $K$  for each pulse. From Eq. (5.2), note that the amplitudes and phases of the transmitted waveforms towards communication receivers in different directions can be distinct during each radar pulse. Depending on the choice of  $N$  and  $K$ , different schemes [46] can be realized using Eqs. (5.2) and (5.3).

## 5.1 Proposed Information Embedding Strategy

We observed that the existing JRC techniques do not optimize the maximum possible energy which can be transmitted in the direction of radar main beam. Moreover, each waveform  $\psi_k(t)$  in the radar pulse is transmitted with an equal power towards the main beam of radar. In practice, it is desirable that the radar beam be operated on the highest possible amplitude to efficiently detect long-distance targets. In addition, modern radars change the power allocation for each transmitted frequency to ensure the best performance when the RCS of the target is frequency-dependent [43]. Therefore, it is also important for future JRC systems to offer power allocation capabilities.

### 5.1.1 Proposed Information Embedding

In our proposed approach, we optimize the amplitude of each radar waveform towards the radar main beam given the RCS-dependent power allocation for each waveform. Fig. 5.1 shows the basic principle of the proposed method. We generate  $K$  ( $\leq \hat{K}$ ) beamforming weight vectors  $\mathbf{u}_k$  such that each vector corresponds to one of the available radar waveforms  $\psi_k(t)$  where  $1 \leq k \leq K$ . The signal transmitted from the JRC platform can be expressed in the following form:

$$\mathbf{s}(t, \tau) = \sum_{k=1}^K \mathbf{u}_k^*(\tau)(\tau)\psi_k(t), \quad (5.4)$$

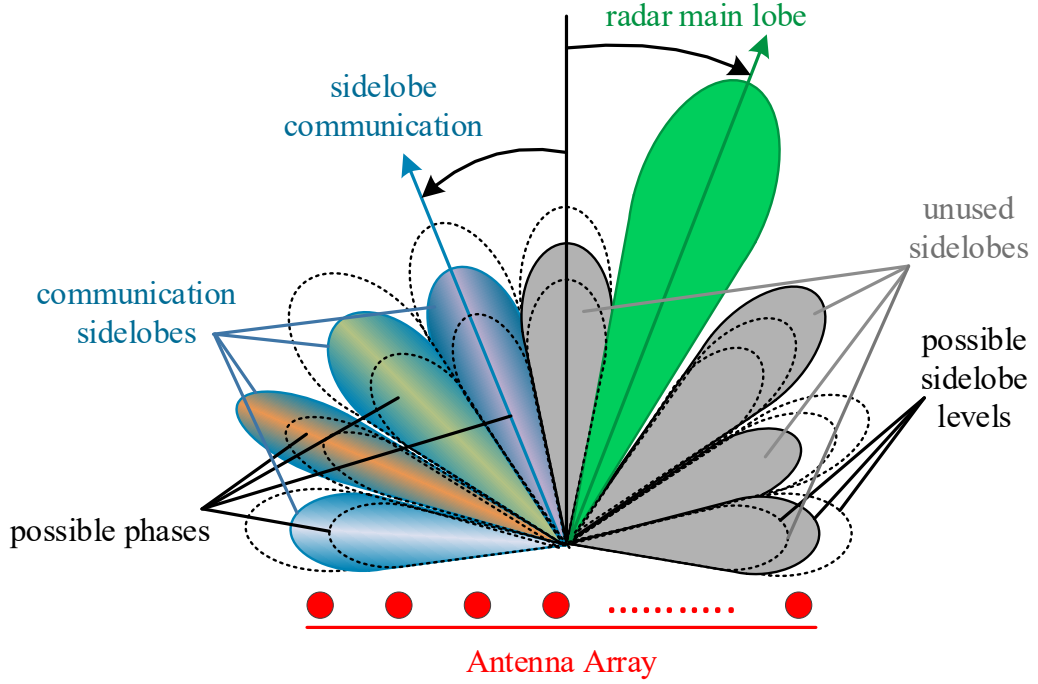


Figure 5.1. The proposed JRC strategy.

where  $\mathbf{u}_k$  can be changed for each pulse time  $\tau$  depending on the desired phase and amplitude levels towards the radar beam and the CUs. The beamforming weight vector  $\mathbf{u}_k$  can be calculated using the following optimization problem (note that  $\tau$  is omitted for notational simplicity) [45]:

$$\begin{aligned}
 & \max_{\mathbf{u}_k} G_k \\
 & \text{subject to } |G_k e^{j\varphi_k(\theta_i)} - \mathbf{u}_k^H \mathbf{a}(\theta_i)| = 0, & \theta_i \in \Theta_{\text{rad}}, \\
 & \mathbf{u}_k^H \mathbf{a}(\theta_u) = \delta_u e^{j\phi(\theta_u)}, & \theta_u \in \Theta_{\text{com}}, \\
 & |\mathbf{u}_k^H \mathbf{a}(\theta_p)| \leq \varepsilon, & \theta_p \in \Theta_{\text{sll}}, \\
 & \sum_{\theta_q} |\mathbf{u}_k^H \mathbf{a}(\theta_q)|^2 = P_k, & \theta_q \in \Theta_{\text{all}}, \\
 & \sum_{\theta_i} |\mathbf{u}_k^H \mathbf{a}(\theta_i)|^2 = \gamma_k P_k, & \theta_i \in \Theta_{\text{rad}}, \\
 & \sum_{\theta_p} |\mathbf{u}_k^H \mathbf{a}(\theta_p)|^2 = (1 - \gamma_k) P_k, & \theta_p \in \bar{\Theta}_{\text{rad}},
 \end{aligned} \tag{5.5}$$

where  $G_k$  is the amplitude of each transmitted waveform  $\psi_k(t)$  in the direction of the radar main beam, and  $P_k$  denotes the total power available to the JRC platform for the waveform  $\psi_k(t)$ . Moreover,  $\gamma_k$  ( $\gamma_k \in [0, 1]$ ) and  $1 - \gamma_k$ , respectively, denote the power proportion designated for radar operation and for radar sidelobes  $\Theta_{\text{com}} \cup \Theta_{\text{sll}}$  by the waveform  $\psi_k(t)$ . In addition,  $\Theta_{\text{all}}$  contains all the angles from  $-90^\circ$  to  $90^\circ$  and  $\bar{\Theta}_{\text{rad}}$  represents the complement set of  $\Theta_{\text{rad}}$ . Note that the proposed approach aims to maximize the transmitted power in the radar main beam while considering the power allocated to radar and communication systems.

Alternatively, the optimization problem in Eq. (5.5) can be relaxed as a convex optimization problem as follows [45]:

$$\begin{aligned}
& \min_{\mathbf{u}_k} \quad -G_k \\
& \text{subject to} \quad |G_k e^{j\varphi_k(\theta_i)} - \mathbf{u}_k^H \mathbf{a}(\theta_i)| \leq \beta_{\text{tol}}, \quad \theta_i \in \Theta_{\text{rad}}, \\
& \quad \mathbf{u}_k^H \mathbf{a}(\theta_u) = \delta_u e^{j\phi(\theta_u)}, \quad \theta_u \in \Theta_{\text{com}}, \\
& \quad |\mathbf{u}_k^H \mathbf{a}(\theta_p)| \leq \varepsilon, \quad \theta_p \in \Theta_{\text{sll}}, \\
& \quad |\mathbf{u}_k^H \mathbf{A}(\Theta_{\text{all}})|_2 \leq \sqrt{P_k}, \\
& \quad |\mathbf{u}_k^H \mathbf{A}(\Theta_{\text{rad}})|_2 \leq \sqrt{\gamma_k P_k}, \\
& \quad |\mathbf{u}_k^H \mathbf{A}(\bar{\Theta}_{\text{rad}})|_2 \leq \sqrt{(1 - \gamma_k) P_k},
\end{aligned} \tag{5.6}$$

where  $\beta_{\text{tol}}$  is the error tolerance for the desired radar beampattern in the main beam and  $\mathbf{A}(\Theta) = [\mathbf{a}(\theta_1), \mathbf{a}(\theta_2), \dots, \mathbf{a}(\theta_j)]$  with  $\{\theta_1, \theta_2, \dots, \theta_j\} \in \Theta$ . From Eqs. (5.4)-(5.6), the maximum power  $P_{\text{rad}}$  and  $P_{\text{com}}$  transmitted in the radar main beam and the sidelobe region, respectively, can be expressed as:

$$P_{\text{rad}} \leq \sum_{k=1}^K \gamma_k P_k, \quad P_{\text{com}} \leq \sum_{k=1}^K (1 - \gamma_k) P_k. \tag{5.7}$$

Thus, the maximum power transmitted from antenna array is  $P_{\text{total}} = P_{\text{rad}} + P_{\text{com}}$ .

From Eqs. (5.4) and (5.6), it can be observed that different radar waveforms can be transmitted with different power levels towards the main lobe. Moreover, we have an added flexibility to maximize the transmitted power in radar main beam while ensuring the communication performance within the power constraints for the

communications and radar purpose. These power allocations can change with respect to target response and communication environment.

For example, we can control the maximum transmitted energy of each frequency component for the transmission based on OFDM by controlling the power  $P_k$  of the corresponding subcarrier  $\psi_k(t)$ . This can be helpful to enhance the target characterization with frequency-dependent RCS [43]. In this context, a higher SNR can be achieved by maximizing the radar amplitudes in the frequencies where RCS is high (by selecting appropriate  $P_k$  and  $\gamma_k$ ). This strategy results in an improved SNR for radar receiver, whereas CUs are still entertained with all the desired frequencies by allowing  $(1 - \gamma_k)P_k$  power towards the radar sidelobe region.

### 5.1.2 Detection Communication Receiver

The signal received at the  $r$ th communication receiver at the angle  $\theta_u$  can be expressed as:

$$x_u(t, \tau) = h_u(\tau) \mathbf{a}^T(\theta_u) \mathbf{s}(t, \tau) + n_u(t), \quad (5.8)$$

where  $h_u(\tau)$  is the channel coefficient summarizing the propagation environment between the transmit array and  $r$ th CU, and  $n_u(t)$  is the zero-mean additive white Gaussian noise. Matched filtering of the received signal  $x_u(t, \tau)$  to each of the  $K$  ( $\leq \hat{K}$ ) possible waveforms at the  $r$ th communication receiver yields the following scalar:

$$\begin{aligned} y_{u,k}(\tau) &= \frac{1}{T_p} \int_0^{T_p} x_u(t, \tau) \psi_k(t) dt \\ &= \begin{cases} \sqrt{\frac{P_{\text{total}}}{K}} \alpha_u(\tau) \delta_u + n_{u,k}(\tau), & \text{if } \psi_k(t) \text{ transmitted,} \\ n_{u,k}(\tau), & \text{otherwise,} \end{cases} \end{aligned} \quad (5.9)$$

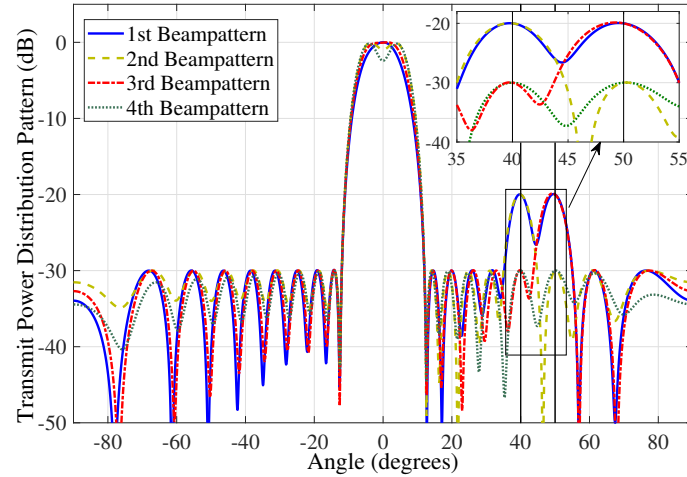
where  $n_{u,k}(\tau)$  is the noise at the output of  $k$ th matched filter. By analyzing  $y_{u,k}(\tau)$  at the  $r$ th communication receiver located in the direction of  $\theta_u$ , the receiver can determine the respective amplitude and phase to decode the embedded communication information.

### 5.1.3 Sum Data Rate Analysis

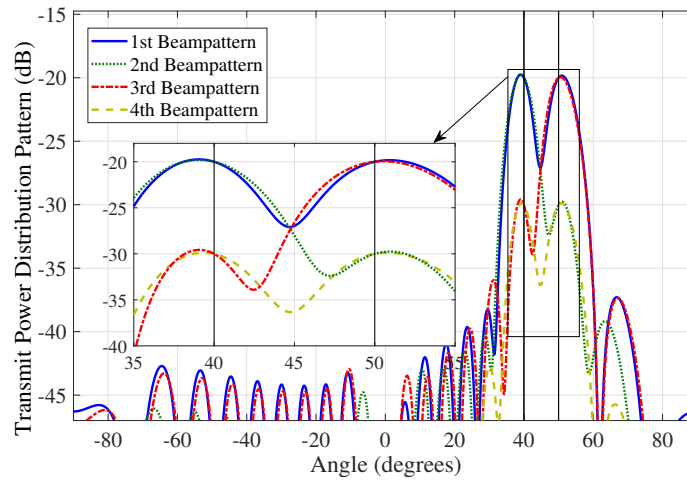
We calculate the sum data rate which can be received by the  $U$  sidelobe CUs located in distinct directions within the sidelobe region of the radar. Considering  $K$  orthogonal waveforms,  $L$  sidelobe levels, and  $Q$  phases for each CU, Eq. (5.4) can be utilized to determine the information capacity during each radar pulse. It can be observed that  $\log(LQ)$  bits can be transmitted with each radar waveform  $\psi_k(t)$  at each communication receiver when  $L$  sidelobe levels and  $Q$  phases are exploited. This implies that the total number of bits which can be transmitted during each radar pulse is  $UK \log(LQ)$ . It is important to note that the information streams transmitted to each communication receiver may or may not be distinct, respectively corresponding to multi-user access and broadcast modes.

## 5.2 Simulation Results

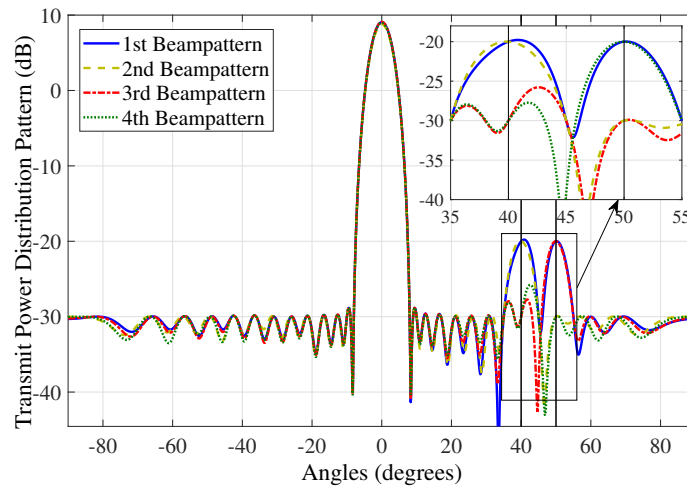
We consider a ULA consisting of 20 transmit antennas. The primary function of the radar is to form a main beam between  $-5^\circ$  and  $5^\circ$ . There are two communication receivers ( $U = 2$ ) located in the sidelobe region at  $40^\circ$  and  $50^\circ$ , respectively. For each CU located at  $\theta_u$  ( $1 \leq u \leq U$ ), we consider two possible sidelobe levels ( $L = 2$ ) and two different phases ( $Q = 2$ ). These corresponding sidelobe levels  $\delta_u$  can either be 0.1 (i.e.,  $-20$  dB) or 0.0316 (i.e.,  $-30$  dB) at each communication receiver during each radar pulse. Similarly, the projected phases  $\phi(\theta_u)$  at each communication receiver can take a value of 0 or  $\pi$  radians. Using Eq. (5.6), we can generate the beamforming weight vectors which satisfy these specifications. We exploit  $K = 1,024$  OFDM subcarriers with a bandwidth of 100 MHz centered at 3 GHz to achieve the JRC objectives. For the case of equal power transmission through all the OFDM subcarriers (i.e.,  $P_1 = P_2 = \dots = P_{1024}$ ), we design four different beampatterns using Eq. (5.6) as shown in Fig. 5.2(a). It can be observed that each beampattern has a unique set of sidelobe levels for the CUs while maintaining the 0 dB amplitude in radar main beam.



(a) Case I: Beam pattern synthesis for equal power in all subcarriers



(b) Case II: Beam patterns for subcarriers with low target reflectivity



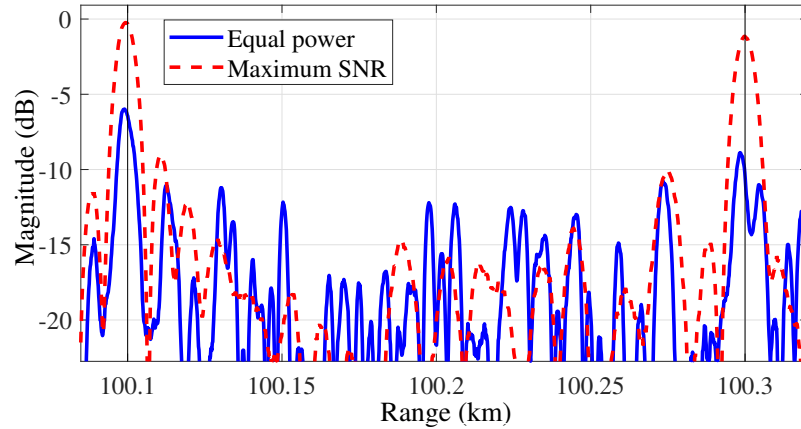
(c) Case II: Beam patterns for subcarriers with high target reflectivity

Figure 5.2. Example beam patterns using the proposed approach (ULA with  $M = 20$ ,  $U = 2$  at  $40^\circ$  and  $50^\circ$ ).

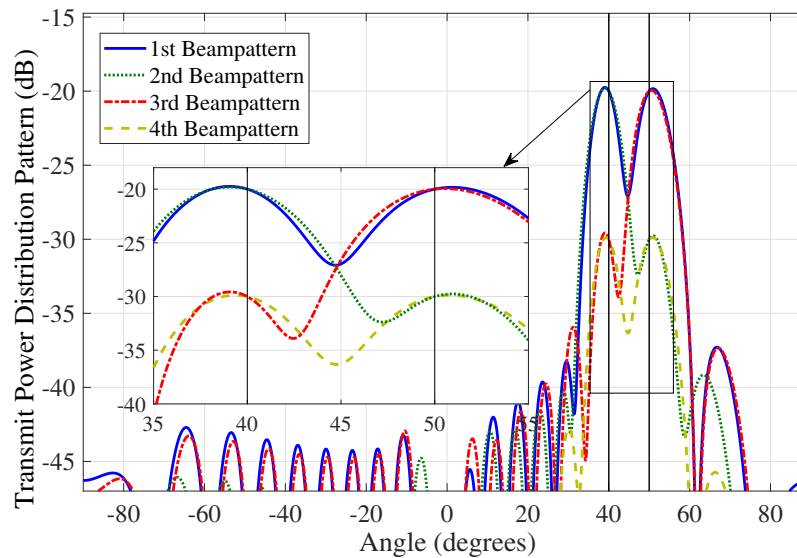
Next, we consider two point targets located within the radar main beam at 100.1 km and 100.3 km, respectively, from the JRC system. The targets are assumed to have a high electromagnetic reflectivity for only 400 OFDM subcarriers clustered at the center of the transmitted bandwidth. This information about RCS can be achieved by calculating the spectrum of the reflected signal at radar receiver. To achieve the optimal SNR for the radar system, the JRC platform is optimized for the subsequent radar pulses such that more power is allocated to the frequencies with a higher target reflectivity. In this context, Fig. 5.2(b) shows the respective transmit beampatterns for the subcarriers with low target reflectivity, whereas Fig. 5.2(c) corresponds to the transmit beampatterns for the highly reflected subcarrier. From Fig. 5.2(b) and Fig. 5.2(c), it can be observed that the transmitted energy in the radar main beam varies for different frequencies without deteriorating the communication performance. It is important to note that the magnitude response of all the beampatterns in Fig. 5.2 remains the same for different possible phases  $\phi(\theta_u)$  at the communication receivers. Therefore, we have only shown the beampatterns for  $\phi(\theta_u) = 0$  at each communication receiver.

In Fig. 5.3, we present the range estimation and symbol error rate performance for the cases of equal power and optimal SNR. The radar range is estimated using the technique illustrated in [23] by considering a radar range cell from 100 km to 101.5 km. Additive white Gaussian noise of equal power is considered for both cases at the radar receiver. It can be observed from Fig. 5.3(a) that the optimal SNR provides considerable performance enhancement in range estimation. This is a significant improvement since the total power transmitted by the array and the total power projected in the radar main beam are kept constant for both cases. The only difference is the transmitted power for different subcarriers based on the RCS. The proposed approach provides better performance because more power is allocated to the frequencies which are highly reflected by the targets.

Communication performance is illustrated in Fig. 5.3(b) in terms of symbol error rate. We consider coherent QAM-based approach [38] by exploiting two phases and two available sidelobe levels for each transmitted OFDM waveform ( $L = 2, Q =$



(a) Radar range profile for equal power and max. SNR case



(b) Case II: Beam patterns for subcarriers with low target reflectivity

Figure 5.3. Range estimation and symbol error rate performance for the proposed technique.

2,  $K = 1,024$ ). Note that independent data streams are transmitted to both communication receivers simultaneously. Only one curve is plotted here because the symbol error rates for the case of equal power and optimal SNR are the same. This is because the change in radar main beam does not deteriorate the required signal amplitudes and phases at the communication receivers which can be observed in Fig. 5.2. Thus, the improvement in radar range estimation is achieved without compromising the performance of communication system and utilizing the same power resources. Thus,

the simulation results illustrate the effective performance achieved by the proposed JRC strategy.

### 5.3 Remarks

A novel JRC strategy was proposed to ensure the maximum SNR in the radar main lobe by optimizing the transmit beampattern considering the power allocations for radar and communication operation. The proposed method allocates the desired power in radar and communication directions for each transmitted waveform based on the RCS. Optimized power allocation results in higher SNR at the radar receivers which enables a better characterization of targets. While ensuring the radar's objectives, the proposed approach transmits distinct amplitudes and phases in different directions enabling the multi-user access. As an example, OFDM subcarriers are used as the radar waveforms for performing JRC objectives. The power of different subcarriers towards radar main beam was varied by inspecting the target returns while keeping the total transmitted energy constant for radar and communication objectives. The proposed JRC strategy resulted in improved target detection without any degradation in the performance of communication system.

## CHAPTER 6

### SENSOR SELECTION FOR BEAMFORMING-BASED JRC SYSTEMS

An antenna array-based JRC system employs the beamforming strategy to steer the transmit signals in different directions such that different beamforming weight vectors are exploited which perform the corresponding radar-communication objectives. Such functionality has been provisioned in the spectrally congested environments where both systems are destined to coexist. The transmit antenna selection has become an increasingly interesting topic as the antennas become significantly cheaper and smaller relative to the up-conversion chains. In this chapter, we address the problem of antenna selection for the JRC system by employing a re-weighted  $\ell_1$ -norm minimization naturally yielding the low-complexity solution compared to the exhaustive  $\ell_0$ -norm-based optimization. We present the mathematical framework for the proposed approach in the context of the individual as well as grouped beamforming weight vectors and analyze the practical applicability of the proposed approach for both cases. We argue that the grouped approach for optimizing the JRC antenna selection is hardware-efficient compared to the antenna selection for individual beamforming weight vectors. Simulation results illustrate that the proposed technique significantly reduces the number of required antennas while simultaneously satisfying the radar and communication system objectives [73, 74].

In a JRC transmitter, a radio transmission chain, which consists of a digital-to-analog converter, a mixer, and a power amplifier, is often much more expensive than the transmit antennas. Therefore, to achieve a high system performance at a low cost, a recent trend is to place more antennas than the available number of expensive radio transmission chains. Ideally, it is desirable to automatically switch the available chains to the best subset of antennas which provides the optimized per-

formance for the whole system. Therefore, optimal antenna selection has a crucial importance in the modern systems. Several research efforts have been made in this direction for different radar and communication applications. In [75, 76], antenna selection has been discussed for a distributed multiple-input multiple-output (MIMO) radar to achieve the radar's objective in terms of desired mean-squared error. For the communication systems, [77–79] discuss the antenna selection strategies using convex optimization and sparsity-aware techniques. Sensor selection-based beamforming is discussed in [80–82]. Distributed JRC systems also enjoy optimal transmit antenna selection such that the desired communication capacity and radar performance are achieved [52]. For antenna array-based JRC systems, an array partitioning-based approach is employed in [83] where the functional antennas are split into two subarrays respectively performing the radar and communications operations. Similarly, [84] addresses the optimal antenna selection at the receiver side of JRC systems to maximize the signal-to-interference-plus-noise ratio. Iterative optimization-based optimal antenna selection for array-based JRC schemes was discussed in [47, 85]. Note that the existing antenna array-based JRC antenna selection schemes employing the sidelobe modulation principle select different antennas for different beamforming weight vectors. Such a scenario results in frequent and unavoidable antenna switching during the JRC operation, complicating the hardware implementation and degrading the applicability in practice.

In this chapter, our focus is on antenna array-based JRC system which exploits beamformers to perform radar operation whereas the communication operation is enabled in the radar sidelobe region by employing QAM-based sidelobe modulation. The waveforms responsible to perform the radar task are also utilized to satisfy the requirements of the communication system. An example of such a system is illustrated in Fig. 6.1. The radar objective in this JRC system is to maintain a specific beamforming gain in the sector of radar interest. The communication information is transmitted by varying the transmit amplitudes as well as the phases towards the communication user directions located in the sidelobe region of the radar. The objective of our optimization approach is to select the minimum number of antennas

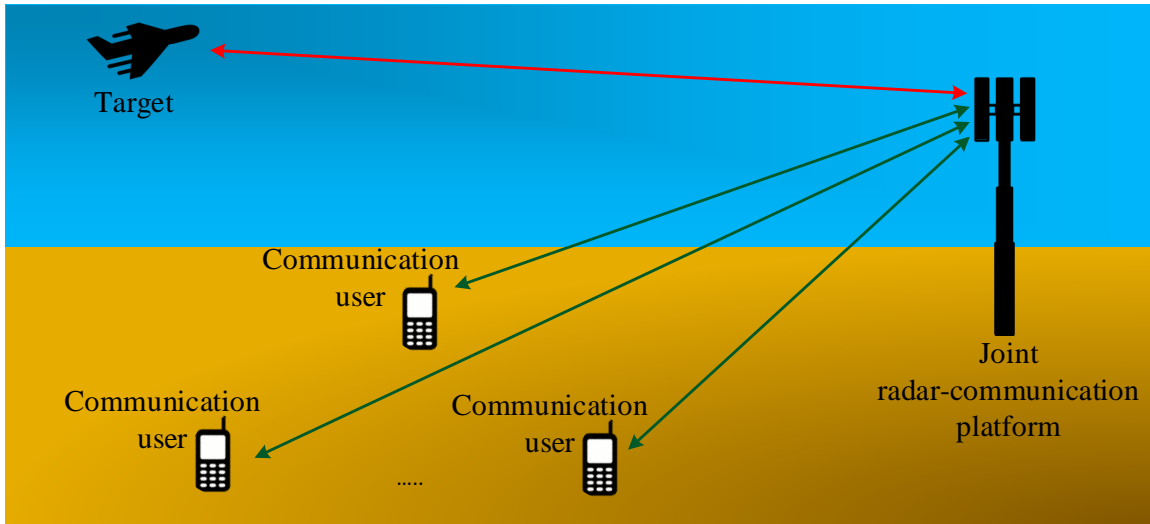


Figure 6.1. Basic principle of the joint radar-communication system.

which satisfy the required radar and communications operations. We present the convex optimization-based mathematical formulation which addresses this objective in two different ways. First, we present an optimal antenna selection strategy for individual beamforming weight vectors employing the QAM-based sidelobe modulation approach. As the selected antennas for different beamformers are generally different, the resulting solutions can result in frequent antenna switching. To tackle this problem, we also develop a group sparsity-based approach in which the same set of antennas is used for all beamformers without any antenna switching.

The chapter is organized as follows. First, we reiterate the JRC system model. Subsequently, the proposed optimal antenna selection strategy for the JRC system is presented. Finally, the comparative analysis of the proposed approaches is provided in in the form of simulation results.

## 6.1 Signal Model of JRC system

We consider an antenna array-based JRC system consisting of  $M$ -element transmit linear array of an arbitrary configuration. The JRC system employs the antenna array beamformers to satisfy the transmit gain objective within the radar main beam. The

same beamformers are responsible to transmit communication information within the sidelobe region such that the radar operation is not perturbed.

Consider the radar surveillance region, the sidelobe region, and the transition region from main beam to sidelobe denoted by  $\Theta_{\text{rad}}$ ,  $\Theta_{\text{sl}}$ , and  $\Theta_{\text{trans}}$ , respectively. There are a total of  $U$  communication users located within the sidelobe region of the radar. The objective of JRC antenna array is to maintain the transmit gain  $G_{\text{rad}}$  in the main beam of the radar, whereas the sidelobe region of the radar should be lower than a threshold  $\varepsilon_{\text{sl}}$ . The communication operation should be enabled by transmitting distinct phases and amplitudes towards the communication receivers. The beamforming weight vector  $\mathbf{u}_n$  which satisfies these objectives can be extracted using the following optimization [26, 46]:

$$\begin{aligned} \min_{\mathbf{u}_n} \max_{\theta_r} & \left| G_{\text{rad}} e^{j\varphi(\theta_r)} - \mathbf{u}_n^H \mathbf{a}(\theta_r) \right|, & \theta_r \in \Theta_{\text{rad}}, \\ \text{s.t.} & \left| \mathbf{u}_n^H \mathbf{a}(\theta_\varepsilon) \right| \leq \varepsilon_{\text{sl}}, & \theta_\varepsilon \in \Theta_{\text{sl}}, \\ & \mathbf{u}_n^H \mathbf{a}(\theta_u) = e^{j\phi_{n,u}} \Delta_{n,u}, & c = 1, \dots, C. \end{aligned} \quad (6.1)$$

where  $\mathbf{u}_n$  achieves the sidelobe level  $\Delta_{n,u}$  and the phase  $e^{j\phi_{n,c}}$  towards the  $u$ th ( $u = 1, \dots, U$ ) communication receiver located at angle  $\theta_u$  such that  $\theta_u \in \Theta_{\text{sl}}$ . The parameter  $e^{j\varphi(\theta_u)}$  represents the phase profile of the radar in the main beam. We use the phase profile  $e^{j\varphi(\theta_r)}$  as a free parameter in the above optimization in order to achieve better approximation of the desired beampattern [47]. Such phase response can be first extracted by designing a beamforming weight vector which only satisfies the radar objective within the main beam. Also, there are other phase adjustment techniques as in [47, 86]. The array response vector of the JRC transmit system at the angle  $\theta$  is given by

$$\mathbf{a}(\theta) = [e^{j2\pi d_1 \sin(\theta)/\lambda}, e^{j2\pi d_2 \sin(\theta)/\lambda}, \dots, e^{j2\pi d_M \sin(\theta)/\lambda}]^T,$$

where  $d_m$  is the location of  $m$ th ( $m = 1, \dots, M$ ) antenna and  $\lambda$  is the transmit signal wavelength.

The optimization (6.1) can be exploited to extract a dictionary of  $N$  beamforming vectors where each vector transmits a specific phase and magnitude towards different

communication receivers. Note that the optimization (6.1) enables multiple-access communication as the values of  $\Delta_{n,u}$  and  $e^{j\phi_{n,u}}$  can be different for each communication receiver for the same beamformer. If  $L$  and  $P$  respectively denote the desired possible number of amplitudes and phases at each communication receiver, we will require  $N = (LP)^U$  unique beamforming weight vectors. Note that if  $\Theta_{\text{rad}}$  contains only one angle, the optimization (6.1) corresponds to the focused beampattern design. On the other hand, if  $\Theta_{\text{rad}}$  contains multiple angles corresponding to a sector, the optimization (6.1) corresponds to the flat-top beampattern synthesis.

The JRC system exploits dual-purpose waveforms, i.e. the same waveforms which serve the radar purpose are also utilized to perform the communication operation. Consider that the JRC system exploits  $K$  possible orthogonal dual-purpose waveforms  $\psi_1(t), \psi_2(t), \dots, \psi_K(t)$  such that:

$$\frac{1}{T} \int_0^T \psi_{k_1}(t) \psi_{k_2}(t - \Delta T) dt = \delta(k_1 - k_2 - \Delta T), \quad 1 \leq k_1, k_2 \leq K, \quad (6.2)$$

where  $t$  denotes the fast time,  $T$  is the time duration of each radar pulse,  $k_1$  and  $k_2$  are the positive integers,  $\delta(\cdot)$  is the Kronecker delta function, and  $\psi_{k_2}(t - \Delta T)$  denotes the time delayed version of  $\psi_{k_2}(t)$  such that  $\Delta T < T$ .

When the beamforming vector  $\mathbf{u}_n$  is selected, the transmit signal from the JRC antenna array takes the following form:

$$\mathbf{x}(t) = \mathbf{u}_n \psi_k(t). \quad (6.3)$$

The above beamforming vector satisfies the gain criteria of the main beam and projects the QAM symbols of amplitude  $\Delta_{n,u}$  and phase  $e^{j\phi_{n,u}}$  towards the communication directions. The JRC system can change the transmitted communication information by changing the beamforming vectors [46].

## 6.2 Transmit Antenna Selection Strategy for JRC System

We propose the antenna selection strategy for transmit beamforming-based JRC system as illustrated in Fig. 6.2. Our objective is two-fold: Design the beamforming weight vector for the JRC system which (a) use the least possible number of antennas,

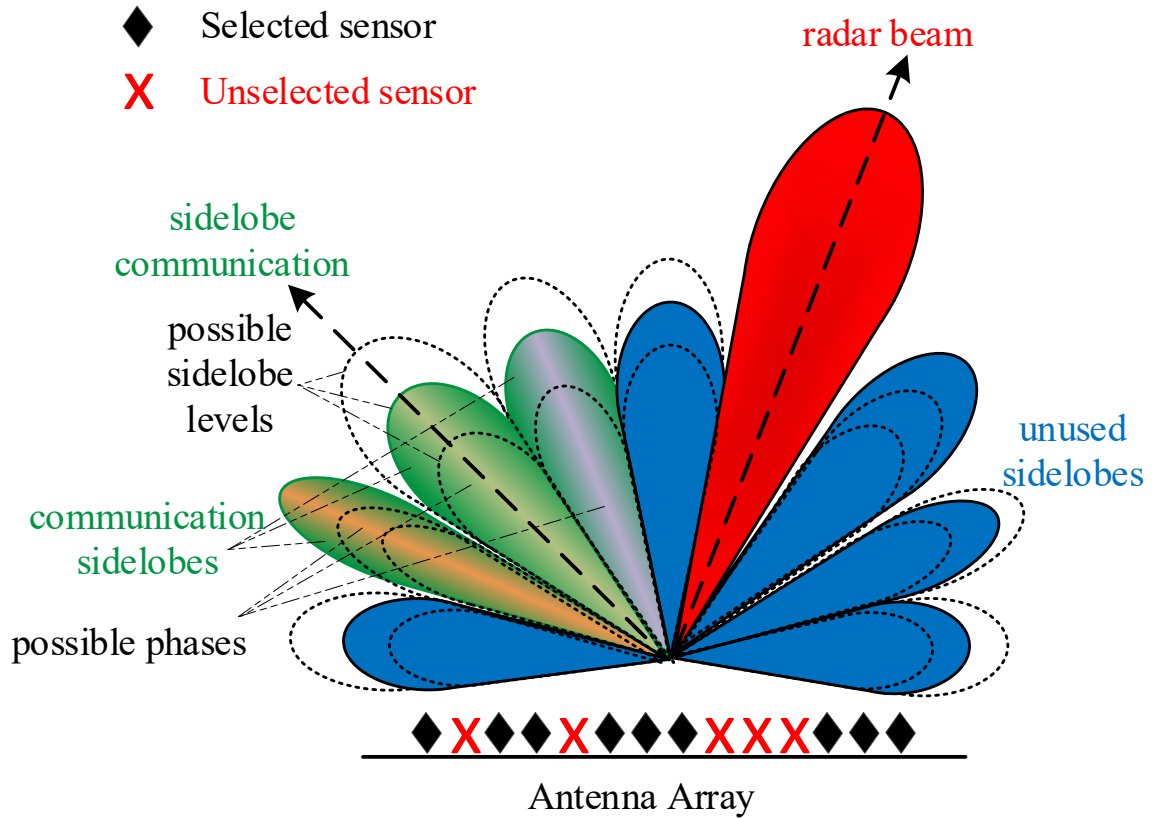


Figure 6.2. The proposed antenna selection strategy for joint radar-communication system.

(b) exploit minimum transmit power. As both objectives can be conflicting, we give more precedence to the first objective. In this context, two cases are discussed. In the first case, transmit antennas are selected for each beamforming weight vector separately. This strategy might result in the activation of different antennas for different beamforming weight vectors. On the other hand, the second approach discusses the joint antenna selection strategy for multiple beamforming weight vectors which exploits the same antennas for all the beamforming weight vectors without any antenna switching.

### 6.2.1 Transmit Antenna Selection for Individual Beamformers

For a given JRC antenna array, beamforming weight vector which minimizes the total transmit power  $|\mathbf{u}_n|_2^2$  can be expressed as follows:

$$\begin{aligned}
& \min_{\mathbf{u}_n} && |\mathbf{u}_n|_2^2 \\
& \text{s.t.} && |G_{\text{rad}}e^{j\varphi(\theta_r)} - \mathbf{u}_n^H \mathbf{a}(\theta_r)| \leq \gamma_{\text{tol}}, \quad \theta_r \in \Theta_{\text{rad}}, \\
& && |\mathbf{u}_n^H \mathbf{a}(\theta_\varepsilon)| \leq \varepsilon_{\text{sl}}, \quad \theta_\varepsilon \in \Theta_{\text{sl}}, \\
& && \mathbf{u}_n^H \mathbf{a}(\theta_u) = \Delta_{n,u} e^{j\phi_{n,u}}, \quad u = 1, \dots, U,
\end{aligned} \tag{6.4}$$

where  $\gamma_{\text{tol}}$  is the tolerance illustrating the maximum possible deviation from the desired main beam profile. Although the above optimization achieves the minimum power for the JRC system, it does not ensure the best antenna selection for the JRC operation because  $\ell_2$ -norm does not encourage sparsity. We can modify the above optimization to select the best  $\bar{M} (< M)$  or fewer antennas in the antenna array as follows:

$$\begin{aligned}
& \min_{\mathbf{u}_n} && |\mathbf{u}_n|_2^2 \\
& \text{s.t.} && |G_{\text{rad}}e^{j\varphi(\theta_r)} - \mathbf{u}_n^H \mathbf{a}(\theta_r)| \leq \gamma_{\text{tol}}, \quad \theta_r \in \Theta_{\text{rad}}, \\
& && |\mathbf{u}_n^H \mathbf{a}(\theta_\varepsilon)| \leq \varepsilon_{\text{sl}}, \quad \theta_\varepsilon \in \Theta_{\text{sl}}, \\
& && \mathbf{u}_n^H \mathbf{a}(\theta_u) = \Delta_{n,u} e^{j\phi_{n,u}}, \quad u = 1, \dots, U, \\
& && |\mathbf{u}_n|_0 \leq \bar{M}.
\end{aligned} \tag{6.5}$$

Instead of enforcing the hard sparsity constraint which allows the selection of a maximum of  $\bar{M}$  antennas,  $\ell_0$ -penalty can be employed in the objective function to promote sparsity as follows:

$$\begin{aligned}
& \min_{\mathbf{u}_n} && |\mathbf{u}_n|_2^2 + \eta |\mathbf{u}_n|_0 \\
& \text{s.t.} && |G_{\text{rad}}e^{j\varphi(\theta_r)} - \mathbf{u}_n^H \mathbf{a}(\theta_r)| \leq \gamma_{\text{tol}}, \quad \theta_r \in \Theta_{\text{rad}}, \\
& && |\mathbf{u}_n^H \mathbf{a}(\theta_\varepsilon)| \leq \varepsilon_{\text{sl}}, \quad \theta_\varepsilon \in \Theta_{\text{sl}}, \\
& && \mathbf{u}_n^H \mathbf{a}(\theta_u) = \Delta_{n,u} e^{j\phi_{n,u}}, \quad u = 1, \dots, U,
\end{aligned} \tag{6.6}$$

where  $\eta$  is the tuning parameter which controls the balance between the desired power optimization and the number of utilized antennas in the above multi-objective

optimization. In optimization (6.6), the constraint handling the number of active antennas in optimization (6.5) is shifted to the objective function, i.e., (6.6) is a relaxed version of (6.5). In optimization (6), the value of  $\bar{M}$  tends to decrease as the value of  $\eta$  increases. If  $\eta$  takes a very high value, the optimization problem (6.6) will only minimize the number of selected antennas irrespective of the power utilized by the antenna array. Note that for each selection of  $\eta$ , (6.6) provides a corresponding solution of  $\bar{M}$  as well as the selected antennas for the beamforming vector  $\mathbf{u}_n$ . If this value of  $\bar{M}$  obtained from (6.6) is used in the optimization problem (6.5), it will also potentially yield the same selected antennas for the beamforming weight vector. In this chapter, we will only emphasize the optimization of problem (6.6).

Unfortunately, due to the non-convex nature of  $\ell_0$ -norm, the optimization (6.6) requires an exhaustive combinatorial search over all  $C_M^M$  possible sparsity patterns of  $\mathbf{u}_n$ , where the optimization (6.4) must be solved for each of these patterns. We can exploit  $\ell_1$ -norm which offers a close convex approximation of  $\ell_0$ -norm, albeit a weaker and indirect measure of sparsity [87], resulting in the following relaxed version of the optimization (6.6):

$$\begin{aligned}
\min_{\mathbf{u}_n} \quad & |\mathbf{u}_n|_2^2 + \eta|\mathbf{u}_n|_1 \\
\text{s.t.} \quad & |G_{\text{rad}}e^{j\varphi(\theta_r)} - \mathbf{u}_n^H \mathbf{a}(\theta_r)| \leq \gamma_{\text{tol}}, \quad \theta_r \in \Theta_{\text{rad}}, \\
& |\mathbf{u}_n^H \mathbf{a}(\theta_\varepsilon)| \leq \varepsilon_{\text{sl}}, \quad \theta_\varepsilon \in \Theta_{\text{sl}}, \\
& \mathbf{u}_n^H \mathbf{a}(\theta_u) = \Delta_{n,u} e^{j\phi_{n,u}}, \quad u = 1, \dots, U.
\end{aligned} \tag{6.7}$$

Here, it is important to consider the crucially defining difference between the  $\ell_0$ - and  $\ell_1$ -norm for our problem. The larger weights in  $\mathbf{u}_n$  are penalized more heavily than the smaller weights in  $\ell_1$ -norm-based penalty. On the other hand,  $\ell_0$ -norm enforces democratized penalization which results in better sparse solutions because it penalizes all the non-zero weights of  $\mathbf{u}_n$  equally. Therefore, the optimization (6.7) is not an ideal formulation for antenna selection problem as the resulting solution might select more antennas than the exhaustive search-based optimization (6.6). To mollify this disparity, we exploit the re-weighted  $\ell_1$ -norm minimization, originally developed in the context of compressed sensing [87], to penalize the non-zero entries in  $\mathbf{u}_n$  more

democratically. Contrary to  $\ell_1$ -norm-based relaxation where absolute values of all the beamforming coefficients are added, we must consider each coefficient as an independent parameter whose value, if selected, significantly improves the beamforming performance.

In order to enforce the democratic selection of antennas, we introduce a weighting function, inspired by [87], which counteracts the influence of beamforming coefficient magnitude in  $\ell_1$ -norm-based penalty as follows:

$$w_{n,m} = \begin{cases} \frac{1}{|u_{n,m}|}, & \text{if } |u_{n,m}| > 0, \\ \frac{1}{\epsilon}, & \text{if } |u_{n,m}| = 0, \end{cases} \quad (6.8)$$

where  $u_{n,m}$  is  $m$ th ( $m = 1, \dots, M$ ) coefficient in  $\mathbf{u}_n$ , and  $\epsilon$  is a very small number. Thus, the weighting vector corresponding to the beamforming weight vector  $\mathbf{u}_n$  can be represented as  $\mathbf{w}_n = [w_{n,1}, w_{n,2}, \dots, w_{n,M}]^T$ . If the optimal solution  $\mathbf{u}_n^{\text{opt}}$  of the optimization (6.6) is  $\bar{M}$ -sparse, i.e.  $|\mathbf{u}_n^{\text{opt}}|_0 = \bar{M}$ , the following optimization will tend to obtain the correct solution analogous to  $\ell_0$ -norm penalty in the optimization (6.6):

$$\begin{aligned} \min_{\mathbf{u}_n} \quad & |\mathbf{u}_n|_2^2 + \eta |\mathbf{u}_n^{(i)} \odot \mathbf{w}_n|_1 \\ \text{s.t.} \quad & |G_{\text{rad}} e^{j\varphi(\theta_r)} - \mathbf{u}_n^H \mathbf{a}(\theta_r)| \leq \gamma_{\text{tol}}, \quad \theta_r \in \Theta_{\text{rad}}, \\ & |\mathbf{u}_n^H \mathbf{a}(\theta_\varepsilon)| \leq \varepsilon_{\text{sl}}, \quad \theta_\varepsilon \in \Theta_{\text{sl}}, \\ & \mathbf{u}_n^H \mathbf{a}(\theta_u) = \Delta_{n,u} e^{j\phi_{n,u}}, \quad u = 1, \dots, U. \end{aligned} \quad (6.9)$$

The above optimization is executed iteratively and  $\mathbf{w}^{(i)}$  denote the weights for the  $i$ th iteration. Such type of weighted optimization strategy is known to have a quick convergence [87]. We have observed the convergence of the algorithm in very few steps through simulations. The weighting vector  $\mathbf{w}_n$  forces the small entries of the beamforming vector  $\mathbf{u}_n$  to zero in the subsequent iteration. The small parameter  $\epsilon$ , which should ideally be slightly smaller than the expected smallest non-zero magnitude of  $\mathbf{u}_n$ , provides stability and ensures that a zero-valued entry does not prohibit a non-zero estimate of the corresponding beamforming coefficient in the next step. The detailed algorithm for extracting the beamforming weight vectors is listed in Table 6.1. This algorithm is employed for extracting all the desired  $N$  beamforming weight vectors individually.

Table 6.1.  
Transmit antenna selection for individual beamformers

---

**Algorithm I:** Transmit Antenna Selection for Individual Beamformers

---

1. *Initialize* the iteration count as  $i = 0$  and the initial weight vector as  $\mathbf{w}_n^{(0)} = \mathbf{1}_{M \times 1}$ .
  2. *Solve* the multi-objective re-weighted  $\ell_1$ -norm optimization problem (6.9).
  3. *Increment*  $i$  and *update* the weighting vector  $\mathbf{w}_n^{(i)}$  using Eq. (6.8).
  4. *Terminate* on convergence or if the maximum number of iterations for  $i$  has reached; Otherwise, go to step 2.
- 

Minimizing the total number of antennas for JRC may result in some spare hardware up-conversion chains which can be further used for other tasks. There are several ways to fully utilize all the available up-conversion chains. For example, a concurrent communication-only operation can be realized by the spare hardware chains to increase the communication data rate. Alternatively, as the final solution results in fewer than  $\bar{M}$  activated antennas, we may turn on the remaining antennas based on the magnitude of the weighting coefficients. Note that the importance of each antenna is inversely proportional to the respective weighting  $w_{n,m}$ . If the optimal solution is achieved in the  $i$ th iteration, the most important antennas correspond to the elements of vector  $\mathbf{w}_n^{(i)}$  which have the smallest amplitudes. Therefore, the  $\bar{M}$  most important antennas can be identified by determining the  $\bar{M}$  smallest elements in  $|\mathbf{w}_n^{(i)}|$  and regenerating the beamforming weight vectors using the array manifold of those antennas by exploiting optimization (6.4). Another possible solution is to suspend the iterative optimization process once the desired number of antennas is achieved.

Our proposed iterative technique also falls in the general class of Majorization Minimization [88] algorithms where a surrogate function is exploited to achieve the optimal result. In our case,  $|\mathbf{u}_n \odot \mathbf{w}_n|_1$  serves as the surrogate objective function of  $|\mathbf{u}_n|_0$ . In this sense, a wide variety of re-weighting techniques can be employed.

### 6.2.2 Joint Transmit Antenna Selection for Multiple Beamforming Vectors via Group-sparsity

The optimal selection of antennas discussed in Subsection 6.2.1 results in different antenna array configurations for different beamforming weight vectors. This is a serious disadvantage because frequent electronic switching of antennas needs to be performed using the fast switching circuitry whenever the beamforming weight vector is changed. For high data rates, this switching will become more frequent, resulting in an added complexity for the JRC system. It is also possible that although the antennas used by each beamformer are very less, practically all the antennas are being used. This happens when each antenna is used by at least one of the  $N$  beamformers. In such a scenario, the spare antennas cannot be used for any other purposes which is not an optimal strategy when the additional radio transmission chains are still available.

We propose a joint optimal antenna selection strategy which optimizes the total number of transmit antennas used by all the beamformers for the JRC operation. For this purpose, the well-known group-sparsity concept [89] can be employed.

We define the mixed  $\ell_{1,q}$ -norm as:

$$|\mathbf{u}|_{1,q} := \sum_{m=1}^M \left( \sum_{n=1}^N |u_{n,m}|^q \right)^{1/q}, \quad (6.10)$$

which induces group-sparsity for  $q > 1$  [90]. Recall that  $u_{n,m}$  denotes the  $m$ th beamforming coefficient of  $\mathbf{u}_n$ . The most extensively used norms to enforce group-sparsity are  $\ell_{1,2}$ - and  $\ell_{1,\infty}$ -norms. For more detail, see [90].

Similar to the previous section, our proposed antenna selection strategy for grouped beamforming vectors takes the form of the following *joint* optimization:

$$\begin{aligned} \min_{\mathbf{u}_n} \quad & \sum_{n=1}^N |\mathbf{u}_n|_2^2 + \eta |\mathbf{u}|_{1,q} \\ \text{s.t.} \quad & |G_{\text{rad}} e^{j\varphi(\theta_r)} - \mathbf{u}_n^H \mathbf{a}(\theta_r)| \leq \gamma_{\text{tol}}, \theta_r \in \Theta_{\text{rad}}; n = 1, \dots, N, \\ & |\mathbf{u}_n^H \mathbf{a}(\theta_\varepsilon)| \leq \varepsilon_{\text{sl}}, \theta_\varepsilon \in \Theta_{\text{sl}}; n = 1, \dots, N, \\ & \mathbf{u}_n^H \mathbf{a}(\theta_u) = \Delta_{n,u} e^{j\phi_{n,u}}, u = 1, \dots, U; n = 1, \dots, N. \end{aligned} \quad (6.11)$$

Note that contrary to the optimization (6.7) which is exploited for each beamforming weight vector separately, the optimization (6.11) jointly solves all the beamforming vectors simultaneously. Moreover, the optimization (6.11) yields the beamforming weight vectors which exploit the same antenna elements for the JRC operation but have different weights depending on their sidelobe communication profile.

In continuation of our discussion in the previous section regarding sparsity enhancement, the group-sparsity can also be significantly enhanced democratically by exploiting a similar weighting function as in (6.8) as follows:

$$v_m = \begin{cases} \frac{1}{\left(\sum_{n=1}^N |u_{n,m}|^q\right)^{1/q}}, & \text{if } \sum_{n=1}^N |u_{n,m}| > 0, \\ \frac{1}{\epsilon}, & \text{if } \sum_{n=1}^N |u_{n,m}| = 0. \end{cases} \quad (6.12)$$

The resulting optimization employing group sparsity which enables optimal antenna selection jointly for all the beamforming weight vectors can now be expressed as follows:

$$\begin{aligned} \min_{\mathbf{u}_n} \quad & \sum_{n=1}^N \|\mathbf{u}_n\|_2^2 + \eta \sum_{m=1}^M \left( v_m^{(i)} \sum_{n=1}^N |u_{n,m}|^q \right)^{1/q} \\ \text{s.t.} \quad & |G_{\text{rad}} e^{j\varphi(\theta_r)} - \mathbf{u}_n^H \mathbf{a}(\theta_r)| \leq \gamma_{\text{tol}}, \theta_r \in \Theta_{\text{rad}}; n = 1, \dots, N, \\ & |\mathbf{u}_n^H \mathbf{a}(\theta_\varepsilon)| \leq \varepsilon_{\text{sl}}, \theta_\varepsilon \in \Theta_{\text{sl}}; n = 1, \dots, N, \\ & \mathbf{u}_n^H \mathbf{a}(\theta_u) = \Delta_{n,u} e^{j\phi_{n,u}}, u = 1, \dots, U; n = 1, \dots, N, \end{aligned} \quad (6.13)$$

where the above optimization is solved iteratively and  $v_m^{(i)}$  denotes the weighting coefficient for the  $i$ th iteration. This multi-objective optimization strategy tends to provide the antenna array design for the JRC operation which ensures the selection of the least number of transmit antennas and minimizes their power utilization. The detailed algorithm for extracting the beamforming weight vectors using this approach is listed in Table 6.2.

It is interesting to note that both proposed iterative algorithms for optimal antenna selection and power optimization iteratively solve a convex optimization problem, whereas the overall algorithm does not. Instead, the overall iterative strategy

Table 6.2.

Transmit antenna selection for grouped beamformers by employing group sparsity

---

**Algorithm II:** Transmit Antenna Selection for Grouped Beamformers

---

1. *Initialize* the iteration count as  $i = 0$  and the initial weight vector as  $v_m^{(0)} = 1$ .
  2. *Solve* the multi-objective re-weighted  $\ell_{1,2}$ -norm-based joint optimization (6.11).
  3. *Increment*  $i$  and *update* the weighting  $v_m^{(i)}$  using Eq. (6.12).
  4. *Terminate* on convergence or if the maximum number of iterations for  $i$  has reached; Otherwise, go to step 2.
- 

forces one part of the objective function to find a local minimum of a non-convex penalty function that resembles  $\ell_0$ -norm for antenna selection through re-weighted  $\ell_1$ -norm. Moreover, the other part of the objective function tends to minimize the power utilization of the selected antennas.

Group sparsity-based approach will utilize more number of antennas than individual beamforming weight vector at a given fast time. However, due to antenna switching, the total number of antennas used by individual beamforming weight vectors are generally more than group sparse version in the slow time.

### 6.3 Comparative Analysis of the Proposed Strategies

Let us compare the antenna selection by individual beamformer design (6.9) and group sparsity-based beamformer design (6.13). The most important difference between the two schemes lies in that the group sparsity-based approach (6.13) extracts the optimal antennas for all beamformers which not only satisfy the radar tasks but also enable transmission of all the given set of communication symbols to all communication users. On the other hand, the individual beamformer design strategy only selects the optimal antenna positions which satisfy the radar tasks and can transmit

only one respective communication symbol to each communication receiver, i.e., only one beamformer is designed at a time (6.9).

Note that the constraints of the maximum allowable sidelobe level and the radar main beam tolerance are common for both schemes (6.9) and (6.13). The only difference lies in the communication constraints. The optimization (6.9) has  $U$  equality constraints corresponding to the communication operation because this approach designs only one beamforming weight vector at a time which serves one communication symbol to each communication receiver. On the other hand, (6.13) has  $NU$  communication constraints as this approach designs all the  $N$  beamforming weight vectors simultaneously which can further be used to deliver all the possible communication information to the communication users. Since (6.13) has more constraints than (6.9), it will generally tend to select more antennas than (6.9) to satisfy all those constraints. However, to deliver all the possible communication information to all the communication users, optimization (6.9) is executed  $N$  times to generate  $N$  beamforming weight vectors which can achieve such task. Optimization (6.9) generally results in different antenna selections for different beamforming weight vectors. In this case, the overall number of antennas used by (6.9) to produce all the desired beamforming weight vectors will likely exceed the number of antennas selected by (6.13). Moreover, (6.9) will require frequent antenna switching for different slow times whenever communication information being transmitted is changed. Therefore, the proposed group sparsity-based approach (6.13) is preferred for antenna selection as it requires fewer number of antennas and prevents frequent antenna switching, thereby easing the hardware implementation.

For a given number of hardware chains  $\bar{M}$ , the total number of feasible antenna configurations is given by:

$$U_{\text{count}} = C_{\bar{M}}^M, \quad (6.14)$$

Therefore, an exhaustive search will require us to evaluate the feasibility of  $U_{\text{count}}$  number of array configurations to achieve the optimal solution. On the other hand,

if the antennas are randomly selected, the probability to achieve the optimal solution will be:

$$P_{\text{opt}} = \frac{1}{U_{\text{count}}} = \frac{1}{C_{\frac{M}{M}}}. \quad (6.15)$$

Note that the array configuration obtained from random antenna selection may not satisfy the radar and communication objectives. Therefore, it is impractical to use random selection or exhaustive search to obtain the desired array configuration.

## 6.4 Simulation Results

In this section, we present simulation results to illustrate the performance of the proposed antenna selection strategy for the beamforming-based JRC system. In all the simulations, we consider a ULA consisting of  $M = 30$  transmit antennas to optimize the radar main beam objectives and serve two ( $C = 2$ ) communication users located in the sidelobe region of the radar at angles  $30^\circ$  and  $40^\circ$ , respectively. We set the inter-sensor spacing of the ULA at  $0.25\lambda$  and the tuning coefficient  $\eta$  for all the multi-objective optimizations is set to unity. The maximum allowable sidelobe level for all the cases is considered to be lower than  $\varepsilon_{\text{sl}} = -20$  dB. We use the open-source SDPT3 solver [68] integrated with the open-source version of CVX toolbox [65] to solve all the optimizations. For the simulations involving the focused beampattern, the JRC radar objective is to focus the main beam with a gain of 0 dB at  $\theta_r = 0^\circ$ . For flat-top beampattern synthesis experiments, the radar objective is to project the main beam with a gain of 0 dB for angles from  $-7^\circ$  to  $7^\circ$ . For this purpose, we consider  $\Theta_{\text{sl}}$  consisting of a grid of angles with a grid spacing of  $0.5^\circ$ . The value of  $q = 2$  for the group-sparse optimization (6.13), i.e. mixed  $\ell_{1,2}$ -norm is used.

### 6.4.1 Convergence Analysis for Individual Beampattern Synthesis

First, we consider the beampattern synthesis for the radar main beam focused at  $\theta_r = 0^\circ$  using Algorithm I. In this scenario, the JRC system aims to project an amplitude of  $-20$  dB towards both communication receivers. Fig. 6.3(a) demonstrates

the power distribution profile of the beamforming weight vector synthesized using Algorithm I. The corresponding number of selected antennas during each iteration of Algorithm I is illustrated in Fig. 6.3(b). Moreover, Fig. 6.3(c) shows the spatial selection profile during each iteration of the Algorithm I for the first 4 iterations.

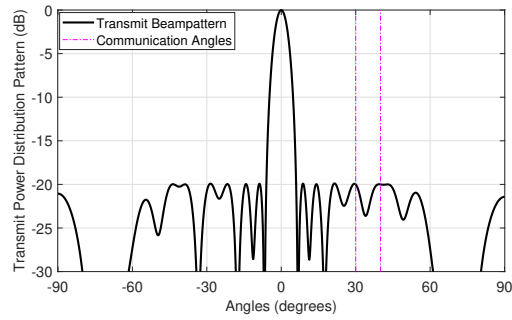
It can be observed that the algorithm converges very fast, i.e. only 4 iterations were enough to achieve the final solution. It can also be observed that the spatial profile of the selected antennas does not change after the convergence. Moreover, we also ran the Algorithm I for up to 100 iterations but did not observe any change in the spatial antenna selection profile.

Fig. 6.4 illustrates the similar results for flat-top beampattern synthesis. In Fig. 6.4(a), we observe the synthesized beampattern derived from Algorithm I and note that it achieves both radar and communication objectives. The corresponding number of selected antennas during each iteration is shown in Fig. 6.4(b). It can be observed that the Algorithm I converged within 4 iterations. We extended the iteration count up to 100 iterations and noted that the spatial antenna selection profile, as shown in Fig. 6.4(c) illustrating the selection of 14 antennas, did not change after the first 4 iterations.

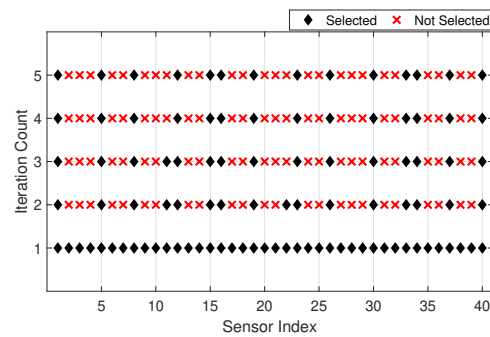
If the optimal number of antennas is known to be 14, an exhaustive search will require us to evaluate  $C_{14}^{40} \approx 2 \times 10^{10}$  different configurations of antennas which is impractical. If the optimal number of antennas is unknown, exhaustive search will require us to evaluate  $\sum_{m=1}^{40} C_m^{40}$  possible array configurations.

#### 6.4.2 Antenna Selection for Individual Beamforming Weight Vectors

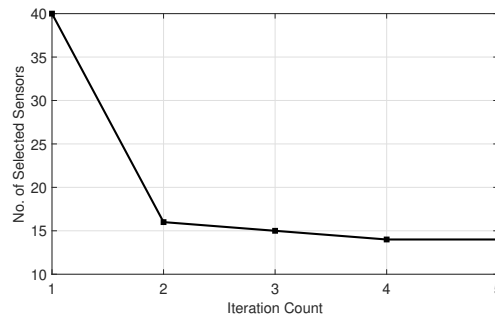
Now we discuss the set of beampatterns that have the same main beam profile but transmit different communication information. Without loss of generality, we consider the ASK multiple-access signaling scheme where the JRC transmit array has an objective to transmit two (same or different) amplitude levels towards both communication receivers. This results in four different combinations of possible beampatterns.



(a)

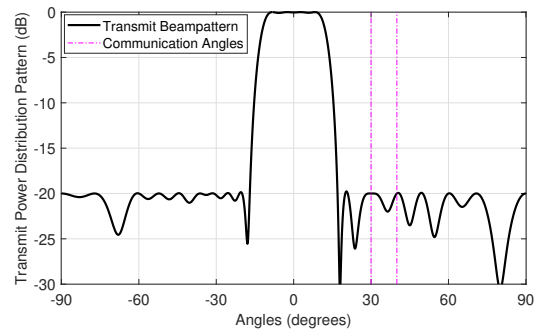


(b)

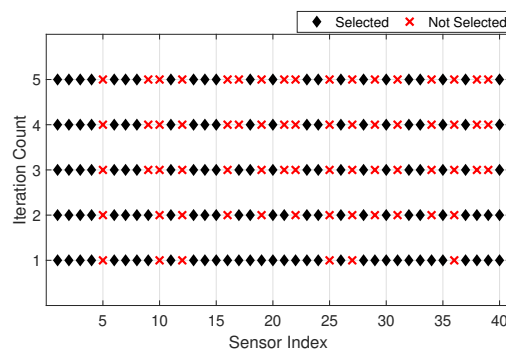


(c)

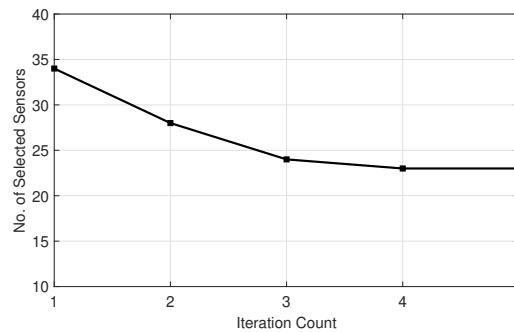
Figure 6.3. Focused beampatterns synthesis using the optimal antenna selection strategy in Algorithm I ( $M = 40$ ,  $\Theta_{\text{rad}} = 0^\circ$ ,  $\Theta_{\text{trans}} = [-6^\circ \ 0^\circ] \cup (0^\circ \ 6^\circ]$ ,  $\Theta_{\text{sl}} = [-90^\circ \ -6^\circ] \cup (6^\circ \ 90^\circ]$ ,  $G_{\text{rad}} = 1$ ,  $\gamma_{\text{tol}} = 10^{-3}$ ,  $\varepsilon_{\text{sl}} = 0.1$  (20 dB below  $G_{\text{rad}}$ ): (a) Transmit power distribution pattern, (b) Total number of selected antennas with respect to the number of iterations, (c) Spatial antenna selection profile for each iteration.



(a)

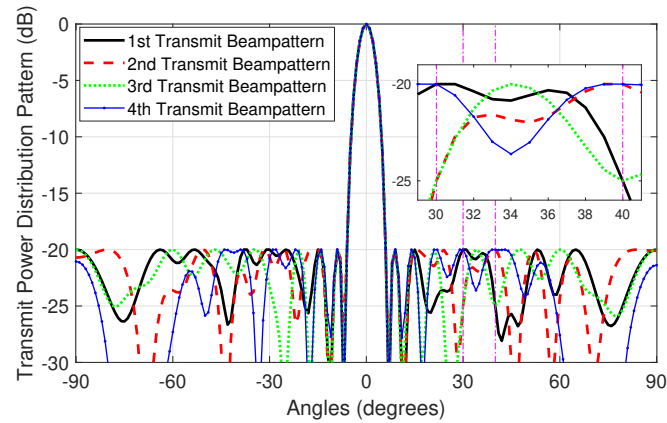


(b)

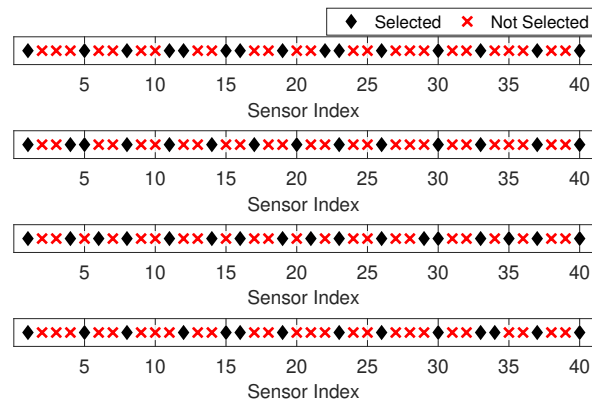


(c)

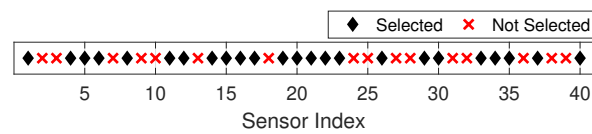
Figure 6.4. Flat-top beampattern synthesis using the antenna selection strategy in Algorithm I ( $M = 40$ ,  $\Theta_{\text{rad}} = [-7^\circ \ 7^\circ]$ ,  $\Theta_{\text{trans}} = [-17^\circ \ -7^\circ) \cup (7^\circ \ 17^\circ]$ ,  $\Theta_{\text{sl}} = [-90^\circ \ -17^\circ) \cup (17^\circ \ 90^\circ]$ ,  $G_{\text{rad}} = 1$ ,  $\gamma_{\text{tol}} = 10^{-3}$ ,  $\varepsilon_{\text{sl}} = 0.1$  (20 dB below  $G_{\text{rad}}$ ): (a) Transmit power distribution pattern, (b) Total number of selected antennas with respect to the number of iterations, (c) Spatial antenna selection profile with increasing number of iterations



(a)



(b)



(c)

Figure 6.5. Focused beampattern synthesis using the antenna selection strategy in Algorithm I for different communication objectives ( $M = 40$ ,  $\Theta_{\text{rad}} = 0^\circ$ ,  $\Theta_{\text{trans}} = [-6^\circ \ 0^\circ] \cup (0^\circ \ 6^\circ]$ ,  $\Theta_{\text{sl}} = [-90^\circ \ -6^\circ] \cup (6^\circ \ 90^\circ]$ ,  $G_{\text{rad}} = 1$ ,  $\gamma_{\text{tol}} = 10^{-3}$ ,  $\varepsilon_{\text{sl}} = 0.1$  (20 dB below  $G_{\text{rad}}$ ): (a) Transmit power distribution pattern, (b) Final antenna selection profile for each beampattern, (c) Overall antenna selection profile containing the antennas selected at least once by any of the beamforming weight vectors.

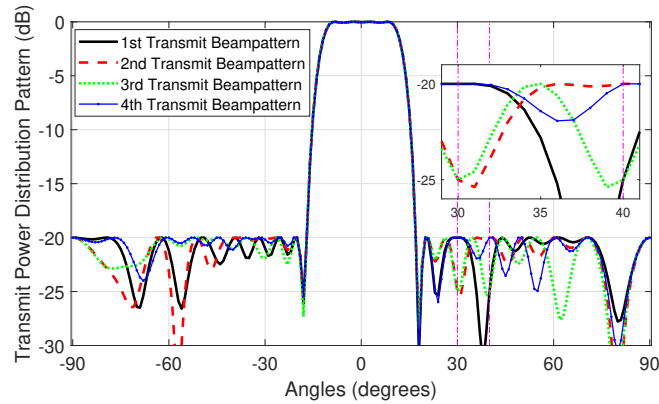
Using Algorithm I, we synthesized the focused beampatterns for the JRC system as illustrated in Fig. 6.5(a). The final spatial optimal antenna selection profile for these respective beamformers is shown in Fig. 6.5(b). It can be observed that the number of antennas used for each beampattern is not the same. Note that a maximum of 17 antennas will be exploited by any of the beamformers at a given time. Fig. 6.5(c) shows all the individual antennas which are selected at least once by the respective four beampatterns. It shows that the overall number of antennas collectively used by all the beamformers is 24. This means that 24 antennas will remain in operation by the JRC system, which is more than the number of antennas individually required by each beamformer. Extensive antenna switching will be also be required inviting hardware complexity.

Similar results have been obtained for the flat-top beampattern synthesis, shown in Fig. 6.6(a), using the Algorithm I by exploiting ASK signaling strategy. It can be observed from Fig. 6.6(b) that the four beamformers exploit 21, 21, 20, and 23 antennas, respectively. However, the total number of antennas used by all the beamformers collectively is 36 as shown in Fig 6.6. This signifies our previous analysis that the antenna array utilization might be sub-optimal if the beamforming weight vectors are synthesized individually.

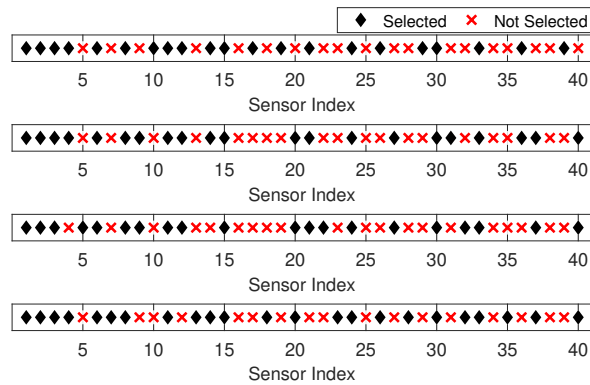
### 6.4.3 Antenna Selection by Employing Group Sparsity

The simulation results from Subsection 6.4-6.4.2 motivate to inspect the optimal antenna selection performance for a group of beamforming weight vectors collectively. We exploit the same scenario as in Subsection 6.4-6.4.2 where ASK signaling strategy is exploited. We find the optimal antenna selection for a group of four beamforming weight vectors using the group-sparsity Algorithm II which satisfies radar and communication objectives simultaneously.

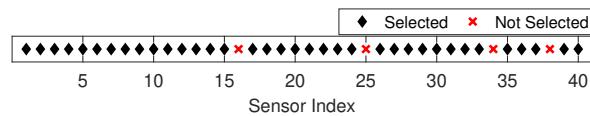
Fig. 6.7(a) shows the power distribution pattern of the four beamforming weight vectors for the focused main beam synthesized by using Algorithm II. Note that in this approach, all the beamforming weight vectors exploit the same antenna array



(a)

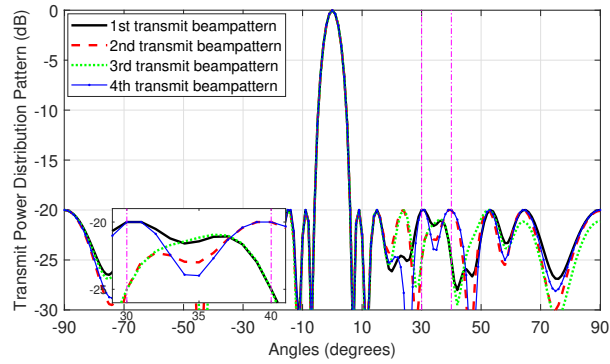


(b)

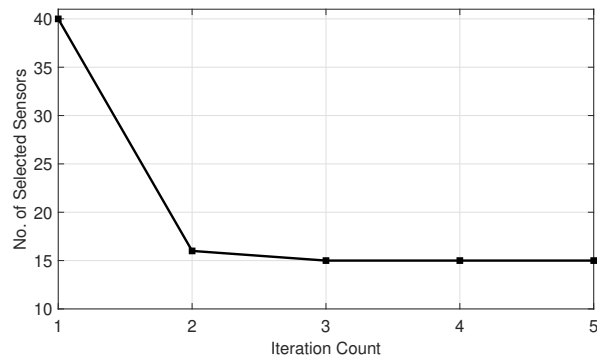


(c)

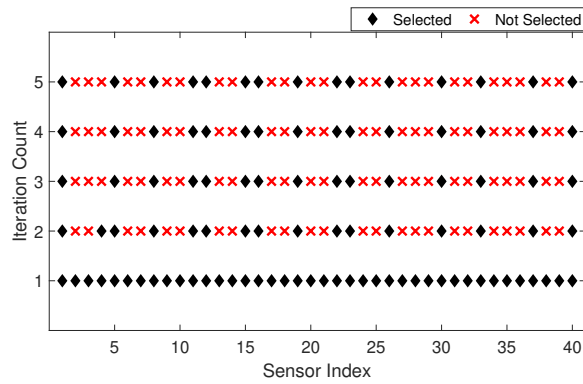
Figure 6.6. Flat-top beampattern synthesis using the antenna selection strategy in Algorithm I for different communication objectives ( $M = 40$ ,  $\Theta_{\text{rad}} = [-7^\circ \ 7^\circ]$ ,  $\Theta_{\text{trans}} = [-17^\circ \ -7^\circ] \cup (7^\circ \ 17^\circ]$ ,  $\Theta_{\text{sl}} = [-90^\circ \ -17^\circ] \cup (17^\circ \ 90^\circ]$ ,  $G_{\text{rad}} = 1$ ,  $\gamma_{\text{tol}} = 10^{-3}$ ,  $\varepsilon_{\text{sl}} = 0.1$  (20 dB below  $G_{\text{rad}}$ ): (a) Transmit power distribution pattern, (b) Final antenna selection profile for each beampattern, (c) Overall antenna selection profile containing the antennas selected at least once by any of the beamforming weight vectors.



(a)



(b)



(c)

Figure 6.7. Focused beampattern synthesis by employing the group-sparsity for antenna selection Algorithm II ( $M = 40$ ,  $\Theta_{\text{rad}} = 0^\circ$ ,  $\Theta_{\text{trans}} = [-6^\circ \ 0^\circ] \cup (0^\circ \ 6^\circ]$ ,  $\Theta_{\text{sl}} = [-90^\circ \ -6^\circ] \cup (6^\circ \ 90^\circ]$ ,  $G_{\text{rad}} = 1$ ,  $\gamma_{\text{tol}} = 10^{-3}$ ,  $\varepsilon_{\text{sl}} = 0.1$  (20 dB below  $G_{\text{rad}}$ ): (a) Transmit power distribution pattern, (b) Number of selected antennas with increasing number of iterations, (c) Spatial antenna selection profile for the first 5 iterations.

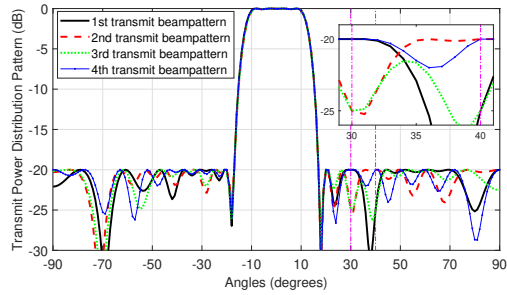
elements. Contrary to the results using Algorithm I in Fig. 6.5(c), where an overall 24 antennas of the JRC transmit array are used, Figs. 6.7(b)-(c) show that the grouped approach exploits only 15 antennas. Fig. 6.7(b) shows the number of selected antennas with the increasing number of iterations. Note that the Algorithm II converged within 3 iterations.

A similar result has been observed for the flat-top beam pattern synthesis in Fig. 6.8 using group-sparsity Algorithm II. Fig. 6.8(a) shows the power distribution pattern for the four beamforming weight vectors resulting from Algorithm II. It can be observed that all the beam patterns satisfy the radar and communication objectives. Contrary to Fig. 6.6, where 36 antenna elements were selected at least once by the beamforming vectors, Fig. 6.8 shows that only 21 antennas are exploited when all the beamforming vectors were extracted simultaneously as a group using the Algorithm II. Fig. 6.8(b) shows the number of selected antennas with the increasing number of iterations. It can be observed that the Algorithm II converged within 4 iterations. The corresponding spatial antenna selection profile is illustrated in Fig. 6.8(c).

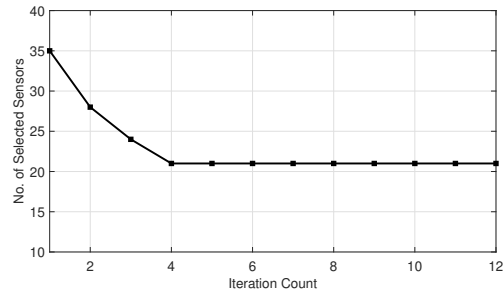
It has been observed that when the beamforming weight vectors are derived simultaneously as a group, they exploit overall fewer number of antennas compared to the case when the beamforming weight vectors are synthesized individually. These results show a significant advantage of utilizing Algorithm II. In such a scenario, the additional antennas can be exploited to perform other objectives. Moreover, the grouped antenna selection-based strategy prevents frequent antenna switching when the beamforming weights are changed, which eases the implementation of the JRC system. The fast convergence of the proposed algorithms also emphasizes their importance.

#### 6.4.4 Computation Time

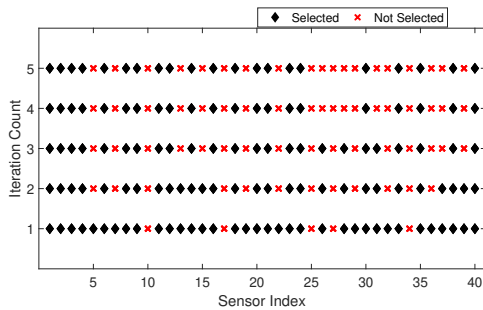
Now we compare the computation time for both proposed antenna selection algorithms outlined in Tables I and II. Fig. 6.10 illustrates the run-time of generating all the required beamforming weight vectors in Figs. 6.5–6.8. For these simulations, we



(a)

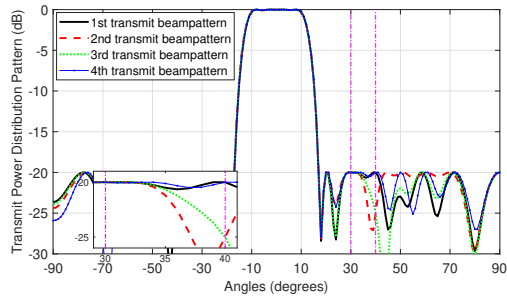


(b)

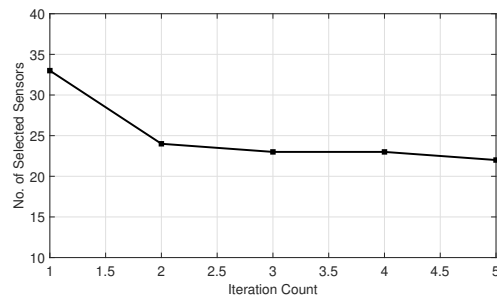


(c)

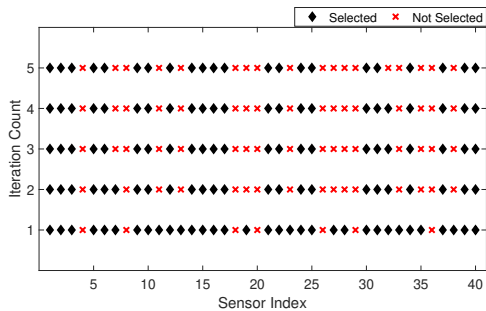
Figure 6.8. Flat-top beampattern synthesis by employing the group-sparsity based antenna selection Algorithm II ( $M = 40$ ,  $\Theta_{\text{rad}} = [-7^\circ \ 7^\circ]$ ,  $\Theta_{\text{trans}} = [-17^\circ \ -7^\circ] \cup [7^\circ \ 17^\circ]$ ,  $\Theta_{\text{sl}} = [-90^\circ \ -17^\circ] \cup [17^\circ \ 90^\circ]$ ,  $G_{\text{rad}} = 1$ ,  $\gamma_{\text{tol}} = 10^{-3}$ ,  $\varepsilon_{\text{sl}} = 0.1$  (20 dB below  $G_{\text{rad}}$ ): (a) Transmit power distribution pattern, (b) Number of selected antennas with increasing number of iterations, (c) Spatial antenna selection profile for the first 5 iterations.



(a)



(b)



(c)

Figure 6.9. Flat-top beampattern synthesis by employing the group-sparsity based antenna selection Algorithm II using QAM-based side-lobe modulation ( $M = 40$ ,  $\Theta_{\text{rad}} = [-7^\circ \ 7^\circ]$ ,  $\Theta_{\text{trans}} = [-17^\circ \ -7^\circ] \cup (7^\circ \ 17^\circ]$ ,  $\Theta_{\text{sl}} = [-90^\circ \ -17^\circ) \cup (17^\circ \ 90^\circ]$ ,  $G_{\text{rad}} = 1$ ,  $\gamma_{\text{tol}} = 10^{-3}$ ,  $\varepsilon_{\text{sl}} = 0.1$  (20 dB below  $G_{\text{rad}}$ ): (a) Transmit power distribution pattern for the first four beampatterns, (b) Number of selected antennas with increasing number of iterations, (c) Spatial antenna selection profile for the first 5 iterations.

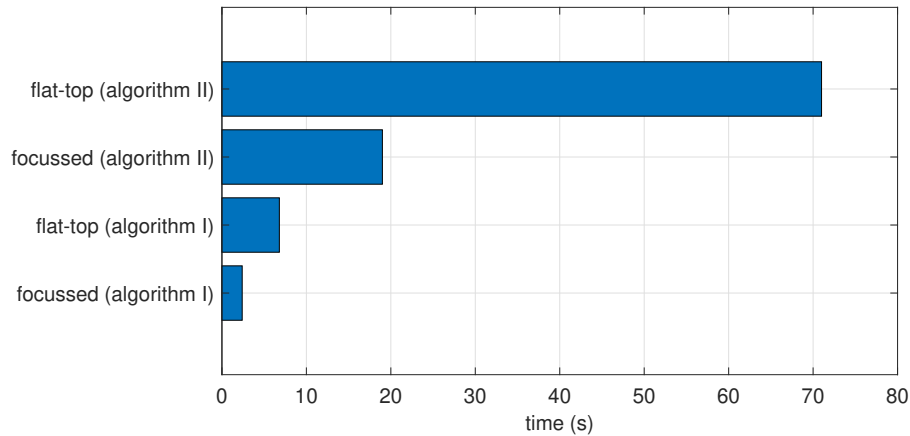


Figure 6.10. Computation time required to compute the beamforming weight vectors using the proposed approaches.

used a computer equipped with Intel(R) Core(TM) i7-6700 processor, 16 GB DDR3 (1600 MHz) RAM, 64-bit Windows 8.1 Enterprise, and MATLAB R2017b (64-bit). It can be observed that the group sparsity-based antenna selection strategy takes longer computation time as compared to the antenna selection strategy developed for individual beamformers. This is expected from the formulation of both strategies as the group sparsity-based approach exploits  $\ell_2$ -norm of all the beamforming weight vectors during the optimization as well as for computing the weighting coefficients.

#### 6.4.5 Antenna Selection for QAM-based Sidelobe Modulation

Now we modify the parameters used in Fig. 6.8 to investigate the antenna selection performance for QAM-based sidelobe modulation by employing two possible phases for each communication user. We find the optimal antenna selection for a group of sixteen beamforming weight vectors using the group sparsity-based Algorithm II which satisfies radar and communication objectives simultaneously.

Fig. 6.9(a) shows the power distribution pattern of the first four beamforming weight vectors for the flat-top main beam synthesized by using Algorithm II. All the beamformers exploit the same antenna array elements. Contrary to Fig. 6.8 where

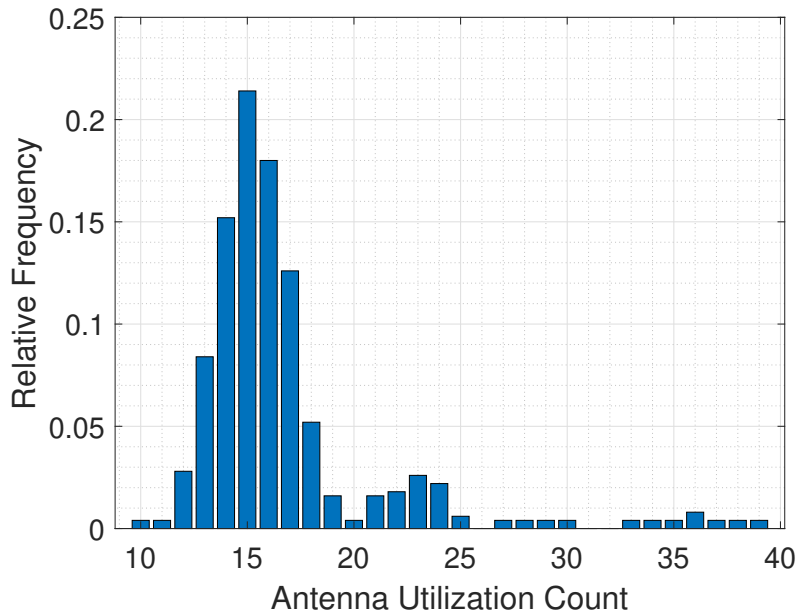


Figure 6.11. Relative frequency of antenna utilization for randomly generated simulation events.

21 antenna elements are selected, Fig. 6.9 shows that 22 antennas are exploited. Although the QAM-based signaling increased the number of required beamforming weight vectors from 4 to 16, only one additional antenna was required to satisfy the radar and communication objectives compared to ASK signaling.

#### 6.4.6 Antenna Selection for Randomly Located Communication Users

In this simulation, we investigate the performance of the group sparsity-based antenna selection approach for the case where communication users are randomly located in the sidelobe region. We use the same simulation parameters as in Fig. 6.9, but communication user locations are randomly selected such that they do not lie within the radar main beam and their angular separation is at least  $10^\circ$ . We perform 500 Monte Carlo trials for this case and the simulation results are presented in Fig. 6.11. Note that the antenna utilization count is very low for most of the simulation experiments. High antenna utilization is observed for the cases when the

communication users are either very close to the radar main beam, or very close to  $90^\circ$  or  $-90^\circ$ . This is because the JRC transmit array requires more degrees-of-freedom to satisfy all the constraints for those cases.

## 6.5 Remarks

In this chapter, we present a novel antenna selection strategy for JRC operation. We formulate a multi-objective optimization framework that aims to select the least possible number of antennas for the beamforming-based JRC system and minimize their respective power consumption. We show that the desired sparsity levels for antenna selection can be achieved for individual beamformers, as well as for the group of beamformers by using the same set of antennas. Simulation results illustrate that the proposed approach significantly reduces the number of antennas required to meet the prescribed service level for radar and communication operations. Furthermore, the performance of the proposed approach is analogous to that of  $\ell_0$ -norm-based exhaustive search optimization at a significantly reduced computational complexity.

## CHAPTER 7

### DISTRIBUTED JRC SYSTEMS

In this chapter, we propose a novel distributed JRC MIMO system capable of simultaneously performing radar and communication tasks. Note that this is the first research effort in this direction where spectrum sharing in a distributed radar-communication network is considered.

The radar objective is to achieve the desired target localization performance whereas the communication objective is to optimize the overall data rate. The distributed JRC MIMO system performs both objectives by optimizing the power allocation of the different transmitters in the JRC system. A dictionary of radar waveforms is used at each transmitter and the communication information is embedded in the radar waveform by exploiting waveform diversity. The proposed strategy can serve multiple communication receivers located in the vicinity of the distributed JRC MIMO system. Simulation results illustrate the performance of the proposed strategy.

#### 7.1 System Model

##### 7.1.1 Radar Subsystem

The radar signal corresponding to the  $m$ th transmitter and the  $n$ th receiver is expressed as:

$$s_{m,n}(t) = \sqrt{\alpha_{m,n} p_{m_{tx}}} h_{m,n} s_m(t - \tau_{m,n}) + w_{m,n}(t), \quad (7.1)$$

where  $\alpha_{m,n}$  represents the signal variation due to path loss effects,  $p_{m_{tx}}$  is the transmit power of signal  $s_m(t)$  emitted from the  $m$ th transmitter,  $h_{m,n}$  denotes the target RCS<sup>1</sup> for the propagation path from the  $m$ th transmitter to the  $n$ th receiver, and

---

<sup>1</sup>See Section A of Appendix A

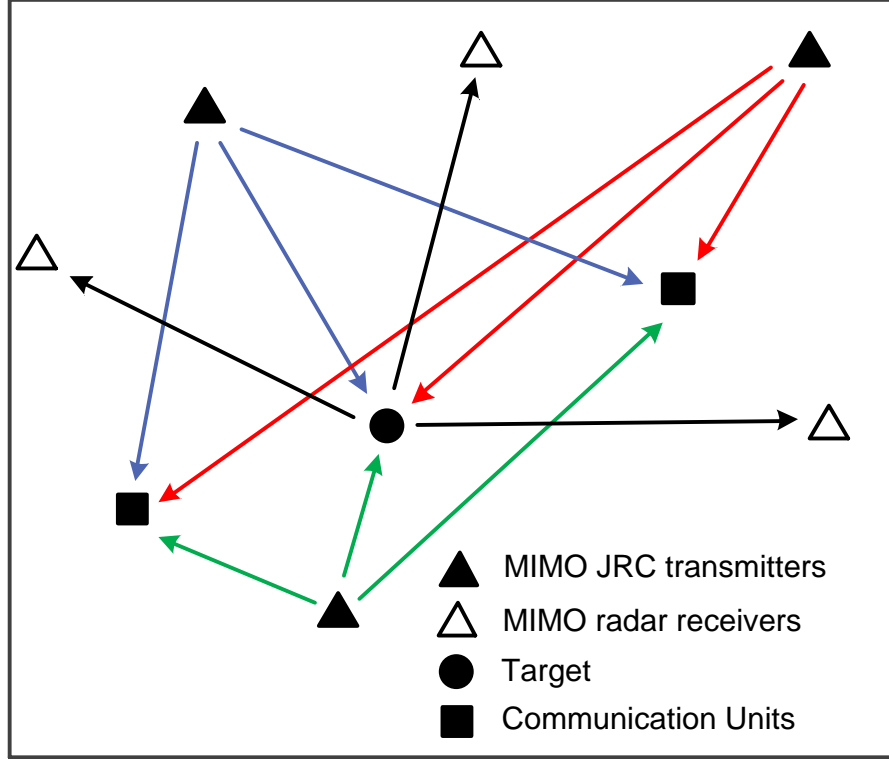


Figure 7.1. Distributed JRC MIMO system.

$w_{m,n}(t) \sim \mathcal{CN}(0, \sigma_w^2)$  represents the circularly symmetric zero-mean complex white Gaussian noise. The propagation delay  $\tau_{m,n}$  due to the propagation path from the  $m$ th transmitter to the  $n$ th receiver is denoted as  $\tau_{m,n} = (D_{m\text{tx}} + D_{n\text{rx}})/c$ , where  $D_{m\text{tx}}$  and  $D_{n\text{rx}}$  are the range to target from the  $m$ th transmitter and that from the  $n$ th receiver, respectively, and  $c$  is the propagation velocity of the transmitted signals. The path loss factor takes the form of  $\alpha_{m,n} \propto D_{m\text{tx}}^{-2} D_{n\text{rx}}^{-2}$ . Moreover, let  $\mathbf{h} = [h_{1,1}, h_{1,2}, \dots, h_{M,1}, h_{2,1}, \dots, h_{M,N}]^T$  be the  $MN \times 1$  vector of all bi-static RCS of the targets, and  $\mathbf{p}_{\text{tx}} = [p_{1\text{tx}}, p_{2\text{tx}}, \dots, p_{M\text{tx}}]^T$  be the  $M \times 1$  vector containing all the transmit powers from all transmitters of the JRC system.

We will optimize the total transmit power for the desired localization error performance for the radar subsystem. Let's denote  $\mathbf{p}_{\text{tx,max}} = [p_{1\text{tx,max}}, p_{2\text{tx,max}}, \dots, p_{M\text{tx,max}}]^T$  and  $\mathbf{p}_{\text{tx,min}} = [p_{1\text{tx,min}}, p_{2\text{tx,min}}, \dots, p_{M\text{tx,min}}]^T$  be the  $M \times 1$  vectors respectively representing the maximum and the minimum allowable transmit power from the  $M$

transmitters. We further denote  $P_{\text{total,max}} \leq \sum_{m=1}^M p_{m_{\text{tx,max}}}$  as the maximum allowable power to be transmitted from the JRC transmitters collectively.

The Cramer-Rao Bound (CRB) expresses a lower bound on the variance of unbiased estimators of a deterministic (fixed, though unknown) parameter and serves as a popular performance metric. Here, the radar performance is evaluated in terms of the CRB representing the lower bound on the mean squared error of the target's location estimates. For the case of distributed radar, CRB is derived in [75,76,91] as:

$$\sigma_{x,y}(\mathbf{p}_{\text{tx}}) = \frac{\mathbf{q}^{\text{T}} \mathbf{p}_{\text{tx}}}{\mathbf{p}_{\text{tx}}^{\text{T}} \mathbf{A} \mathbf{p}_{\text{tx}}}, \quad (7.2)$$

where  $\mathbf{q} = \mathbf{q}_a + \mathbf{q}_b$ ,  $\mathbf{A} = \mathbf{q}_a \mathbf{q}_b^{\text{T}} - \mathbf{q}_c \mathbf{q}_c^{\text{T}}$ ,  $\mathbf{q}_a = [q_{a_1}, q_{a_2}, \dots, q_{a_M}]^{\text{T}}$ ,  $\mathbf{q}_b = [q_{b_1}, q_{b_2}, \dots, q_{b_M}]^{\text{T}}$  and  $\mathbf{q}_c = [q_{c_1}, q_{c_2}, \dots, q_{c_M}]^{\text{T}}$ . Here,

$$\begin{aligned} q_{a_m} &= \xi_m \sum_{n=1}^N \alpha_{m,n} |h_{m,n}|^2 \left( \frac{x_m - x}{D_{m_{\text{tx}}}} + \frac{x_n - x}{D_{n_{\text{rx}}}} \right)^2, \\ q_{b_m} &= \xi_m \sum_{n=1}^N \alpha_{m,n} |h_{m,n}|^2 \left( \frac{y_m - x}{D_{m_{\text{tx}}}} + \frac{y_n - x}{D_{n_{\text{rx}}}} \right)^2, \\ q_{c_m} &= \xi_m \sum_{n=1}^N \alpha_{m,n} |h_{m,n}|^2 \left( \frac{x_m - x}{D_{m_{\text{tx}}}} + \frac{x_n - x}{D_{n_{\text{rx}}}} \right) \left( \frac{y_m - x}{D_{m_{\text{tx}}}} + \frac{y_n - x}{D_{n_{\text{rx}}}} \right), \end{aligned} \quad (7.3)$$

where  $\xi_m = 8\pi^2 \mathcal{B}_m^2 / (\sigma_w^2 c^2)$ , and  $\mathcal{B}_m$  is the effective bandwidth of the signal transmitted from the  $m$ th transmitter.

### 7.1.2 Communication Subsystem

Consider  $U$  communication receivers that are located in the vicinity of the distributed JRC MIMO system. Assume that the signals reflected from the radar target and received at each communication receiver have a significantly lower magnitude compared to the line-of-sight transmission from the transmitters and, thus, are ignored. Then, we can express the received signal at the  $u$ th ( $1 \leq u \leq U$ ) receiver as:

$$s_{m,u}(t) = \sqrt{\beta_{m,u} p_{m_{\text{tx}}}} g_{m,u} s_m(t - \kappa_{m,u}) + w_{m,u}(t), \quad (7.4)$$

where  $g_{m,u}$  denotes the complex channel gain,  $\kappa_{m,u}$  is the propagation delay, and  $\beta_{m,u} \propto \mathcal{D}_{m,u}^{-2}$  incorporates the path loss effects, and  $\mathcal{D}_{m,u}$  is the distance between the  $m$ th transmitter and the  $u$ th communication receiver. We assume  $w_{m,u}(t) \sim$

$\mathcal{CN}(0, \sigma_{m,u})$  be circularly complex white Gaussian noise whose statistics are known at the transmitter. The channel state information, expressed as the complex channel gain vector  $\mathbf{g} = [g_{1,1}, g_{1,2}, \dots, g_{M,1}, \dots, g_{M,U}]^T$ , is also assumed to be known at the radar fusion center.

The communication performance is evaluated in terms of the achieved Shannon capacity. The data rate from the  $m$ th transmitter to the  $u$ th receiver is expressed in terms of Shannon's capacity as:

$$\mathfrak{R}_{m,u} = \log \left( 1 + \frac{|g_{m,u}|^2 p_{m,\text{tx}}}{\Gamma_{m,u} \sigma_{m,u}^2} \right) = \log \left( 1 + \frac{p_{m,\text{tx}}}{\gamma_{m,u}} \right), \quad (7.5)$$

where  $\Gamma_{m,u} \geq 1$  represents the SNR gap which translates the loss in the data rate into the loss in the SNR and is determined by the coding scheme, and  $\gamma_{m,u} = \Gamma_{m,u} \sigma_{m,u}^2 / |g_{m,u}|^2$ . The sum data rate per radar pulse can be calculated as  $\mathfrak{R} = \sum_{m=1}^M \sum_{u=1}^R \mathfrak{R}_{m,u}$ .

## 7.2 Optimal Power Allocation for Distributed JRC MIMO System

### 7.2.1 Radar-Only Operation

The optimal power allocation for radar-only operation is derived in [75] as:

$$\begin{aligned} & \text{minimize} && \mathbf{1}_{1 \times M} \mathbf{p}_{\text{tx}} \\ & \text{s.t.} && \mathbf{p}_{\text{tx},\min} \leq \mathbf{p}_{\text{tx}} \leq \mathbf{p}_{\text{tx},\max}, \\ & && \sigma_{x,y}(\mathbf{p}_{\text{tx}}) = \eta. \end{aligned} \quad (7.6)$$

The optimization in (7.6) minimizes the total transmit power for the distributed MIMO radar such that a desirable localization accuracy, described in terms of the CRB  $\eta$ , is achieved. The optimization problem (7.6) can be relaxed to the following convex form [75]:

$$\begin{aligned} & \text{minimize} && \mathbf{1}_{1 \times M} \mathbf{p}_{\text{tx}} \\ & \text{s.t.} && \mathbf{p}_{\text{tx},\min} \leq \mathbf{p}_{\text{tx}} \leq \mathbf{p}_{\text{tx},\max}, \\ & && \mathbf{q} - \eta \mathbf{A} \mathbf{p}_{\text{tx}} \leq \mathbf{0}. \end{aligned} \quad (7.7)$$

The solution of the convex optimization problem (7.7) yields the optimized transmit power vector  $\mathbf{p}_{\text{tx,opt}}$ , which can be used as a starting point for a local optimization applied to the original optimization (7.6).

### 7.2.2 Communication-Only Operation

We assume that the waveform transmitted from each transmitter is broadcast to all communication users (CUs) located in the vicinity of the JRC transmitters. We also assume that the channel side information is known at the JRC transmitter and communication receivers. We optimize the power allocation for communication operation by exploiting the conventional water-filling approach [70]. In such an approach, the transmit power is amplified for each user to the pre-determined power level compensating for the channel impairments. The desired power level is determined by considering the SNR ratio of each user with the JRC transmitters. Generally, water-filling approach invests more resources in the communication channels which have better SNR.

The water-filling for the maximum allowable transmit power is achieved by solving the following equation simultaneously for all the communication receivers ( $1 \leq u \leq U$ ):

$$\mathbf{U} \begin{bmatrix} \mathbf{p}_{\text{tx}} \\ X_u \end{bmatrix} = \begin{bmatrix} P_{\text{total,max}} \\ \gamma_u \end{bmatrix}, \quad (7.8)$$

where

$$\mathbf{U} = \begin{bmatrix} \mathbf{1}_{1 \times M} & 0 \\ \mathbf{I}_{M \times M} & -\mathbf{1}_{1 \times M}^T \end{bmatrix}, \quad \gamma_u = - \begin{bmatrix} \gamma_{1,r} \\ \gamma_{2,r} \\ \vdots \\ \gamma_{M,r} \end{bmatrix},$$

where  $X_u$  represents the water-filling power level. Eq. (7.8) may provide different optimal power distributions for different CUs depending on their channel side information. Moreover, the solution of Eq. (7.8) can also provide negative power if any

channel has a deep fade. Therefore, we can write Eq. (7.8) for all the communication receivers as the following constrained least-square optimization problem:

$$\begin{aligned}
& \text{minimize} && \sum_{u=1}^U \left| \mathbf{V} \begin{bmatrix} \mathbf{p}_{\text{tx}} \\ X_u \end{bmatrix} - \gamma_u \right|_2 \\
& \text{s.t.} && \mathbf{p}_{\text{tx},\min} \leq \mathbf{p}_{\text{tx}} \leq \mathbf{p}_{\text{tx},\max}, \\
& && \mathbf{1}^T \mathbf{p}_{\text{tx}} \leq P_{\text{total,max}}, \\
& && X_u \geq 0, \quad u = 1, 2, \dots, U,
\end{aligned} \tag{7.9}$$

where  $\mathbf{V} = \begin{bmatrix} \mathbf{I}_{M \times M} & -\mathbf{1}_{1 \times M}^T \end{bmatrix}$  and  $|\cdot|_2$  is the  $l_2$  norm. Note that  $X_u$  is a free parameter and its optimal value is also determined by the above optimization. The optimization problem (7.9) is convex. However, unlike (7.6) and (7.7) where the least power required for satisfactory radar operation is extracted, it utilizes the maximum allowable power and distributes it with respect to channel quality for all the CUs. For a given maximum power  $P_{\text{total,max}}$ , the optimization problem (7.9) tends to maximize the water-filling level  $X_u$ , thus resulting in high data rate for the communication channels which have better channel conditions.

### 7.2.3 Joint Radar-Communication System

The optimal power allocation extracted from the optimization problems (7.7) and (7.9), respectively designed for radar-only and communication-only operations, are not favorable for the acceptable joint operation JRC system. The power allocation from optimization (7.7) provides the minimal required power from all the transmitters of the distributed radar. As such, this scheme may not establish an acceptable communication data rate as most of the transmitters work on a low power in ideal radar conditions, resulting in unacceptable SNR and data rate for CUs. Moreover, the resulting power from the optimization problem (7.7) is independent of the communication channel side information. Likewise, the resource allocation from the optimization problem (7.9) is not suitable for radar operation as the power distribution for this

case is independent of the radar performance and may result in unacceptable target tracking performance, even after the maximum allowable power is utilized.

We can add the radar performance constraint in the optimization problem (7.9) to obtain the following modified convex optimization problem:

$$\begin{aligned}
& \text{minimize} && \sum_{u=1}^U \left\| \mathbf{V} \begin{bmatrix} \mathbf{p}_{\text{tx}} \\ X_u \end{bmatrix} - \gamma_u \right\|_2 \\
& \text{s.t.} && \mathbf{p}_{\text{tx},\min} \leq \mathbf{p}_{\text{tx}} \leq \mathbf{p}_{\text{tx},\max}, \\
& && \mathbf{q} - \eta \mathbf{A} \mathbf{p}_{\text{tx}} \leq \mathbf{0}, \\
& && \mathbf{1}^T \mathbf{p}_{\text{tx}} \leq P_{\text{total,max}}, \\
& && X_u \geq 0, \quad u = 1, 2, \dots, U.
\end{aligned} \tag{7.10}$$

The optimization problem (7.10) provides the optimal power allocation for distributed JRC transmitters under the maximum allowable power constraint such that the localization error for the radar operation is bounded by  $\eta$ . At the same time, our objective function tends to maximize the water-filling level  $X_u$  to improve the communication data rate.

### 7.3 Information Embedding

The information embedding can be accomplished by utilizing waveform diversity. If each transmitter is assigned a dictionary of  $K$  radar waveforms, the total bits transmitted from the distributed JRC MIMO system during one radar pulse is  $M \log K$ , provided that the dictionaries are non-overlapping and all transmitters are active.

The signal received at the communication receiver  $u$  can be expressed as:

$$\begin{aligned}
s_u(t) &= \sum_{m=1}^M s_{m,u}(t) \\
&= \sum_{m=1}^M \sqrt{\beta_{m,u} p_{m,\text{tx}}} g_{m,u} s_m(t - \kappa_{m,u}) + w_u(t),
\end{aligned} \tag{7.11}$$

where  $w_u(t) = \sum_{m=1}^M w_{m,u}(t)$ . Matched filtering can be exploited at the communication receivers to synthesize the embedded information by feeding the time delayed versions of  $s_u(t)$  in the matched filter as follows:

$$\begin{aligned} y_u(k) &= \frac{1}{T} \int_0^T s_u(t + k\Delta t) s_m^*(t) dt \\ &= \begin{cases} \sqrt{\beta_{m,u} p_{m_{tx}}} g_{m,u} + w_{u,k}(t), & \text{if } s_m(t) \text{ transmitted,} \\ w_{u,k}(t), & \text{otherwise,} \end{cases} \end{aligned} \quad (7.12)$$

where  $\Delta t$  is the time delay defining the time resolution of delay matched filtering,  $k$  is a non-negative integer with  $0 \leq k \leq T/\Delta t$  and  $w_{u,k}(t)$  is the noise output.

#### 7.4 Simulation Results

Consider a distributed JRC MIMO system consisting of  $M = 5$  isotropic transmitters located at (100, 1900) m, (250, 700) m, (1150, 1100) m, (1700, 300) m and (1900, 1250) m, respectively, in the two-dimensional space. The radar uses  $N = 5$  receive antennas located at (100, 1000) m, (450, 300) m, (1000, 1950) m, (1400, 150) m and (1800, 950) m, respectively. A point target is located at the coordinate of (1000, 1000) m. Two communication receivers are located at (250, 200) m and (1150, 300) m, respectively. Fig. 7.2 shows the arrangement of the distributed JRC MIMO system and the communication receivers in the two-dimensional coordinate system. Each transmitter can transmit a maximum of 100 W power during each radar pulse whereas the minimum allowed power for each transmitter is 1 W. Moreover, the maximum total allowable transmit power from the distributed JRC MIMO system,  $P_{\text{total}_{\max}}$ , is 400 W. The data rate for the communication system is calculated in terms of Shannon's capacity.

The magnitude of all elements of the RCS vector  $\mathbf{h}$  is assumed to be uniformly distributed between 0.9 to 1. For this simulation, we took the magnitude of  $\mathbf{h}$  as [0.962, 0.912, 0.969, 0.977, 0.907, 0.918, 0.945, 0.952, 0.982, 0.957, 0.946, 0.945, 0.952, 0.982, 0.957, 0.964, 0.941, 0.915, 0.956, 0.909, 0.906, 0.979, 0.980, 0.996, 0.902]<sup>T</sup> whereas their phases independently follow the uniform distribution. The path loss coefficients

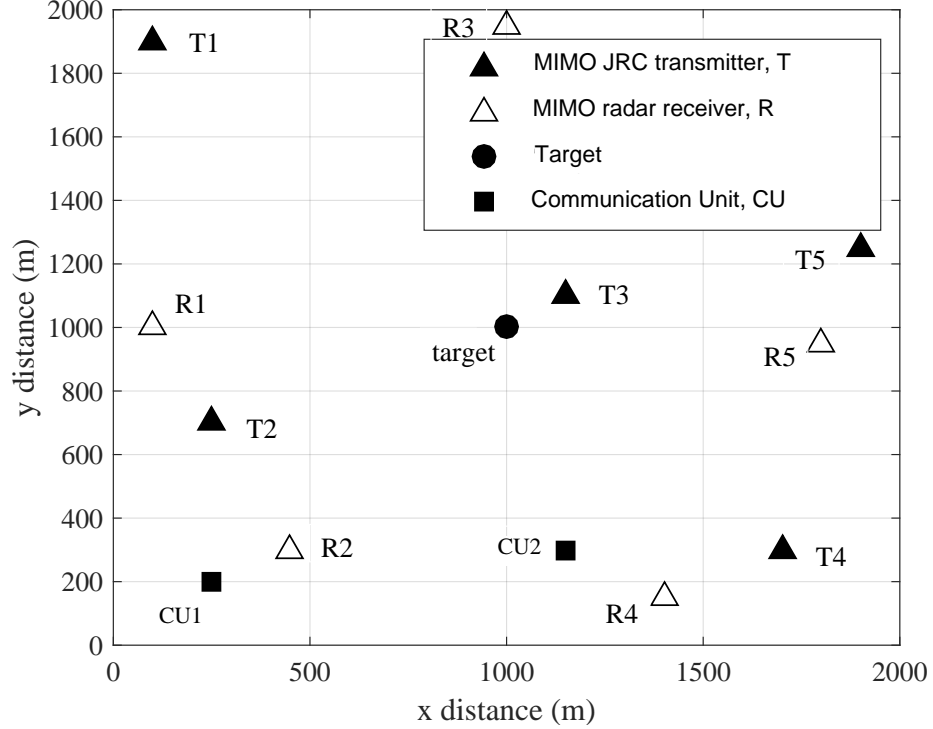


Figure 7.2. Simulation layout for distributed JRC MIMO system.

$\alpha_{m,n}$  and  $\beta_{m,u}$  are calculated using the location coordinates of the distributed JRC MIMO system, the communication receivers, and the target, whereas  $\xi_m = 8.773 \times 10^5$  is assumed for all  $1 \leq m \leq M$ . For the communication purpose, we considered  $\gamma_1 = -[1/0.8, 1/1, 1/0.01, 1/0.9, 1/0.95]^T$  and  $\gamma_2 = -[1/0.6, 1/0.9, 1/0.01, 1/0.85, 1/0.73]^T$ . In this case, both communication receivers experience deep fading with the third transmitter of the distributed JRC MIMO system. On the other hand, the path loss coefficients  $\alpha_{m,n}$  are the highest for the third transmitter of the JRC system because of its proximity with the target. This implies that the third transmitter is the most important in determining the target localization. However, it is the least important for optimizing the data rate for the communication system due to the smallest communication SNR (deep fading) with both communication receivers.

Table 7.1 summarizes the power allocation results and the radar as well as communication performance for the optimization strategies of the radar-only case [75], the

Table 7.1.  
 Power allocation for proposed JRC system for  $M = N = 5$  and  $U = 2$ ,  
 $P_{\text{total}_{\max}} = 400$  W,  $\eta_{\text{desired}} = 10$  m<sup>2</sup>

	Radar-only (7.7)	Communication-only (7.9)	JRC (7.10)
$\mathbf{p}_{\text{tx}}$ (W)	1.0	99.45	89.39
	1.0	99.95	81.27
	90.46	1.02	72.22
	1.0	99.86	79.43
	1.0	99.72	77.69
$P_{\text{total}}$ (W)	94.46	400	400
$\eta$ (m <sup>2</sup> )	9.97	30.59	8.21
$\mathfrak{R}$ (bits/pulse)	8.87	51.16	50.44

communication-only case, and the proposed JRC case. The desired radar performance is the mean squared localization error of  $\eta_{\text{desired}} = 10$  m<sup>2</sup>.

The radar-only optimization scheme described in (7.7) provides the optimal power required for the acceptable operation of radar. It allocates most of the transmit power to the third transmitter because it provides the best target localization accuracy due to its lowest path loss coefficient. However, the third transmitter has poor communication channel conditions, thus making it unsuitable for joint radar-communication operation because the yielding communication sum data rate is only 8.87 bits/pulse.

The communication-only scheme (7.9) exploits water-filling under the available power constraint to achieve the optimal sum data rate of 51.16 bits/pulse. It can be observed that the least power is allocated to the third transmitter due to its worst communication conditions and more power is allocated to other transmitters with better communication channel conditions. Although this scheme is the best to achieve the optimal data rate, it results in a high CRB of  $\eta = 30.59$  m<sup>2</sup> while using 400 W power, thus failing to achieve the desired radar performance, even consuming the maximum allowable total power.

The distributed JRC MIMO scheme described in (7.10) allocates the optimal power to different transmitters by simultaneously considering the communication and radar objectives. As the radar objective is the primary one, it is observed that the JRC scheme allocates a considerable amount of power to the third transmitter, resulting in the desired target localization accuracy with  $\eta = 8.21 \text{ m}^2$ , whereas the secondary communication operation achieves a sum data rate of 50.44 bits/pulse. The results clearly confirm the promising performance of the proposed strategy.

## 7.5 Remarks

In this chapter, we proposed a distributed JRC MIMO system which optimizes the power allocation for a desired localization accuracy of the radar and improves the communication data rate by considering the channel side information. The power allocation was derived for the maximum allowable total power of the JRC transmitters ensuring the desired radar-communication performance. Simulation results verify the effectiveness of the proposed scheme.

## CHAPTER 8

### FUTURE DIRECTIONS

The research carried out towards this dissertation has opened up several avenues in spectrum sharing related to JRC systems. In the following, we recommend the investigation of following research problems that stem from this study:

#### **1. Spectrum Sharing Under Channel Uncertainties**

In the dissertation, we mostly focused on spectrum sharing strategies where the radar target response and communication channel are precisely known, whereas some preliminary results have been presented for channel conditions following Rayleigh distribution. However, it would be of great interest to work in this direction accounting for channel uncertainties for radar as well as communication systems simultaneously for a wide variety of channel uncertainties. Further research can be beneficial to develop effective methods in this domain.

#### **2. Massive Access Management**

The radar subsystem estimates the target locations using the received pulsed signals reflected by the target. However, the JRC system is also receiving data from massive number of communication users in the same frequency band. Therefore, it is important for the JRC systems to be able to distinguish between the target echos and received communication signals.

#### **3. Location-Dependent Resource Allocation**

The spatial location of radar, communication users, and target play critical role in JRC system performance. The main challenge for JRC systems is to understand the effect of mobility and adapt resource allocation according to it. Therefore, resource-

dependent JRC strategies can be helpful to effectively optimize time, frequency, and energy resources.

#### **4. Incentive Mechanisms for JRC Systems**

In distributed JRC systems, all the distributed sensors are responsible to detect as much information about the target as possible. However, each node in the network requires high bandwidth to perform this task. Game theoretic approaches can be developed that distribute the spectrum resources in an intelligent manner such that more incentive is provided to the nodes with better performance. Such approaches can also be used in internet-of-things that sense the surrounding environments.

#### **5. Security Issues**

The radar systems are susceptible to jamming and eavesdropping attacks. Such attacks can be easier in JRC systems as the system resources are shared with communication users. Due to the uncertainty of jamming patterns and the presence of active eavesdroppers, JRC systems need to enable optimal defense strategies that counter these problems.

**REFERENCES CITED**

- [1] H. Griffiths, S. Blunt, L. Cohen, and L. Savy, "Challenge problems in spectrum engineering and waveform diversity," in *Proc. IEEE Radar Conf.*, Ottawa, Canada, Apr.–May 2013, pp. 1–5.
- [2] H. Griffiths, L. Cohen, S. Watts, E. Mokole, C. Baker, M. Wicks, and S. Blunt, "Radar spectrum engineering and management: Technical and regulatory issues," *Proc. IEEE*, vol. 103, no. 1, pp. 85–102, Jan. 2015.
- [3] C. Baylis, M. Fellows, L. Cohen, and R. J. Marks, "Solving the spectrum crisis: Intelligent, reconfigurable microwave transmitter amplifiers for cognitive radar," *IEEE Microw. Mag.*, vol. 15, no. 5, pp. 94–107, July-Aug. 2014.
- [4] H. T. Hayvaci and B. Tavli, "Spectrum sharing in radar and wireless communication systems: A review," in *Proc. Int. Conf. Electromagn. in Advanced Appl.*, Palm Beach, Aruba, Aug. 2014, pp. 810–813.
- [5] N. C. Luong, X. Lu, D. T. Hoang, D. Niyato, and D. I. Kim, "Radio resource management in joint radar and communication: A comprehensive survey," *ArXiv*, vol. abs/2007.13146, 2020.
- [6] F. Liu, C. Masouros, A. P. Petropulu, H. Griffiths, and L. Hanzo, "Joint radar and communication design: Applications, state-of-the-art, and the road ahead," *IEEE Trans. Commun.*, vol. 68, no. 6, pp. 3834–3862, June 2020.
- [7] S. Kumar, G. Costa, S. Kant, B. F. Flemming, N. Marchetti, and P. Mogensen, "Spectrum sharing for next generation wireless communication networks," in

- Proc. First Int. Workshop on Cognitive Radio and Advanced Spectr. Manag.*, Aalborg, Denmark, Feb 2008, pp. 1–5.
- [8] E. Biglieri, *Principles of Cognitive Radio*. Cambridge University Press, 2012.
- [9] Q. Wu, Y. D. Zhang, M. G. Amin, and B. Himed, “High-resolution passive SAR imaging exploiting structured Bayesian compressive sensing,” *IEEE J. Sel. Topics Signal Process.*, vol. 9, no. 8, pp. 1484–1497, 2015.
- [10] H. D. Griffiths and C. J. Baker, *An Introduction to Passive Radar*, ser. Artech House radar library. Norwood, MA, USA: Artech House Publishers, 2017.
- [11] Y. D. Zhang, M. G. Amin, and B. Himed, “Structure-aware sparse reconstruction and applications to passive multistatic radar,” *IEEE Aerosp. Electron. Syst. Mag.*, vol. 32, no. 2, pp. 68–78, Feb. 2017.
- [12] R. Saruthirathanaworakun, J. M. Peha, and L. M. Correia, “Opportunistic sharing between rotating radar and cellular,” *IEEE J. Sel. Areas Commun.*, vol. 30, no. 10, pp. 1900–1910, Nov. 2012.
- [13] D. W. Bliss, “Cooperative radar and communications signaling: The estimation and information theory odd couple,” in *Proc. IEEE Radar Conf.*, Cincinnati, OH, May 2014, pp. 50–55.
- [14] B. Paul, A. R. Chiriyath, and D. W. Bliss, “Survey of RF communications and sensing convergence research,” *IEEE Access*, vol. 5, pp. 252–270, Dec. 2017.
- [15] Z. Geng, H. Deng, and B. Himed, “Adaptive radar beamforming for interference mitigation in radar-wireless spectrum sharing,” *IEEE Signal Process. Lett.*, vol. 22, no. 4, pp. 484–488, April 2015.

- [16] Kuan-Wen Huang, M. Bica, U. Mitra, and V. Koivunen, "Radar waveform design in spectrum sharing environment: Coexistence and cognition," in *Proc. IEEE Radar Conf.*, Johannesburg, South Africa, May 2015, pp. 1698–1703.
- [17] B. Li and A. P. Petropulu, "Joint transmit designs for coexistence of MIMO wireless communications and sparse sensing radars in clutter," *IEEE Trans. Aerosp. Electron. Syst.*, vol. 53, no. 6, pp. 2846–2864, Dec. 2017.
- [18] B. Li, A. P. Petropulu, and W. Trappe, "Optimum co-design for spectrum sharing between matrix completion based MIMO radars and a MIMO communication system," *IEEE Trans. Signal Process.*, vol. 64, no. 17, pp. 4562–4575, Sep. 2016.
- [19] A. Khawar, A. Abdelhadi, and T. C. Clancy, "Coexistence analysis between radar and cellular system in los channel," *IEEE Antennas Wireless Propag. Lett.*, vol. 15, pp. 972–975, Oct. 2016.
- [20] J. A. Mahal, A. Khawar, A. Abdelhadi, and T. C. Clancy, "Spectral coexistence of MIMO radar and MIMO cellular system," *IEEE Trans. Aerosp. Electron. Syst.*, vol. 53, no. 2, pp. 655–668, April 2017.
- [21] F. Paisana, N. Marchetti, and L. A. DaSilva, "Radar, TV and cellular bands: Which spectrum access techniques for which bands?" *Commun. Surveys & Tuts.*, vol. 16, no. 3, pp. 1193–1220, 2014.
- [22] F. Liu, C. Masouros, A. Li, and T. Ratnarajah, "Robust MIMO beamforming for cellular and radar coexistence," *IEEE Wireless Commun. Lett.*, vol. 6, no. 3, pp. 374–377, June 2017.
- [23] C. Sturm, T. Zwick, and W. Wiesbeck, "An OFDM system concept for joint radar and communications operations," in *Proc. IEEE 69th Veh. Technol. Conf.*, Barcelona, Spain, April 2009, pp. 1–5.

- [24] S. C. Surender, R. M. Narayanan, and C. R. Das, "Performance analysis of communications & radar coexistence in a covert UWB OSA system," in *Proc. IEEE Global Telecommun. Conf.*, Miami, FL, Dec. 2010, pp. 1–5.
- [25] S. D. Blunt, M. R. Cook, and J. Stiles, "Embedding information into radar emissions via waveform implementation," in *Proc. Intl. Waveform Diversity Design Conf.*, Niagara Falls, Canada, Aug. 2010, pp. 195–199.
- [26] A. Hassaniien, M. G. Amin, Y. D. Zhang, and F. Ahmad, "Signaling strategies for dual-function radar communications: an overview," *IEEE Aerosp. Electron. Syst. Mag.*, vol. 31, no. 10, pp. 36–45, Oct. 2016.
- [27] J. Euziere, R. Guinvarc'h, M. Lesturgie, B. Uguen, and R. Gillard, "Dual function radar communication time-modulated array," in *Proc. International Radar Conf.*, Lille, France, Oct. 2014, pp. 1–4.
- [28] A. Hassaniien, M. G. Amin, Y. D. Zhang, and F. Ahmad, "A dual function radar-communications system using sidelobe control and waveform diversity," in *Proc. IEEE Radar Conf.*, Arlington, VA, May 2015, pp. 1260–1263.
- [29] —, "Dual-function radar-communications: Information embedding using sidelobe control and waveform diversity," *IEEE Trans. Signal Process.*, vol. 64, no. 8, pp. 2168–2181, April 2016.
- [30] —, "Efficient sidelobe ASK based dual-function radar-communications," in *Proc. SPIE Defense + Security, Radar Sensor Technology Conf.*, Baltimore, MD, April 2016.
- [31] —, "Dual-function radar-communications using phase-rotational invariance," in *Proc. European Signal Process. Conf.*, Nice, France, Aug. 2015, pp. 1346–1350.

- [32] A. Hassanien, M. G. Amin, Y. D. Zhang, F. Ahmad, and B. Himed, “Non-coherent PSK-based dual-function radar-communication systems,” in *Proc. IEEE Radar Conf.*, Philadelphia, PA, May 2016, pp. 1–6.
- [33] A. Hassanien, M. G. Amin, Y. D. Zhang, and F. Ahmad, “Phase-modulation based dual-function radar-communications,” *IET Radar, Sonar, Navig.*, vol. 10, no. 8, pp. 1411–1421, March 2016.
- [34] A. Hassanien, B. Himed, and B. D. Rigling, “A dual-function MIMO radar-communications system using frequency-hopping waveforms,” in *Proc. IEEE Radar Conf.*, Seattle, WA, May 2017, pp. 1721–1725.
- [35] A. Hassanien, M. G. Amin, and Y. D. Zhang, “Computationally efficient beam-pattern synthesis for dual-function radar-communications,” in *Proc. SPIE Defense + Security, Radar Sensor Technology Conf.*, Baltimore, MD, April 2016.
- [36] P. M. McCormick, S. D. Blunt, and J. G. Metcalf, “Simultaneous radar and communications emissions from a common aperture, part I: Theory,” in *IEEE Radar Conf.*, May 2017, pp. 1685–1690.
- [37] A. R. Chiriyath, B. Paul, and D. W. Bliss, “Radar-communications convergence: Coexistence, cooperation, and co-design,” *IEEE Trans. Cogn. Commun. Netw.*, vol. 3, no. 1, pp. 1–12, March 2017.
- [38] A. Ahmed, Y. D. Zhang, and B. Himed, “Multi-user dual-function radar-communications exploiting sidelobe control and waveform diversity,” in *Proc. IEEE Radar Conf.*, Oklahoma City, OK., Apr. 2018, pp. 698–702.
- [39] P. Kumari, J. Choi, N. González-Prelcic, and R. W. Heath, “IEEE 802.11ad-based radar: An approach to joint vehicular communication-radar system,” *IEEE Trans. Vehicular Technol.*, vol. 67, no. 4, pp. 3012–3027, April 2018.

- [40] F. Liu, L. Zhou, C. Masouros, A. Li, W. Luo, and A. Petropulu, "Toward dual-functional radar-communication systems: Optimal waveform design," *IEEE Trans. Signal Process.*, vol. 66, no. 16, pp. 4264–4279, Aug. 2018.
- [41] H. Deng and B. Himed, "Interference mitigation processing for spectrum-sharing between radar and wireless communications systems," *IEEE Trans. on Aerosp. Electron. Syst.*, vol. 49, no. 3, pp. 1911–1919, July 2013.
- [42] J. R. Guerci, R. M. Guerci, A. Lackpour, and D. Moskowitz, "Joint design and operation of shared spectrum access for radar and communications," in *Proc. IEEE Radar Conf.*, Arlington, VA, May 2015, pp. 0761–0766.
- [43] K. W. Huang, M. Bică, U. Mitra, and V. Koivunen, "Radar waveform design in spectrum sharing environment: coexistence and cognition," in *Proc. IEEE Radar Conf.*, Arlington, VA, May 2015, pp. 1698–1703.
- [44] I. P. Eedara, A. Hassaniien, M. G. Amin, and B. D. Rigling, "Ambiguity function analysis for dual-function radar communications using PSK signaling," in *Proc. Asilomar Conf. Signals, Systems, Comput.*, Pacific Grove, CA, Oct. 2018, pp. 900–904.
- [45] A. Ahmed, Y. Gu, D. Silage, and Y. D. Zhang, "Power-efficient multi-user dual-function radar-communication," in *Proc. IEEE Int. Workshop Signal Process. Advances in Wireless Commun.*, Kalamata, Greece, June 2018, pp. 1–5.
- [46] A. Ahmed, Y. D. Zhang, and Y. Gu, "Dual-function radar-communications using QAM-based sidelobe modulation," *Digital Signal Process.*, vol. 82, pp. 166–174, Nov. 2018.
- [47] X. Wang, A. Hassaniien, and M. G. Amin, "Sparse transmit array design for dual-function radar communications by antenna selection," *Digital Signal Process.*, vol. 83, pp. 223–234, Dec. 2018.

- [48] S. D. Blunt, J. G. Metcalf, C. R. Biggs, and E. Perrins, “Performance characteristics and metrics for intra-pulse radar-embedded communication,” *IEEE J. Sel. Areas in Commun.*, vol. 29, no. 10, pp. 2057–2066, Dec. 2011.
- [49] Y. Liu, G. Liao, J. Xu, Z. Yang, and Y. Zhang, “Adaptive OFDM integrated radar and communications waveform design based on information theory,” *IEEE Commun. Lett.*, vol. 21, no. 10, pp. 2174–2177, Oct. 2017.
- [50] M. Bică and V. Koivunen, “Radar waveform optimization for target parameter estimation in cooperative radar-communications systems,” *IEEE Trans. Aerosp. Electron. Syst.*, vol. 55, no. 5, Oct. 2019.
- [51] —, “Multicarrier radar-communications waveform design for RF convergence and coexistence,” in *Proc. IEEE Int. Conf. Acoust., Speech, Signal Process.*, Brighton, U.K., May 2019, pp. 7780–7784.
- [52] A. Ahmed, Y. D. Zhang, and B. Himed, “Distributed dual-function radar-communication MIMO system with optimized resource allocation,” in *Proc. IEEE Radar Conference*, Boston, MA, April 2019, pp. 1–5.
- [53] A. Ahmed, S. Zhang, V. S. Amin, and Y. D. Zhang, “Spectrum sharing strategy for radio frequency based medical services,” in *Proc. IEEE Signal Process. in Medicine and Biol. Symp.*, Philadelphia, PA, Dec. 2019.
- [54] A. Ahmed, Y. D. Zhang, A. Hassanien, and B. Himed, “OFDM-based joint radar-communication system: Optimal sub-carrier allocation and power distribution by exploiting mutual information,” in *Proc. Asilomar Conf. Signals, Systems, Comput.*, Pacific Grove, CA, Nov. 2019, pp. 559–563.
- [55] C. Shi, Y. Wang, F. Wang, S. Salous, and J. Zhou, “Power resource allocation scheme for distributed MIMO dual-function radar-communication system based

- on low probability of intercept,” *Digital Signal Process.*, vol. 106, p. 102850, Nov. 2020.
- [56] M. Bică and V. Koivunen, “Generalized multicarrier radar: Models and performance,” *IEEE Trans. Signal Process.*, vol. 64, no. 17, pp. 4389–4402, September 2016.
- [57] A. Hassanien, S. A. Vorobyov, and A. Khabbazibasmenj, “Transmit radiation pattern invariance in MIMO radar with application to DOA estimation,” *IEEE Signal Process. Lett.*, vol. 22, no. 10, pp. 1609–1613, Oct. 2015.
- [58] A. D. Maio and M. Lops, “Design principles of MIMO radar detectors,” *IEEE Trans. Aerosp. Electron. Syst.*, vol. 43, no. 3, pp. 886–898, July 2007.
- [59] Y. Yang and R. S. Blum, “MIMO radar waveform design based on mutual information and minimum mean-square error estimation,” *IEEE Trans. Aerosp. Electron. Syst.*, vol. 43, no. 1, pp. 330–343, Jan. 2007.
- [60] T. M. Cover and J. A. Thomas, *Elements of Information Theory*. Wiley, 2006.
- [61] Y. Gu and Y. D. Zhang, “Information-theoretic pilot design for downlink channel estimation in FDD massive MIMO systems,” *IEEE Trans. Signal Process.*, vol. 67, no. 9, pp. 2334–2346, May 2019.
- [62] M. R. Bell, “Information theory and radar waveform design,” *IEEE Trans. Inf. Theory*, vol. 39, no. 5, pp. 1578–1597, Sep. 1993.
- [63] Gurobi Optimization, *Gurobi Optimizer Reference Manual*, 2020. [Online]. Available: <http://www.gurobi.com>
- [64] MOSEK ApS, *The MOSEK Optimization Toolbox for MATLAB Manual. Version 9.0.*, 2019. [Online]. Available: <http://docs.mosek.com/9.0/toolbox/index.html>

- [65] CVX Research, Inc., “CVX: Matlab software for disciplined convex programming, version 2.0,” <http://cvxr.com/cvx>, 2012.
- [66] M. Grant and S. Boyd, “Graph implementations for nonsmooth convex programs,” in *Recent Advances in Learning and Control*, V. Blondel, S. Boyd, and H. Kimura, Eds. Springer-Verlag Limited, 2008, pp. 95–110.
- [67] R. H. Tütüncü, K. C. Toh, and M. J. Todd, “Solving semidefinite-quadratic-linear programs using SDPT3,” *Math. Program.*, vol. 95, no. 2, pp. 189–217, Feb 2003.
- [68] K. C. Toh, M. J. Todd, and R. H. Tütüncü, “SDPT3 — a Matlab software package for semidefinite programming, version 1.3,” *Optim. Methods. Softw.*, vol. 11, no. 1-4, pp. 545–581, 1999.
- [69] A. Ahmed, D. Silage, and Y. D. Zhang, “Chance constrained beamforming for joint radar-communication systems,” in *Proc. IEEE Sensor Array Multichannel Signal Process. Workshop*, Hangzhou, China, June 2020, pp. 1–5.
- [70] A. Goldsmith, *Wireless Communications*. Cambridge University Press, 2005.
- [71] R. H. Tütüncü, K. C. Toh, and M. J. Todd, “Solving semidefinite-quadratic-linear programs using SDPT3,” *Math. Program.*, vol. 95, no. 2, pp. 189–217, Feb. 2003.
- [72] K. C. Toh, M. J. Todd, and R. H. Tütüncü, “SDPT3 — a Matlab software package for semidefinite programming, version 1.3,” *Optim. Methods. Softw.*, vol. 11, no. 1-4, pp. 545–581, 1999.
- [73] A. Ahmed, S. Zhang, and Y. D. Zhang, “Optimized sensor selection for joint radar-communication systems,” in *Proc. IEEE Int. Conf. Acoust., Speech, Signal Process.*, Brighton, UK, May 2020, pp. 4682–4686.

- [74] A. Ahmed, S. Zhang, and Y. D. Zhang, “Antenna selection strategy for transmit beamforming-based joint radar-communication system,” *Digital Signal Process.*, vol. 105, p. 102768, October 2020.
- [75] H. Godrich, A. P. Petropulu, and H. V. Poor, “Power allocation strategies for target localization in distributed multiple-radar architectures,” *IEEE Trans. Signal Process.*, vol. 59, no. 7, pp. 3226–3240, July 2011.
- [76] —, “Sensor selection in distributed multiple-radar architectures for localization: A knapsack problem formulation,” *IEEE Trans. Signal Process.*, vol. 60, no. 1, pp. 247–260, Jan 2012.
- [77] O. Mehanna, N. D. Sidiropoulos, and G. B. Giannakis, “Joint multicast beamforming and antenna selection,” *IEEE Trans. Signal Process.*, vol. 61, no. 10, pp. 2660–2674, May 2013.
- [78] O. T. Demir and T. E. Tuncer, “Antenna selection and hybrid beamforming for simultaneous wireless information and power transfer in multi-group multicasting systems,” *IEEE Trans. Wireless Commun.*, vol. 15, no. 10, pp. 6948–6962, Oct. 2016.
- [79] L. Blanco and M. Nájjar, “Sparse multiple relay selection for network beamforming with individual power constraints using semidefinite relaxation,” *IEEE Trans. Wireless Commun.*, vol. 15, no. 2, pp. 1206–1217, Feb. 2016.
- [80] S. A. Hamza and M. G. Amin, “Hybrid sparse array design for under-determined models,” in *Proc. IEEE Int. Conf. Acoust., Speech, Signal Process.*, Brighton, U.K., May 2019, pp. 4180–4184.
- [81] —, “Sparse array DFT beamformers for wideband sources,” in *Proc. IEEE Radar Conf.*, Boston, MA, Apr. 2019, pp. 1–5.

- [82] S. A. Hamza and M. G. Amin, "Sparse array design for maximizing the signal-to-interference-plus-noise-ratio by matrix completion," *Digital Signal Process.*, vol. 105, p. 102678, Oct. 2020.
- [83] H. Nosrati, E. Aboutanios, and D. Smith, "Array partitioning for multi-task operation in dual function MIMO systems," *Digital Signal Process.*, vol. 82, pp. 106–117, Nov. 2018.
- [84] A. Deligiannis, M. Amin, S. Lambotharan, and G. Fabrizio, "Optimum sparse subarray design for multitask receivers," *IEEE Trans. Aerosp. Electron. Syst.*, vol. 55, no. 2, pp. 939–950, April 2019.
- [85] X. Wang, A. Hassanien, and M. G. Amin, "Dual-function MIMO radar communications system design via sparse array optimization," *IEEE Trans. Aerosp. Electron. Syst.*, vol. 55, no. 3, pp. 1213–1226, June 2019.
- [86] A. Koochakzadeh and P. Pal, "Beam-pattern design for hybrid beamforming using Wirtinger flow," in *Proc. IEEE Int. Workshop Signal Process. Advances in Wireless Commun.*, Kalamata, Greece, June 2018.
- [87] E. J. Candès, M. B. Wakin, and S. P. Boyd, "Enhancing sparsity by reweighted  $l_1$  minimization," *J. Fourier Anal. Appl.*, vol. 14, no. 5, pp. 877–905, Dec. 2008.
- [88] K. Lange, *Optimization*. Springer, New York, 2004.
- [89] M. Yuan and Y. Lin, "Model selection and estimation in regression with grouped variables," *J. R. Stat. Soc. B.*, vol. 68, pp. 49–67, Feb. 2006.
- [90] F. Bach, R. Jenatton, J. Mairal, and G. Obozinski, "Optimization with sparsity-inducing penalties," *Found. Trends Mach. Learn.*, vol. 4, no. 1, pp. 1–106, Jan. 2012.

- [91] H. Godrich, A. M. Haimovich, and R. S. Blum, "Target localization accuracy gain in MIMO radar-based systems," *IEEE Trans. Inf. Theory*, vol. 56, no. 6, pp. 2783–2803, June 2010.

## APPENDIX A

### RADAR TERMINOLOGY

Radar is an acronym for RAdio Detection And Ranging. In simple words, it is an object detection system that transmits electromagnetic waves and analyzes the echoes reflected from the objects. However, modern radars can perform quite a lot number of tasks apart from target detection and tracking.

#### **Categorization of Radars**

Radars can be broadly categorized into several categories. In the following, we discuss only the most common characteristics on the basis of which the radars are usually classified:

##### *Illuminator*

Active radars are equipped with transmitter(s) which illuminate the target. On the other hand, passive radars rely on the illuminators of opportunity, like communication networks, to perform the radar tasks.

##### *Transmission Rate*

Pulsed radars emit the transmit waveforms in the forms of pulses. The time duration between the activation of two pulses is called *pulse repetition interval*. The inverse of pulse repetition interval is regarded as *pulse repetition frequency*.

Continuous wave radars transmit the radar waveforms continuously. The reflected signals from the target are inspected to perform the radar tasks.

## *Geometry*

Monostatic radars perform the transmit and receive operation at the same physical location. On the other hand, transmitters and receivers are spatially employed at different locations in the bistatic or multistatic radars.

### **Basic Operation**

The simplest radar operation can be divided into 4 steps:

- The radar is transmitting an electromagnetic pulse.
- The radar switches to listening mode.
- The pulse is reflected by a target.
- The radar receives the echoes from the transmitted pulse.

Using various properties of the received echo, the radar can extract parameters such as the range and velocity of the target

## *Radar Cross-section*

Radar cross-section is a measure of how detectable an object is by radar. A larger RCS indicates that an object is more easily detected.

All objects reflect a limited amount of radar energy back to the radar. The factors that influence this include:

- The material of which the object is made;
- Size of the object relative to the radar wavelength;
- Absolute size of the object;
- Incident and reflected angles of the radar signals with the object;
- polarization of the radar transmit signals and the signals reflected by the target.

## Radar Equation

The radar equation provides the mathematical framework for the basic radar operation. According to this equation, the receive power of the radar  $P_r$  due to target echo can be represented in terms of the transmit power  $P_t$  as follows:

$$P_r = \frac{P_t G^2 \lambda^2 \sigma}{(4\pi)^3 R^4 L}. \quad (\text{A.1})$$

Here,

- $P_t$ : transmit power of the radar;
- $P_r$ : received power at the radar from the target echo;
- $G$ : antenna gain;
- $\lambda$ : operating wavelength;
- $\sigma$ : target radar cross-section
- $R$ : range from the radar to the target;
- $L$ : Other losses (system, propagation).

Rearranging the radar equation we get:

$$R = \left( \frac{P_t G^2 \lambda^2 \sigma}{(4\pi)^3 P_r L} \right)^{1/4}. \quad (\text{A.2})$$

This implies that the low frequencies are preferable for long-range targets.

## Range Calculation

The *range* of the target from the radar can be determined by the time-delay of the echoed signal from the target. Mathematically,

$$R = \frac{c\tau}{2}, \quad (\text{A.3})$$

where  $c$  is the speed of electromagnetic waves and  $\tau$  is the time-delay of the target echo. The factor of 2 in the above equation is due to the fact that the radar signals

cover the distance equal to twice the range. This is because the signals travel from the radar transmitter to the target and then from the target to their way back to the radar receiver.

### *Range Resolution*

*Range resolution* is the ability of the radar to separate the closely spaced targets. The range resolution  $\rho$  can be mathematically expressed as:

$$\rho \geq \frac{cT}{2} \approx \frac{c}{2B}, \quad (\text{A.4})$$

where  $T$  is the pulse duration and  $B$  is the bandwidth.

If the distance between the two targets is less than  $cT/2$ , the reflected signal from the both targets merge with each other. Advanced technique like pulse compression can enhance the range resolution. The above equation shows that the range resolution can be improved if the radar bandwidth is very high.

### *Maximum Unambiguous Range*

Radar is not able to discriminate between echoes from an older and the current pulse transmission. In this context, we can define the maximum unambiguous range as follows:

$$R_{\max} = \frac{cT_{\text{pri}}}{2} = \frac{c}{2f_{\text{prf}}}, \quad (\text{A.5})$$

where  $T_{\text{pri}}$  and  $f_{\text{prf}}$  respectively represent the pulse repetition interval and pulse repetition frequency.

### **Slow Time and Fast Time**

Radar signals from each pulse repetition interval are sorted in memory for further processing. In this context, following two definitions are important:

- Fast time: refers to the different sampling time slots composing a pulse repetition interval. Fast time is dependent on the sampling rate of radar analog-to-digital converter.
- Slow time: It can be considered as the pulse repetition index. It is updated once at each pulse repetition interval.

Suppose that a radar transmits pulses with a pulse repetition interval of 1 msec. The reflected signals will be recorded by the radar receiver in the fast time. The slow time index will start from 0 and will update on each pulse. If the sampling time of radar receiver is 1  $\mu$ sec, it will record 1000 fast-time samples corresponding to each slow-time index or pulse.

## APPENDIX B

### SOFTWARE IMPLEMENTATION

In this appendix, we give a brief overview of the software packages used during this dissertation.

#### **MATLAB**

MATLAB is a multi-paradigm numerical computing environment and proprietary programming language developed by MathWorks. It allows matrix manipulations, plotting of functions and data, implementation of algorithms, creation of user interfaces, and interfacing with programs written in other languages.

MATLAB has served as the main programming environment for this thesis. We have integrated other useful toolboxes and solvers with MATLAB for carrying out the simulations.

#### **CVX**

CVX is a MATLAB-based modeling system for solving convex optimizations. CVX helps the users to model their optimization in the form of MATLAB expressions.

Different commercial and academic solvers can also be integrated with CVX; however, CVX default repository contains SeDuMI, SDPT3, Gurobi, Mosek, and GLPK. Each solver has different capabilities and different levels of performance. For instance, SeDuMi, SDPT3, and MOSEK support all of the continuous (non-integer) models that CVX itself supports, while Gurobi is more limited, in that it does not support semidefinite constraints; and GLPK is limited even further. On the other hand, Gurobi, GLPK, and MOSEK support mixed-integer optimizations, while SeDuMi and SDPT3 do not.

Gurobi and Mosek require additional academic or commercial license. Academic licenses are free to download and install on educational networks. Both of these solvers can also be used with Python.

## **Gurobi**

The Gurobi Optimizer is a commercial optimization solver for linear programming, quadratic programming, quadratically constrained programming, mixed integer linear programming, mixed-integer quadratic programming, and mixed-integer quadratically constrained programming.

The Gurobi Optimizer also includes a number of features to support the building of optimization models including support for:

- Multiple objectives with flexibility in how they are prioritized General constraints such as MIN/MAX, ABS, AND/OR, and indicator constraints help avoid having to turn commonly occurring constraints in linear constraints.
- Models with convex, piecewise-linear objective functions, to capture certain non-linear problems.
- Arbitrary piecewise-linear objective functions, to make it easier to express this common modeling feature.
- Distributed tuning, to speed the exploration of parameter settings to speed solve times.
- The Gurobi Optimizer also has options to deploy on the cloud and for client-server computing.

The Gurobi optimizer can also be used within the CVX toolbox. Currently, Gurobi is free for academic use.

## **MOSEK**

MOSEK is a software package for the solution of linear, mixed-integer linear, quadratic, mixed-integer quadratic, quadratically constraint, conic and convex non-

linear mathematical optimization problems. The emphasis in MOSEK is on solving large scale sparse problems, particularly the interior-point optimizer for linear, conic quadratic and semi-definite. The software is particularly very efficient solving the latter set of problems.

A special feature of the MOSEK interior-point optimizer is that it is based on the so-called homogeneous model. This implies that MOSEK can reliably detect a primal and/or dual infeasible status as documented in several published papers.

The MOSEK optimizer can also be used within the CVX toolbox. Currently, MOSEK is free for academic use.